Charles University
Faculty of Science

Study programme:
Physical Chemistry

Mgr. Marie Olšinová

The effect of peptides derived from protein transmembrane domains on membranes

Vliv peptidů odvozených od transmembránových domén proteinů na membrány

Type of thesis:
Doctoral thesis

Supervisor: Mgr. Marek Cebecauer Ph.D.

Prague, 2018

Prohlášení:

Prohlašuji, že jsem závěrečnou práci zpracovala samostatně a že jsem uvedla všechny použité informační zdroje a literaturu. Tato práce ani její podstatná část nebyla předložena k získání jiného nebo stejného akademického titulu.

V Praze,

Podpis:

Acknowledgement

I would like to express my gratitude to all the people who were supporting me during my PhD studies and without whom finishing my PhD would not be possible. Firstly, I would like to thank my supervisor Marek Cebecauer for the possibility of working in his team and for his patient guidance, insightful advices, human approach and never ending optimism. In the same way, I would like to thank Martin Hof for enabling me to work in his department, for his support through the whole time I was working there and for his friendly attitude (Fridays included).

I would like to thank all my colleagues at J. Heyrovsky Institute of Physical Chemistry for teaching me all the fluorescence techniques and vesicle preparations, for helpful discussions, and willingness to answer all my questions. Also, big thanks for creating so friendly atmosphere!

I would like to thank Petr Novák, Petr Pompach and Ján Sabó for characterization of transmembrane peptides used in the thesis by mass spectrometry.

I would also like to thank my colleagues in BIOCEV, who enabled me to finish my PhD and simultaneously work in the Imaging Methods Core Facility. Thank you for your patience!

My big thank belongs to my family and to my husband Jan. Without their support I would not be able to finish my PhD.

Abstract

Rich structure of cell membranes raises broad number of questions regarding the mechanisms driving and regulating processes taking place on membranes. The thesis presents four articles investigating organization of lipid membranes and peptide-lipid interactions. The experiments were performed on model lipid membranes. These simplified systems that partially mimic cell membranes enable to study protein-lipid interactions at the molecular level and membrane physico-chemical properties in a controlled way. Advanced fluorescence techniques such as FCS, TDFS, FLIM and anisotropy were used for the system characterization. First publication describes newly designed fluorescence dyes based on boron dipyrromethene structure, the so-called molecular rotors, which are reported to be viscosity-sensitive probes. Detailed analysis of fluorescence lifetime of excited state of the molecular rotors inserted into lipid membranes showed diverse incorporation of dyes into membranes and their reorientation in membranes of different rigidity. The second part investigates existence of lipid nanodomains in membranes caused by the presence of a cross-linker. Even though standard fluorescence microscopy techniques do not allow direct visualization of the nanodomains, we were able to detect these structures by employment of FCCS and FLIM-FRET techniques supported by Monte-Carlo simulations. The study showed two mechanisms of nanodomain formation depending on the membrane lipid composition and concentration of the cross-linker. In the third part, TDFS method was newly applied to determine the peptide orientation with respect to the membrane normal. The results from the previous studies set the basis for the fourth paper investigating membrane dynamics in the presence of peptides. Experimental and computational results show that increasing amount of the peptide reduces diffusion rate of all membrane components due to temporal lipid acyl chain trapping on the rough surface of the peptide. In cholesterol-containing membranes, the sterol segregates from peptide surface. Due to the fact that rough surface is an intrinsic property of literally all integral membrane proteins the results of our work can be generalized to most eukaryotic cell membranes. Distribution of membrane proteins and cholesterol in cell membranes could therefore affect a variety of intermolecular interactions and reaction kinetics of cellular processes associated with membranes, thus affecting vital functions of living cells.

Abstrakt

Složitá struktura buněčných membrán vyvolává mnoho otázek týkajících se mechanismu procesů relevantních pro správnou funkci membrán. Dizertační práce představuje čtyři články zabývající se organizací lipidových membrán a interakcemi mezi lipidy a peptidy. Experimenty byly prováděny na modelových lipidových membránách. Tyto zjednodušené systémy napodobující buněčné membrány umožňují studium protein-lipidových interakcí na molekulární úrovni a studium fyzikálně-chemických vlastností membrán kontrolovaným způsobem. Pro charakterizaci systému byly použity pokročilé fluorescenční techniky jako FCS, TDFS, FLIM a anizotropie. První publikace popisuje nově navržené fluorescenční značky založené na struktuře boron dipyrromethenu, tzv. molekulární rotory, které jsou využívány jako sondy pro měření viskozity. Podrobná analýza doby života excitovaného stavu molekulárních rotorů zanořených do lipidových membrán ukázala na různou inkorporaci jednolivých značek do membrány a na změnu orientace fluoroforů v membránách o různé rigiditě. Druhá část práce se zabývá studiem vzniku lipidových nanodomén v membráně v přítomnosti cross-linkeru. Přestože standardní fluorescenční mikroskopické techniky neumožňují přímou vizualizaci nanodomén, jejich existenci jsme byli schopni detekovat pomocí FCCS a FLIM-FRET technikami. Naše závěry byly podpořené Monte-Carlo simulacemi. Studie ukazuje dva mechanismy vzniku nanodomén v závislosti na složení lipidové membrány a koncentraci cross-linkeru. Ve třetím článku byla nově použita metoda TDFS pro stanovení orientace peptidu vzhledem k normále membrány. Předchozí výsledky poskytly základ pro čtvrtý článek věnující se studiu vlivu transmembránových peptidů na dynamiku membrán. Experimentální a výpočetní data ukazují, že zvyšující se množství peptidu v membráně zpomaluje rychlost difuze všech membránových složek v důsledku dočasného zachycení lipidových acylových řetězců hrubém povrchu peptidu. Přidání cholesterolu do studovaného systému ukázalo na vyloučení cholesterolu z blízkosti peptidu. Protože hrubý povrch je vlastní doslova všem integrálním membránovým proteinům, výsledky naší práce lze zobecnit na většinu eukaryotických buněčných membrán. Distribuce membránových proteinů a cholesterolu v buněčných membránách by proto mohla ovlivnit celou řadu intermolekulárních interakcí nebo kinetiku buněčných procesů odehrávajících se na membráně a tím ovlivňovat životně důležité funkce živých buněk.

Table of contents

1 Introduction

Interactions of transmembrane proteins and lipids play an important role in a majority of cell membrane processes, yet they are still poorly understood. Cells are difficult to study directly, as they are very complex and controlling relevant parameters is problematic. Simple model systems provide unique tool for detailed investigations of protein-lipid interactions in well-established systems. The doctoral thesis presents results of my research on the properties and organization of model lipid membranes mainly in the presence of transmembrane peptides – a model system representing protein transmembrane domains. Significant part of the work is dedicated to design of an appropriate model system and development of proper tools for the main experimental studies. The systems of choice for cell membrane representation were unilamellar lipid vesicles with optional transmembrane peptides enrichment. Model membrane properties, such as membrane dynamics and lipid clustering, were studied by various time-resolved fluorescence techniques. The aim of the model systems is to mimic particularly mammalian cell membranes. The focus on mammalian cells is motivated by the fact that human white blood cells are the main area of expertise of the research group in which I worked during my postgradual studies.

The thesis comprises of the introductory chapters describing necessary theoretical basics and the experimental part summarizing the motivation, results and discussion of my research. Theoretical introduction covers basic properties of eukaryotic cell membranes, describes recent models used for cell membrane organization and proteo-lipid model systems. It also provides a basic introduction to several time-resolved fluorescence techniques. The experimental part is based on four papers. The first one (Paper I) is dedicated to the characterization of novel dyes for membrane viscosity measurements. The second one (Paper II) addresses the topic of organization of three-component lipid membranes and conditions under which the nano-domains can form. The third one (Paper III) newly employs the information about local membrane polarity and mobility to determine transmembrane or peripheral orientation of peptides in membranes. The last article (Paper IV) investigates the dynamics of membrane components in the presence of transmembrane peptides. Presented results on model membrane systems suggest implications for organization of cell membranes in vivo.

2 Cell membranes and model systems

2.1 Cell membranes

Lipid membranes are indispensable parts of all living cells. In eukaryotes, they form a barrier between inner and outer space and compartmentalize the cell into several sectors (organelles). The cells are encompassed by the plasma membrane which has several vital functions: it protects cells by controlling import and export of protons, ions, molecules and even whole microorganisms, ensures communication between cells and the environment, and is involved in regulation of signaling or other molecular processes including cell growth and motility. Plasma membrane can be described as a highly dynamic and heterogeneous structure formed by a lipid bilayer densely populated by peripheral or integrated proteins, covered by oligosaccharide mesh from the extracellular space and supported by the cytoskeleton scaffold in the cytosolic side.

2.2 Lipids

Basic building blocks of the plasma membrane are lipids and proteins. A lipid bilayer of cell membranes was originally considered as a simple matrix in which proteins can float [1]. Nowadays, the importance of specific lipids in various aspects of cellular membranes is more appreciated [2,3]. For example, it was shown that lipids form complexes with proteins, which allows correct function of proteins and controls protein stability [4–6]. Moreover, various cell membranes have different thicknesses and a variety of lipid compositions, which indicates diverse functional environment for proteins [7]. (Mis)match between thickness of lipid bilayer and a length of the transmembrane segments of proteins directly regulates protein function and protein organization (e.g. clustering) [3,8]. All these examples indicate that lipids play an active part in the membrane processes.

Based on their structure, lipids of cell membranes can be divided into three main groups: glycerophospholipids, sphingolipids and sterols (Figure 1A). Phospholipids are amphipathic molecules meaning that they are composed of polar and apolar parts (Figure 1B). A polar part is also called a lipid headgroup and is facing towards aqueous environment; apolar part is formed by acyl chains. The hydrophobic backbone of glycerophospholipids contains diacylglycerol with saturated or cis-unsaturated fatty

acyl chains of various lengths. The most abundant type of lipid headgroup among the eukaryotic membrane lipids is phosphatidylcholine; other frequent groups are phosphatidylserine, phosphatidylinositol, phosphatidylethanolamine or phosphatidic acid [7]. Sphingolipids are based on sphingosine structure; the most frequent sphingolipids are sphingomyelin and glycosylated sphingolipids (glycosphingolipids). In gangliosides, there is one or more sialic acids attached to the sugar moiety of glycosphingolipids. Hydrophobic part of sphingolipids is mainly represented by saturated or trans-unsaturated acyl chains which have a tendency to rigidify the membrane. Maintaining the membrane fluidity is a key role of sterols (e.g. cholesterol in mammals, ergosterol in yeasts). A rich diversity of lipid headgroups and acyl chains ensures the existence of thousands of different lipid species present in cell membranes [9]. Lipids do not possess only structural function, they also play an important role in signal transduction and energy storage [7].

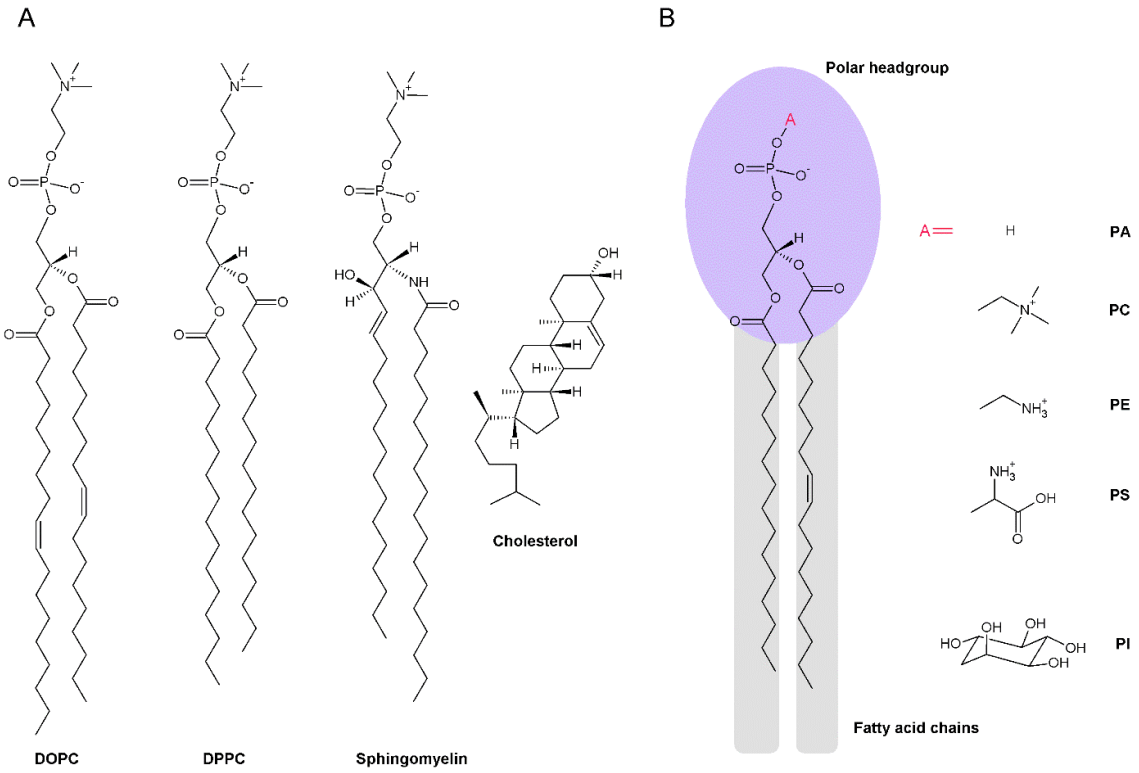

Figure 1. Examples of lipid structures. A. Structure of selected lipids: 1,2-dioleoyl-*sn*-glycero-3-phosphocholine (DOPC; unsaturated lipid) and 1,2-dipalmitoyl-*sn*-glycero-3-phosphocholine (DPPC; saturated lipid) belonging to glycerophospholipids, sphingomyelin (sphingolipid) and cholesterol (sterol). **B**. Scheme of a lipid structure (grey – apolar lipid acyl chains; violet – polar lipid headgroup) and the most frequent variants of lipid headgroups: phosphatidic acid (PA), phosphatidylcholine (PC), phosphatidylethanolamine (PE), phosphatidylserine (PS), phosphatidylinositol (PI).

2.3 Membrane proteins

Plasma membrane contains structurally diverse membrane proteins that function in a large variety of cellular processes. They are involved in metabolic enzymatic reactions, transport of molecules across the membrane and signaling events, for example, in the form of signal sensors. They are standardly divided into two groups: integral and peripheral, depending on their interaction with a membrane. Peripheral proteins are usually bound to membrane lipids or anchored to the membrane via a lipid covalently attached to their structure but typically do not penetrate into the hydrophobic part of membrane. Integral proteins are at least partly embedded in a membrane via one or more transmembrane domains (TMDs) possessing α-helical or β-sheet secondary structure. Several strands of β-sheets could be arranged to a barrel forming a transmembrane channel. β-barrels are frequent in proteins of the outer membrane of mitochondria, chloroplasts, and bacteria [10]. The majority of transmembrane proteins are spanning a membrane via a single or multiple α-helical segments. The transmembrane segments contain hydrophobic region and membrane-water interface region which matches the hydrophobic core of lipid membranes and area of lipid headgroups, respectively [11] (Figure 2). The hydrophobic core and the membrane-water interface differ in their amino acid composition.

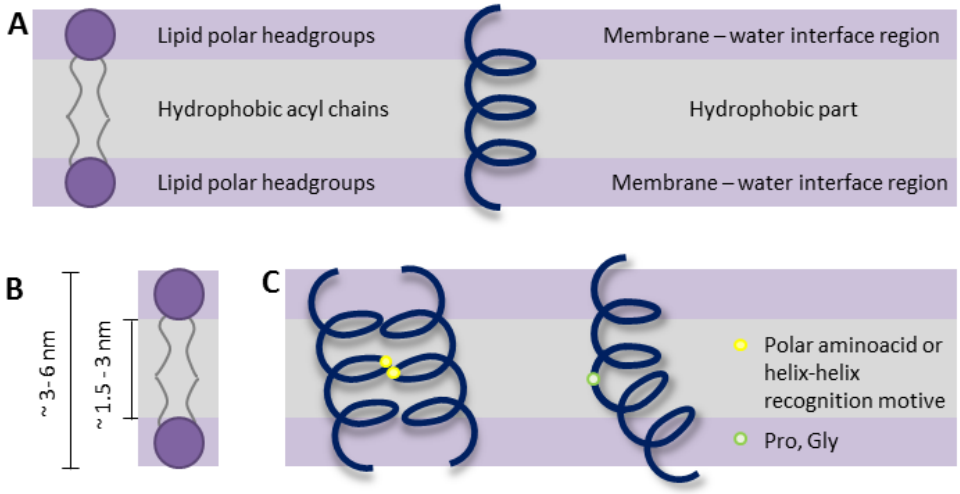

Figure 2. Schematic illustration of proteo-lipid membranes. A. Representation of polar and hydrophobic membrane environment. **B.** Typical lipid membrane dimensions. **C.** Helix-helix association and peptide kink induced by specific amino acid composition.

Hydrophobic regions of proteins are buried in the membrane core and are in direct contact with lipid acyl chains. Therefore, these regions are enriched in non-polar amino

acid residues including valine, leucine, alanine, isoleucine, and phenylalanine [12]. The presence of polar amino acid residues is less frequent and points towards a clustering of helices (Figure 2) [13]. Similarly, particular amino acid sequences, like GXXXG, were found to cause association of more helices together [13,14]. Proline and glycine residues induce kinks in a rather cylindrical α-helical structure of TMDs.

The membrane-water interface is an environment covering a zone of lipid headgroups. This is a very heterogeneous environment covering unpolar region near lipid carbonyls up to a polar part of headgroups encompassed by water molecules. The composition of the corresponding part of the transmembrane domain needs to reflect this environment. Typical is abundance of aromatic amino acids (tryptophan and tyrosine) and positively charged residues (lysine and arginine) [15,16]. The aromatic rings of the aromatic amino acids tend to bury into the hydrophobic membrane core. Similarly, the positively charged amino acids adapt to the water-lipid interface by snorkeling of their relatively long aliphatic chains into membrane hydrophobic core, while their polar functional groups form hydrogen bonds at the level of polar lipid headgroups.

Negatively charged residues also show their increased presence at flanking areas close to the transmembrane part. They are more abundant in the extracellular part of membrane compared to positively charged residues that are preferentially located on the cytosolic part of a membrane (phenomenon known as “positive inside rule”) [16]. In contrast to positively charged residues, negatively charged residues contain just a short aliphatic chain making snorkeling scarcer.

2.4 Cell membrane characteristics

Plasma membranes can be characterized by several intrinsic properties valid for all mammalian cells. Among the most important is the *fluidity of membranes* [1], which allows lateral diffusion of proteins and lipids in a membrane. This property is crucial for membrane processes such as protein cluster formation, hypothetical lipid raft formation, and is vital for dynamics of chemical and biological reactions. In addition, fluid membrane allows for molecular rotation and conformational adaptations of membrane components in the membrane plane. Lipid flip-flop and transbilayer mobility are much slower processes compared to the lateral membrane mobility and they occur very rarely

without specific mechanism allowing this process (transporters, flippasses, floppases, scramblases, etc.)

Lateral and rotational diffusion and conformational adaptation are related to the membrane lipid packing (Figure 3), which refers to the mutual orientation and arrangement of lipid molecules. The lipid packing influences mobility of individual molecules and thus the membrane fluidity. For example, lipids with longer, fully saturated acyl chains are more tightly packed compared to lipids with shorter acyl chains because of higher number of possible van der Waals interactions between neighboring chains. Such interactions restrict movement of the molecules. Similarly, presence of double bonds disturbs firm contacts between lipid acyl chains resulting in higher fluidity of membranes composed of unsaturated lipids than of saturated lipids. Cholesterol counteracts these general trends by making membranes formed of saturated lipids more fluid and *vice versa* for the membranes containing unsaturated lipids. Cells actively control fluidity by changing saturation level of lipids and the amount of cholesterol in its membranes [17,18].

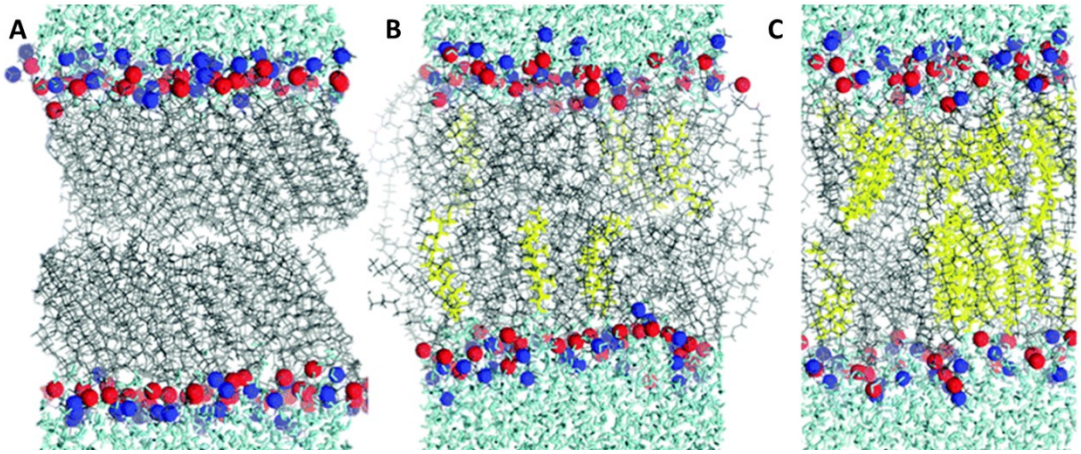

Figure 3. Lipid packing defines freedom of lipid movement. A. Tight arrangement of lipids at gel phase (see later in the text). Stretched lipid acyl chains maximize interactions between two neighboring molecules resulting in restricted lateral and rotational movement. **B.** Relaxed arrangement of lipid acyl chains in fluid membranes allowing fast lipid transfer within membrane leaflet. **C.** Ordering effect of cholesterol. The membrane maintains its fluidity but the higher level of ordering causes slower motions compared to cholesterol-free membranes. Color coding: lipid acyl chains gray, phosphates red, choline blue, cholesterol yellow, water cyan. Adopted from Drolle at al [19].

Plasma membrane is asymmetric. Lipid composition of the outer and inner membrane leaflets differs. Cytosolic leaflet is enriched in phosphatidylserines, phosphatidylethanolamines and phosphatidylinositols, extracellular leaflet contains high amounts of sphingomyelin and glycosphingolipids. The plasma membrane asymmetry is very important and its loss leads to cell death. The unbalanced distribution is allowed by the fact that the transition of lipids between leaflets is very rare and allowed only by special proteins, such as scramblases, flippases and lipid transporters. Spontaneous flip-flop of lipids to the other leaflet was observed in model membranes, but its rate depends on a size and charge of a lipid headgroup [20]. Plasma membrane is asymmetric also in having unequal ion distribution along outer and inner membrane leaflet. Ion concentration gradients form membrane potential which is vital for many cellular processes.

Inner and outer leaflets of membrane face different environment. Cytosolic parts of proteins might be temporarily attached to the membrane cytoskeleton. Such interactions support membrane structure and could cause its compartmentalization. In contrast, sugar moieties of glycosylated proteins are always oriented towards the extracellular space. The layer of sugars, attached to both proteins and lipids, is called glycocalyx and covers the whole cell surface. It serves as a protection against chemicals and is involved in cell adhesion.

Membranes are inhomogeneous. Membranes represent a rich environment full of diverse lipids and proteins that are able to reorganize into spatially heterogeneous compartments. Proteins and lipids are not ordered randomly, but can form structures or compartments, which can limit molecular mobility. For example the picket-fence model predicts compartmentalization of membrane due to the interaction of membrane proteins with cortical actin [21] (see below for more details). Another type of nanoheterogeneities was proven to exist as a result of lipid self-assemblies, lipid-protein interactions or protein clustering. To name a few examples: glycosylphosphatidylinositol anchored protein and receptor protein were found in distinct membrane nanodomains [22], multi-protein-assemblies with nano-scale internal organization were found in plasma membrane [23] and lipid nanodomain formation was induced by cross-linking of gangliosides [24]. Of note, cholesterol was crucial component for maintaining the nano-assemblies in all studies mentioned above.

2.5 Overview of membrane organization models

There is an effort to describe the membrane organization and dynamics by a proper physical model based on the aforementioned properties. Together with new discoveries on the cell membrane organization, the way it has been described by models changed. This part briefly summarizes the most notable models used for the description of cell membranes (Figure 4).

Fluid mosaic

Fluid mosaic was one of the first models used for the description of cell membrane structure and thermodynamical properties [1]. The most important assumption of the model is that the membrane is a two-dimensional oriented lipid bilayer with embedded proteins. Membrane fluidity is a critical intrinsic membrane property. According to the model, free-floating proteins in the lipid bilayer can create aggregates and inhomogeneities. From this fact, the name of the model, fluid mosaic, is derived.

Lipid rafts

This model is based on assumption that membranes are heterogeneous and there is a coexistence of two distinct environments with different lipid packing. The more ordered domains are called membrane rafts and are proposed to regulate function of several proteins [25]. Keystone Symposium on Lipid Rafts and Cell Function in 2006 brought a definition of membrane raft: "Membrane rafts are small (10–200 nm), heterogeneous, highly dynamic, sterol- and sphingolipid-enriched domains that compartmentalize cellular processes. Small rafts can sometimes be stabilized to form larger platforms through protein-protein and protein-lipid interactions." [26] It is still an open topic whether lipid rafts truly exist in cell membranes and how would they influence the membrane organization [27,28]. However, the formation of small (< 120 nm) cross-linked lipid assemblies with "raftophilic" protein enrichment in their vicinity were observed in the intact cell membranes [24].

Mattress model

Presence of transmembrane proteins directly influences lipids in their neighborhood. Lipids can, for example, adapt to the protein the presence by local thickening or thinning of a membrane. This typically happens when hydrophobic parts of proteins and lipids do not match in length, i.e. when hydrophobic mismatch occurs. Exposure of polar amino acids to hydrophobic core of lipid bilayer or contact of apolar amino acids with hydrated headgroup layer is energetically unfavorable. Membrane is expected to prevent occurrence of such situations by shortening or stretching lipid acyl chains to match the hydrophobic length of the transmembrane domain or by sorting lipids of appropriate size to the vicinity of proteins. Description of such thickening or thinning of the membrane is provided by the mattress model [29]. This model was proven to be valid for protein sorting to target membrane [30] and is also proposed to influence membrane structure on nanoscopic scale [29].

Membrane compartmentalization by cortical actin network

Cortical actin beneath the membrane forms a meshwork. Actin-binding proteins can be trapped by the meshwork, and as a result, form boundaries of a membrane compartment. The cortical acting mesh acts as a supporting structure ("fence") to the protein bodies ("pickets"). This gives name to the picket-and-fence model [31]. The size of the compartments is estimated to be up to a few hundred nanometers and varies between various cell types but also across the plasma membrane of a single cell [21]. Membrane molecules are transiently trapped inside the compartment and can cross the barrier only by the perturbation of the protein picket-fence.

The model is supported by single particle tracking experiments [31,32]. The barrier of the compartment has direct impact on mobility of both proteins and lipids. Not only does it act as an obstacle for the nanoparticle, but it also has effect similar to hydrodynamic friction [21]. The mobility is reduced in a vicinity of immobilized proteins, but in the center of compartment the diffusion is free.

Another refreshing and insightful point of view is that there is no simple universal model satisfactorily describing all aspects of membrane organization [33]. Rather, it is a result of interplay between the intrinsic and extrinsic membrane properties. However, full understanding of membrane organization is still elusive and requires more biological and biophysical studies.

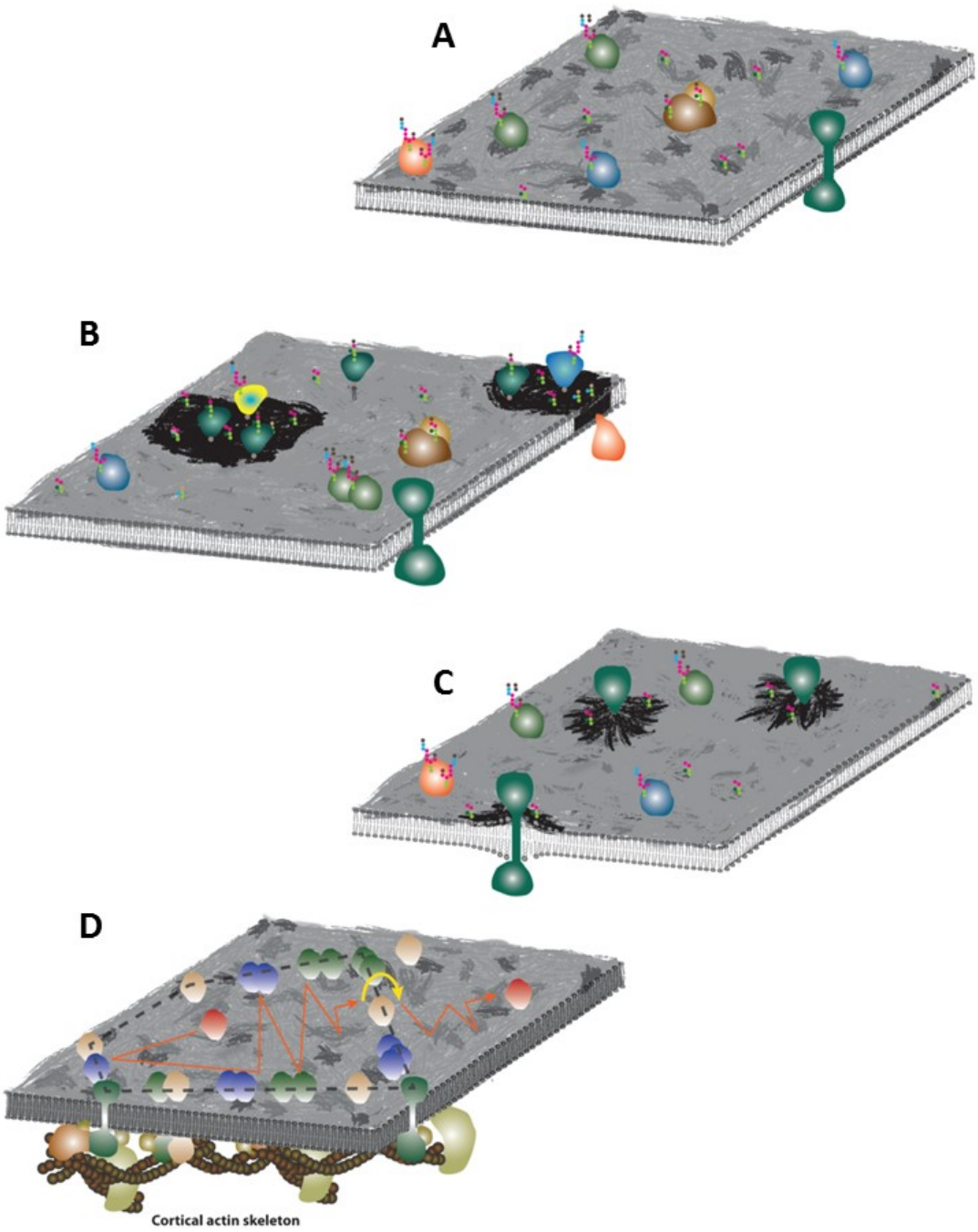

Figure 4. Illustrative representation of current models of membrane organization. A. Fluid mosaic. Membrane is a lipid bilayer with embedded proteins. All membrane components can move. **B.** Lipid rafts. Nanoheterogeneities enriched in specific membrane lipids and possibly proteins. **C.** Mattress model. Lipids adapt to the protein length to reduce hydrophobic mismatch. **D.** Picket-fence model. Membrane compartmentalize by interaction of membrane proteins with cortical actin skeleton. Adapted from [33].

2.6 Model membranes

As described in the previous chapter, cell membranes are enormously complex systems with rich diversity in lipid and protein content. Therefore, simplified systems mimicking cell membranes were introduced to study protein-lipid interactions at the molecular level and to study membrane physico-chemical properties in a controlled way. Moreover, they also enable us to understand the effect of individual parameters, such as membrane thickness, membrane fluidity, and membrane curvature on the membrane organization. A disadvantage of the model membranes is that the membrane asymmetry is difficult to maintain and that these systems lack topology of cellular membranes. Model systems are typically formed by lipid bilayers with a well-defined lipid (and protein) composition. Mostly, lipid bilayer is either encapsulated in vesicles or forming supported lipid bilayers.

Unilamellar vesicles are one of the most favorite model systems because, depending on their size, they resemble cellular membranes. These are typically prepared from a mixture of synthetic or natural lipids in defined ratios. In the presence of an aqueous solute, selected lipids spontaneously form multilamellar membranes to minimize interactions of hydrophobic acyl chains and polar water molecules. Importantly, bilayer-forming lipids are mainly those which constitute the plasma membrane of mammalian cells (e.g. phosphatidylcholines or sphingolipids). Synthetic vesicles are considered as free standing bilayers. They can be prepared in several ways depending on the desired size. Briefly, small unilamellar vesicles (SUV, < 50 nm) are prepared by the sonication of multilamellar membranes (MLV) [34], large unilamellar vesicles (LUVs, 50 – 1000 nm) are generated by the extrusion of MLV using carbonate filters with a defined size of pores [35]. Finally, electro-formation or gentle hydration are used for the preparation of giant unilamellar vesicles (GUVs, > 1000 nm) [36,37]. Small proteins and peptides can be also incorporated into lipid vesicles [36,38,39].

Lipid bilayers spread on a solid support represent another model membrane system, namely supported lipid bilayers [40]. The interaction of support and membranes reduces membrane dynamics compared to the dynamics of unattached membranes (e.g. top of GUVs) [41]. If the interaction with a support is not desirable, cushion polymers or solid spacers might be inserted to lift bilayer out of support [42]. Planar lipid bilayers free of support were also prepared by spreading the membrane over a small holes that separates the two aqueous environments (black lipid membranes [43]).

"Vesicles" and "layers" are not the only shapes that can be accomplished by mixing of lipids or proteins with lipids. There are several other model membrane systems, e.g. micelles, bicelles and nanodiscs which are composed of lipids and detergents or proteins and can be used for some specific studies of membranes and their components.

The choice of a system always depends on specific needs of the particular scientific question, i.e. a specific question requires selection of the best technique(s) in terms of geometry (e.g. whether one needs 2D or 3D setup), stability (e.g. nanodiscs are more stable than bicelles), ease of preparation (e.g. insertion of peptides and proteins) or how well the system mimics the membrane of interest (micelles generated from detergents are often insufficient). In this thesis, lipid vesicles were selected due to their stability, accessibility of membrane for imaging and possibility to incorporate transmembrane peptides in a controlled way.

Apart from the aforementioned model systems, there is an intermediate step between lipid model systems and native cellular membranes: the so-called membrane blebs. These systems better maintain a lipid and protein complexity of cell membranes but lack the cytoskeleton and cell interior. Also, in contrast to the plasma membrane, these membranes are symmetric and lack membrane potential. Membrane blebbing could be induced chemically to obtain so called Giant Plasma Membrane Vesicles (GPMVs) or by osmotic shock (cell-swelling) in the procedure called preparation of Plasma Membrane Spheres (PMS) [44,45]. The bleb isolation method influences the composition and organization of resulting spheres [46,47]. Nevertheless, these cell-derived vesicles still serve as an interesting model for the studies focused on lipid membranes and associated processes.

2.7 Phase transitions in model lipid membranes

One of the topics of this thesis is formation of nanodomains in lipid membranes. The nanodomain formation is closely related to phase transitions of lipids in membranes with various compositions. Apart from the membrane composition, temperature is an important parameter affecting the occurrence of phase transition. Phase transition temperature (Tm) defines the temperature at which lipids change their physical state from solid (gel) phase (So) characterized by the ordered and tightly packed lipids to

liquid disordered (liquid-crystalline) phase (Ld) with typically highly mobile and less ordered lipid arrangement (Figure 3). Liquid disordered phase is typically represented by phospholipids with short and/or unsaturated acyl chains which undergo phase transition at lower temperatures (e.g. -18°C for DOPC [48]). On the contrary, lipids with long saturated acyl chains have usually higher transition temperatures (e.g. 41°C for DPPC [49]) and, therefore, rigidify cellular membranes at 37°C. Addition of cholesterol counterweights these effects, membranes composed of long saturated lipids and cholesterol become more fluid and *vice versa*, unsaturated lipids membranes become more condense after cholesterol enrichment [50]. Cholesterol is also needed for a formation of so-called liquid ordered phase (Lo). The definition of Lo phase is relatively vague. This phase is typically characterized by lateral diffusion coefficients comparable to Ld phase (e.g. ~1 $\mu m^2 s^{-1}$) but a relatively high lipid packing more comparable to a So phase. For example, mixture of DPPC and cholesterol in ratio 2:1 is considered to be Lo phase at room temperature. Removal of cholesterol would rigidify the membrane and lead to formation of So phase.

In membranes formed by a mixture of lipids with different transition temperatures can lead to the separation of phases – the situation is comparable to the demixing of two (or more) liquids. At high temperatures, the liquids (resp. lipids) are miscible and form one uniform phase; decrease of temperatures causes the demixing of liquids (resp. lipids), thus the coexistence of two (or more) phases.

We were in particular interested in membranes formed of three components: low Tm and high Tm lipids and cholesterol. Depending on the temperature and concentrations of the components, only one of the phases is present, or two lipid phases coexist (typically liquid ordered phase and liquid disordered phase). The coexistence of phases in a three-component system is captured in phase diagrams (Figure 5). These are usually determined experimentally. There are different ways how to distinguish between the borders of different phases: a frequently used approach is based on fluorescence microscopy imaging of model lipid bilayers and detection of visible large scale phase separation [51]. The visibility is enabled by preferential localization of a fluorescent probe in one of the phases. Phase separated systems or systems close to phase separation are favorite objects of studies because they might help to clarify properties of lipid rafts (if they exist), and their role in membrane heterogeneities.

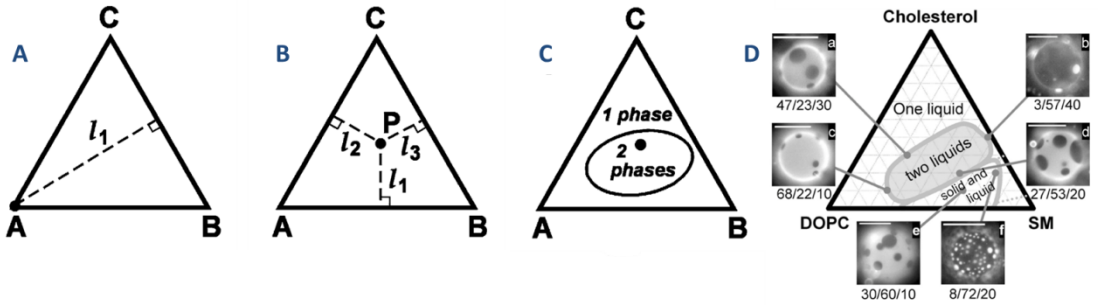

Figure 5. Representation of phase diagram of ternary lipid mixture at given temperature and pressure. A. One-component system is represented by point in a vertex of triangle, in this figure it is the vertex A. Such system contains only compound A. Molar fraction of compound A is determined by length of line l_1 perpendicular to the line segment BC. Maximal length is $l_{1,\,max} = 1$. **B.** Three component system depicted by point P. Molar fraction of compound C is determined by length of l_1 (line perpendicular to AB segment), molar fraction of compound B by length of l_2 (line perpendicular to AC segment) and molar fraction of compound A by length l_3 (line perpendicular to BC segment), where $l_1 + l_2 + l_3 = 1$. **C.** Example of ternary phase diagram providing information about expected number of phases for different ratios of lipids. For specific composition of two phases we still need information about the directions of so called tie-lines, connecting opposite areas of two-phase region. **D.** Example of phase diagram for DOPC/sphingomyelin (SM)/cholesterol system at 25°C and corresponding images of phase separated GUVs. Numbers below GUV images denote molar lipid composition. Bright parts of GUVs are enriched in DOPC, dark parts are enriched in SM and cholesterol [51]. The images were adopted from Veatch and Keller works [51,52].

2.8 Model transmembrane peptides

Similar to membranes represented by simpler lipid bilayers, protein TMDs might be mimicked by simplified synthetic peptides. Model peptides are usually chosen to be monomeric and have a simple primary structure for a better control. Hydrophobic core is usually formed by a simple sequence prevalently composed of hydrophobic residues forming the α-helix. To anchor the peptide into the membrane, hydrophobic sequence is flanked by one or two residues of tryptophan or lysine (or both) on each side of the hydrophobic core. Comparison of tryptophan and lysine amino acids located at similar positions of model peptides showed that tryptophan residue is preferentially located at the level of lipid carbonyl groups, whereas the positively charged lysine prefers negatively charged phosphate groups [53,54]. On the contrary, occurrence of less hydrophobic amino acids in transmembrane sequences (Gly, Ser) is limited due to the loss of transmembrane orientation in case of their abundance [55]. In biophysical

studies, synthetic transmembrane peptides typically employ poly-Leu or poly-Leu/Ala sequence flanked by Trp and Lys residues [55–57]. The length of model peptide is determined by the type of membrane where it should locate. Cellular membranes were shown to have different thickness; plasma membrane is thicker compared to e.g. endoplasmic reticulum or Golgi apparatus membrane [58]. Herein, we were interested in the plasma membrane organization, therefore we used model TMD with 21 hydrophobic residues. Addition of flanking residues to the hydrophobic core of a transmembrane peptide further stabilizes its orientation.

3 Fluorescence methods

Fluorescence is a type of luminescence where a photon is emitted from excited singlet state after excitation by light. It can be employed in many methods which are highly sensitive, chemically specific and compatible with living cells, which makes fluorescence methods optimal for studying biological systems. In addition to cellular structures, fluorescence has turned out to be an excellent tool to study a variety of materials and model systems; including lipid membranes. Fluorescence methods applied to model membranes allow us to visualize various aspects of membrane biophysics, such as membrane dynamics, viscosity, peptide/protein clustering, protein binding reactions and lipid phase separation. Scaling fluorescence techniques down to single molecule sensitivity allowed understanding of what is happening in a sample at molecular level.

Fluorescence measurements fall into one of two main categories: steady-state or time resolved. The steady state measurements typically consist of measuring average intensity or emission spectra over time under constant illumination. The time resolved methods detect fluorescence intensity decay after pulsed excitation. Although, the instrumentation for the time resolved techniques is more expensive and sophisticated, the extra information is valuable. For example, by the exponential fluorescence intensity decay fitting, we obtain information on the fluorescence lifetimes. The lifetimes carry information about the environment surrounding the molecule. The information is typically not available in the steady-state measurements. The following chapters present a basic introduction to time-resolved fluorescent methods relevant for this work and the essential theoretical background. First section presents a brief introduction to the types and properties of fluorescent probes. The second section describes basic principles of time-resolved methods and how they can be employed to measure specific membrane properties, e.g. lateral diffusion or formation of nanodomains. Third section describes the instrumentations and methods for sample preparation used in the thesis.

The complete theory behind the methods is complex and its mathematical description would be extensive. This work does not intend to be a fluorescence technique manual or textbook and does not cover all the details. It aims to explain basic principles and why these methods were suitable for my studies.

3.1 Fluorophores

There are several naturally occurring fluorophores, e.g. aromatic amino acids (tryptophan, phenylalanine, tyrosine), NADH, flavins, chlorophyll, and others. However the most molecules, in particular lipids and peptides lacking tryptophan, phenylalanine or tyrosine, are non-fluorescent by nature. We need to label these structures of interest by suitable fluorescent organic compounds or fluorescent proteins. Fluorescent proteins (e.g. GFP, mCherry) are frequently used in cell biology, but their size limits their use for labeling of lipids: molecular weight of GFP is about 27000 g/mol, molecular weight of DOPC lipid is 786 g/mol. Large protein weight might influence lipid properties. Also, number of photons emitted by fluorescent proteins per molecule in excited state is much lower compared to synthetic organic dyes. There is a large spectrum of commercially available small and bright synthetic dyes (Alexa, Atto, DyLight, Abberior,… dye families) typically derived from structures of well-established fluorophores such as fluorescein, rhodamine or cyanine, with improved fluorescence properties. Choice of the proper dye has to be made according to the experimental requirements, as will be discussed later in the chapter.

Membrane probes need to have a hydrophobic part in order to incorporate into the lipid membranes. One way how to achieve this is to conjugate the fluorescent moiety with a structure of interest that resides in the membrane (Figure 6). In order to label components of proteo-lipid membranes, water soluble fluorophores are covalently linked to the lipid headgroup or flanking residues of membrane peptides. Conjugation of a dye to the structure of interest is typically done by reaction of amine in the lipid headgroup (e.g. PE) with succinimidyl ester reaction group or sulfhydryl (typically in cysteine residue) with maleimide reaction group. Lipid acyl chain labeling is also an option but such lipids must be used cautiously, as certain dyes have a tendency to loop back to the water-lipid interface [59].

Another way is to synthetize a fluorescent molecule that resembles a lipid structure. The examples are BODIPY moieties attached to lipid acyl chains and lipophilic dialkylcarbocyanines (DiD, DiO, DiI, … families). These fluorescent probes typically contain hydrophobic chains (e.g. alkyl or acyl chains) which enable their incorporation into lipid membranes. Some dyes, such as perylene, are highly hydrophobic on their own and can be used as membrane markers without conjugation to additional structures (Figure 6).

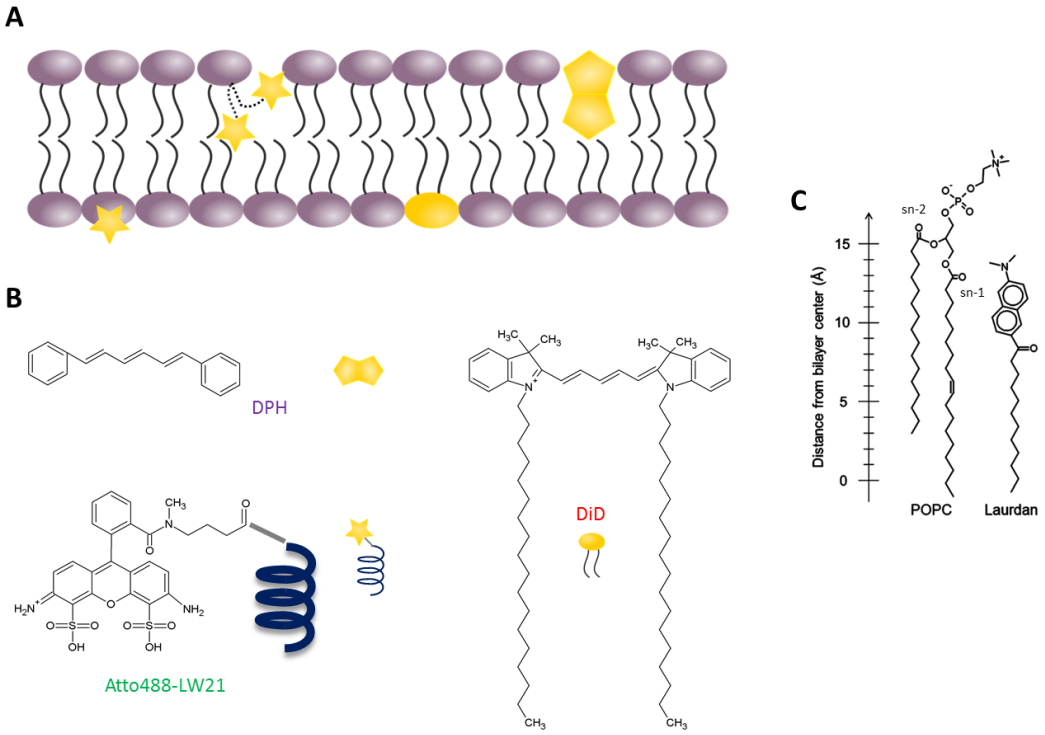

Figure 6. Schematic illustration of some fluorophores used in the thesis and their typical orientation in membranes. A. Different types of fluorophore attachments are indicated in yellow. Stars indicate headgroup or acyl chain labeling. The "yellow lipid" represents fluorescent dyes resembling a lipid structure (e.g. DiD). The two combined yellow pentagons represent a hydrophobic fluorescent probe (e.g. perylene). **B.** Chemical structures of the fluorophores used in the thesis: DPH, Atto488 covalently linked to the LW21 peptide and DiD. **C.** Structure of the Laurdan dye and its location in the membrane composed of POPC lipids. Image C was adapted from Paper III**.**

3.1.1 Selection of fluorophores for specific experiments

The proper choice of a fluorophore is affected by several factors including:

- excitation and emission spectrum
- Stokes shift (difference between excitation and emission spectrum maxima)
- average fluorescence lifetime of the excited state (characteristic time that molecule spends on average in the excited state before a photon emission occurs, typically on the order of nanoseconds)
- quantum yield (ratio of emitted photons to the number of absorbed photons)
- absorption coefficient (describes probability of photon absorption at particular wavelength)
- photobleaching (a disposition to bleaching)

Labeling by fluorescent dye can serve two purposes. One can be used to visualize particular types of molecules to observe their properties, such as protein or lipid dynamics, concentration or oligomerization state. Probes that are bright (high quantum yield, high extinction coefficient), stable and not interacting with other membrane components are required. These probes should not be influenced by changes in fluorophore's environment and should not change the properties of labeled molecules. Specific methods may have specific requirements, e.g. fluorophores with a low triplet state formation are favorable for FCS measurements, those with longer lifetimes are suitable as donors for FLIM-FRET technique, etc.

In another type of experiments, properties of membrane environment are characterized: polarity, viscosity, pH, membrane potential, topology and others. In this case, environment-sensitive membrane dyes are the fluorophores of choice. They respond to changes in the environment by adapting their spectral characteristics. There are numerous environment-sensitive fluorescent probes [60,61], for instance: i) Solvatochromic probes shift their excitation and emission spectra in response to local membrane polarity and mobility. Typical examples are the probes Laurdan or Patman exhibiting a large dipole moment change after excitation. Their emission spectra shift in response to the local membrane environment [62]. The Stokes shift increases with more polar environment and so reports on the level of membrane hydration. Kinetics of emission shift provides information on local membrane mobility. ii) Potentiometric dyes shift their spectra in response to the change in electric field across the membrane (i.e. transmembrane potential). They are used to study membrane potential or electric activity inside small cellular organelles. Fluorophores based on naphthylstyryl-pyridinium cores are examples of relatively non-toxic and fluorescent probes used to study electric activity of neural networks [63]. iii) Molecular rotors, such as substituted BODIPY based rotors [64], are sensing local membrane viscosity. Viscosity is reflected in the quantum yield and lifetime of molecular rotors. iv) Membrane topology sensing probes enable comparison of flat and curved areas. However they are mostly based on amphipathic helical peptides or BAR proteins, molecules of significant weight. Small-sized probes are still missing [60]. v) pH sensitive dyes such as fluorescein and its derivatives alter their spectra and quantum yield depending on pH [65].

Since membranes are three-dimensional structures with rapidly changing properties, the location of probes plays a crucial role in their analytical properties. A broad distribution of probe positioning along membrane normal or probe reorientation

makes data interpretation difficult or even impossible. Environment sensitive probes are potentially very useful tools for membrane studies, but as will be described in more detail in Paper I, their thorough characterization in terms of photophysics, but also membrane location, is needed before implementation in more complex systems such as cells.

3.2 Theoretical introduction to fluorescence methods

3.2.1 Time correlated single photon counting and fluorescence lifetime

Time correlated single photon counting method (TCSPC) can detect the time between pulse excitation and detection of the emitted photon (Figure 7). This directly corresponds to the time the molecule stays in the singlet excited state. In fact, the emission times are random in nature. In order to obtain statistically reliable information about the average fluorescence lifetime of the excited state, thousands of photons have to be gathered. Resulting histogram of photon arrival times is described by a mono- or multi-exponential decay. Fitting data to exponential model provides the information about lifetime of individual components τ_i and their amplitude in sample A_i.

$$I(t) = \sum_{i=1}^{n} A_i e^{-\frac{t}{\tau_i}} \quad (1)$$

Here, $I(t)$ is fluorescence intensity profile (i.e. histogram of photon arrival times). In a real experiment, the measured fluorescence decay is a convolution of an original "true" decay and the broadening in the order of tens or hundreds of picoseconds. This broadening is called Instrument Response Function (IRF) and it is caused by limitations of the electronics, mainly by non-zero temporal response of detectors and non-zero laser pulse width. IRF affects the shape of the original decay especially at short decay times. Its time profile can be measured on a sample with zero lifetime (typically a solution of scattering particles). A reconstruction of the original decay is possible by an iterative reconvolution method [66]. An alternative way is to study events only on the longer timescale by excluding the IRF time window (a tail-fitting approach).

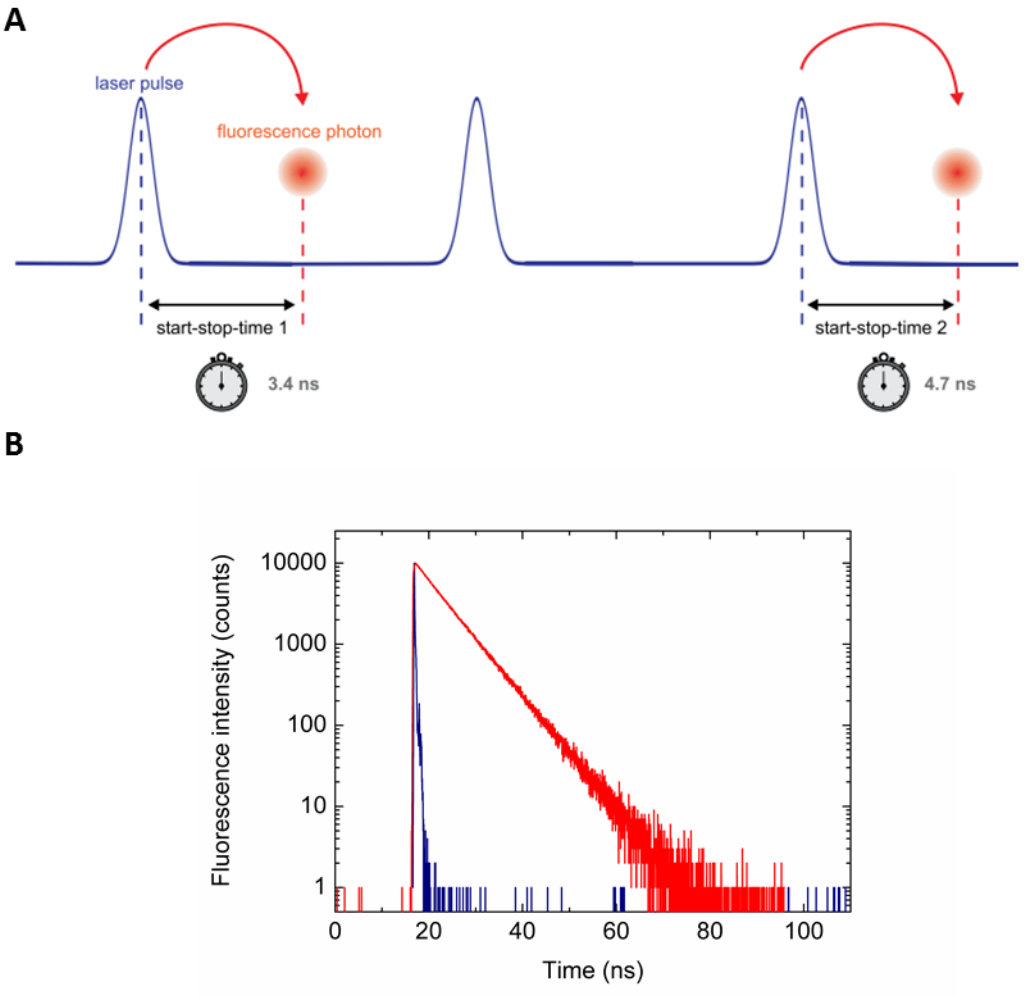

Figure 7. Principle of TCSPC method A. A measurement of time interval between the laser pulse and the photon detection by TCSPC (adopted from Wahl [67]). **B.** An example of photon arrival time histogram of a fluorescent dye (red) and IRF (blue).

3.2.2 Fluorescence lifetime imaging microscopy

Many fluorescence methods, which do not use time-resolved information in their basic setup, can be extended by a TCSPC unit. This is true for both spectroscopy- and microscopy-based methods. For example, a confocal microscope can be extended by TCSPC unit required for Fluorescence Lifetime Imaging Microscopy technique (FLIM). FLIM is capable of measurements of fluorophores' excited state lifetimes for individual pixels of an image. Every detected photon contains the information about its arrival time in respect to its excitation pulse in addition to other parameters such as the location in an image area, wavelength (if more spectral channels are recorded) and time from the

beginning of the experiment. By gathering thousands of photons in every pixel, a lifetime image can be obtained.

Lifetime image calculation and analysis can be performed in several ways, making a compromise between computational demands and accuracy of obtained lifetime information. The most computationally demanding but a very precise method of analysis is iterative reconvolution and fitting of intensity decays to a multi-exponential model for every pixel of an image. Disadvantage of such arrangement is that we need to acquire large amounts of photons, which prolongs the measurement and frequently leads to sample photobleaching. Sometimes, we do not require such detailed description. Information about relative differences in lifetime could also be sufficient. In such cases, we can use the phasor-plot analysis or average lifetime calculation.

Calculation of average lifetime for every pixel is the fastest way how to obtain lifetime image. Average lifetime of the excited state $< \tau >$ is obtained by integration of number of photons over time:

$$< \tau >= \frac{\int_0^\infty tI(t)dt}{\int_0^\infty \mathrm{I(t)dt}} \tag{2}$$

This approach quickly provides lifetime distribution in the image. However, the information about number of components and corresponding individual lifetimes is missing.

Alternative approach is to perform phasor plot analysis which provides not only the lifetime distribution in the image, but also the information whether the intensity decays in image pixels are mono- or multi-exponential [68]. During the phasor-plot analysis, the phasor plot is constructed (Figure 8). For every pixel, fluorescence intensity profile $\mathrm{I(t)}$ is constructed based on the number of photons observed in time t. Then, phasor coordinates g and s in every pixel [i, j] are calculated according to equations

$$g_{i,j}(\omega) = \frac{\int_0^\infty I_{i,j}\,(t)\cos(\omega t)\,dt}{\int_0^\infty I_{i,j}\,(t)dt} \tag{3}$$

$$s_{i,j}(\omega) = \frac{\int_0^\infty I_{i,j}\,(t)\sin(\omega t)\,dt}{\int_0^\infty I_{i,j}\,(t)dt} \tag{4}$$

where ω is laser repetition angular frequency.

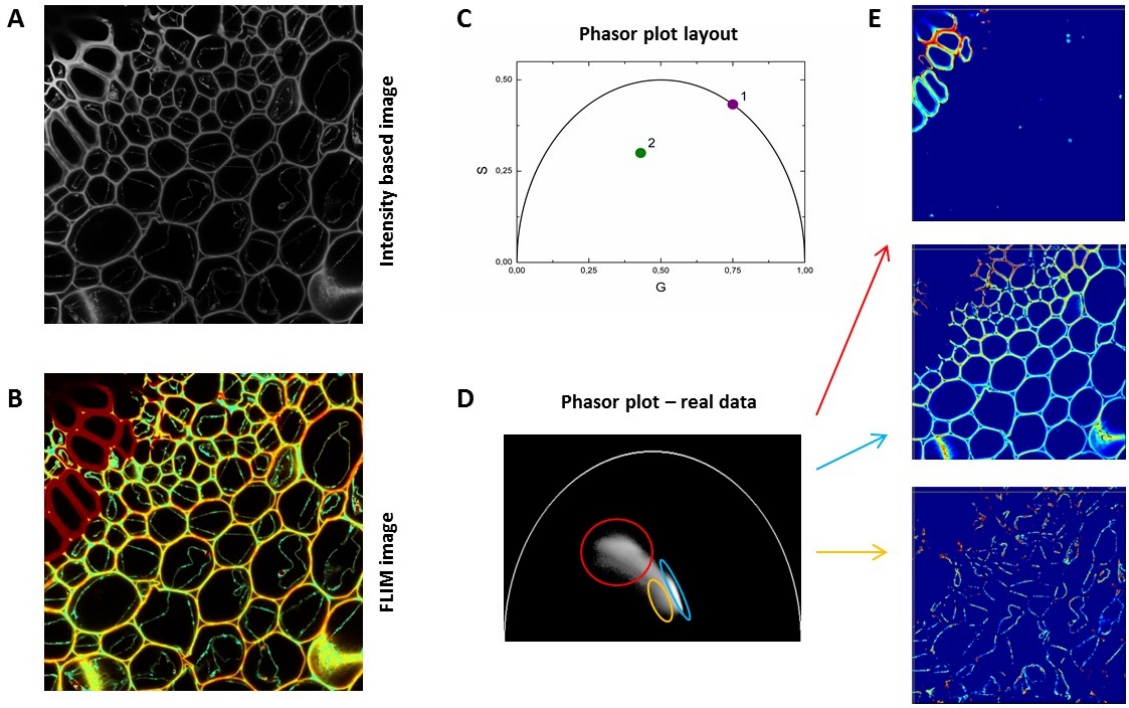

Figure 8. FLIM – Phasor plot representation. Left side: An example showing intensity (**A**) and lifetime distribution (**B**) on 2D image of convallaria. The middle part depicts a phasor plot. The "Phasor plot layout" (**C**) represents schematic phasor plot. It consists of semicircle on which single-exponential decays are localized. Point 1 (purple) represents signal from a probe with mono-exponential decay present on FLIM image. Point 2 (green) represents signal with more complex (multi-exponential) decay. "Phasor plot-real data" (**D**) represents phasor plot calculated from the image on the left. All data are in the multi-exponential region of the plot and they form groups according to the detailed dynamics of their decay in individual image pixels. Application of filter masks on the phasor plot is demonstrated on figures on the right (**E**). The images are reconstructed according to the mask from the red (right top), blue (right middle) and yellow (right bottom) regions of the phasor plot.

Interpretation of the phasor plot allows recognition whether the decay is single- or multi-exponential and allows selecting photons corresponding to certain lifetime distribution. In particular, contribution of single-exponential decay will appear on the so-called universal circle, which has diameter 1 and center [0.5, 0] in the *g*, *s* coordinates of the phasor plot. Contribution of the multi-exponential decay lies inside the circle. Phasor plot from an experiment typically forms a two-dimensional spectrum with well-localized peaks. By choosing photons from the surroundings of a particular peak in the phasor plot, we can set up a filter mask according to which only areas containing molecules with particular decay characteristics are displayed in the resulting FLIM image.

The main advantage of measuring time resolved decays is that fluorescence lifetime is characteristic for individual fluorophores and for the environment they encounter. The fluorescence lifetime of some fluorophores is affected by local pH, temperature, viscosity, but typically not by the local concentration of fluorophores. Thus, such fluorophores can be used as sensors of their local environment. The fluorescence lifetime further allows distinction between background noise or autofluorescence and specific fluorescence signal based on differences between fluorescence decay patterns. Fluorescence lifetime of a fluorophore is also affected by the presence of other de-excitation processes, such as quenching or energy transfer. This way, the presence of another molecule (a quencher or acceptor) in close proximity of the fluorophore can be monitored (e.g. FLIM-FRET, see below).

3.2.3 Fluorescence correlation spectroscopy

Fluorescence correlation spectroscopy (FCS) is a technique which allows detection of highly mobile fluorescent species in a sample and characterization of their translational and rotational diffusion, local concentration, binding constants, molecular weights or photodynamics [69,70]. The most common use of FCS is to measure the translational diffusion, on which we will focus in the further text. FCS is based on analysis of fluorescence intensity fluctuations in time. The fluctuations are caused by a passage of fluorescent molecules through the confocal detection volume. As a fluorescent molecule enters the illuminated volume, it gets excited and emits fluorescence. The burst of photons caused by a repeated excitation and emission of a molecule moving through the detection volume will be displayed as a peak in a recorded intensity time trace. Analysis of the number of peaks and their duration provides information about the concentration and mobility of labeled particles (Figure 9A).

The detection sensitivity has to be high enough to detect photon bursts from individual particles and the ratio of signal from the individual fluorescent bursts to average fluorescence intensity should be high enough to provide a good contrast. This implies that only a low number of particles can be present in the detection volume simultaneously. To match this requirement, nanomolar concentrations of fluorescent probes are used; typically 1-10 molecules in a femtoliter confocal detection volume. The analysis of fluorescence fluctuations is based on calculation and fit of the autocorrelation function $G(\tau)$.

$$G(\tau) = \frac{\langle F(t) \cdot F(t+\tau) \rangle}{\langle F(t) \rangle^2} = 1 + \frac{\langle \delta F(t) \cdot \delta F(t+\tau) \rangle}{\langle F(t) \rangle^2} \quad (5)$$

$$\delta F(t) = F(t) - \langle F(t) \rangle \quad (6)$$

$$\langle F(t) \rangle = \frac{1}{T} \int_0^T F(t) dt \quad (7)$$

where F(t) is fluorescence intensity in time t, δF(t) is fluorescence intensity fluctuation, $\langle F(t) \rangle$ is average fluorescence intensity over total time T, and τ is the so-called lag time. Autocorrelation function describes self-similarity of a signal. It can be interpreted as the probability with which we detect the fluorescence at time t+τ provided we detected signal at time t. G(τ) decays with increasing τ. The magnitude of autocorrelation function is inversely related to the average number of particles present in a detection volume, PN:

$$PN = \frac{1}{G(0)} \quad (8)$$

The full width at half maximum of the autocorrelation function describes characteristic decay time (diffusion time), τ_D, the molecule spends in the detection volume. Fluorescence intensity involved in calculation of the correlation function depends on concentration of the fluorophore, its brightness, geometry of the detection volume and detection efficiency of the optical system. To obtain concrete mathematical model for the fluorescence intensity and thus the autocorrelation function, a priori knowledge of the system has to be applied. In particular, the shape of the detection volume has to be known, and processes that cause fluorescence fluctuations [71,72] have to be described mathematically. The processes are in particular: translational diffusion of molecules through the detection volume, photophysical or photochemical phenomena such as intersystem crossing to non-fluorescent triplet state or cis-trans isomerization, molecular rotation and photobleaching.

Models to fit the autocorrelation function

Translational diffusion is the dominant contribution to the fluorescence intensity fluctuations in point confocal measurement. Free diffusion of fluorescent molecule in solution in a 3D Gaussian detection volume is described by autocorrelation function $G_{3D}(\tau)$:

$$G_{3D}(\tau) = 1 + \frac{1}{PN}(1 + \frac{\tau}{\tau_D})^{-1}(1 + \frac{\tau}{\tau_D SP^2})^{-1/2} \quad (9)$$

where τ_D is the characteristic diffusion time and SP is structural parameter describing the ratio of axial and lateral detection volume width w_z and w_0 ($SP = w_z/w_0$, see Figure 9A).

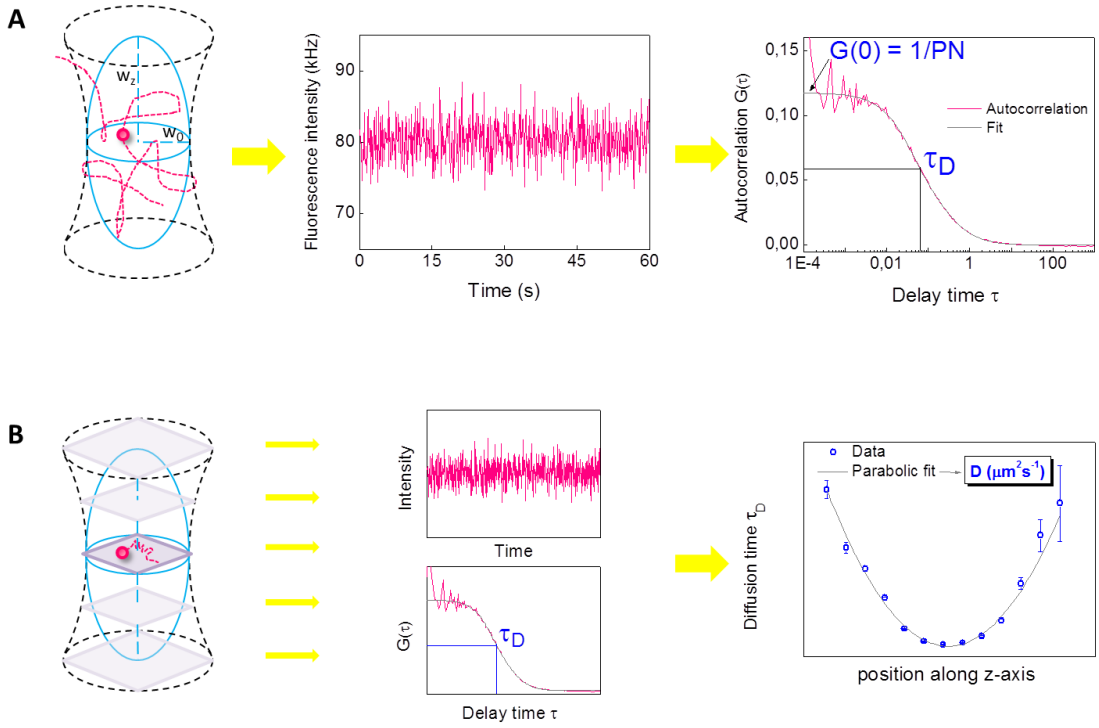

Figure 9. FCS measurement of fluorescent particles in solution and in membrane by FCS technique. A. Diffusion of a particle in solution. Fluorescence intensity of fluorescent molecules moving in and out of the detection volume is recorded and correlated to yield the autocorrelation function. Fit of the autocorrelation curve with an appropriate model provide information about the diffusion time and the average number of particles. If the size of the detection volume is known, particle concentration and diffusion coefficient can be determined. **B.** Diffusion of a particle in membrane measured by z-scan FCS technique. In z-scan FCS, membrane is placed in several positions along the z-axis in regular intervals. In every z-position, intensity time trace is recorded, autocorrelation curve is calculated and fitted to get a parabolic dependence of both diffusion time (and particle number) on z-position. Fitting the data to a parabolic dependence described by equation (13) directly provides the diffusion coefficient D and the radius of the detection volume w_0 without the need of an external calibration.

In membranes, molecules are free to move only in a 2D plane, therefore, a different model has to be applied. It can be obtained from $G_{3D}(\tau)$ in limit $SP \to \infty$. The limit corresponds to the situation, when the detection volume is infinite along the z-axis. Then, the fluorophores cannot leave the detection volume along the z-axis and only their x,y coordinates can cause fluorescence fluctuations. The autocorrelation function yields

$$G_{2D}(\tau) = 1 + \frac{1}{PN}(1 + \frac{\tau}{\tau_D})^{-1} \tag{10}$$

Moreover, virtually all fluorophores used in our experiments undergo triplet state transitions. This is an additional source of fluorescence fluctuations, which has to be included into the model. Thus, the resulting autocorrelation function $G_{2DTr}(\tau)$ yields

$$G_{2DTr}(\tau) = 1 + \left[1 - T + Texp\left(^{-\tau}/_{\tau_r}\right)\right]\frac{1}{PN(1-T)}\frac{1}{1 + \frac{\tau}{\tau_D}} \tag{11}$$

where T is the fraction of molecules in triplet state and τ_r the relaxation time of intersystem crossing. T and τ_r are additional parameters of the model whose values have to be obtained by fitting the data.

In a more complex case, a fraction of a probe is freely diffusing in a solution (FR_{3D}) and some other fraction is embedded in a membrane (FR_{2D}). Assuming that both fractions have the same brightness, autocorrelation function is then described by [73]:

$$G_{3D2DTr}(\tau) = 1 + \left[1 - T + Texp\left(^{-\tau}/_{\tau_r}\right)\right]\frac{1}{PN(1-T)}\left[\frac{FR_{2D}}{1 + \frac{\tau}{\tau_{2D}}} + \frac{FR_{3D}}{1 + \frac{\tau}{\tau_{3D}}} \cdot \frac{1}{(1 + \frac{\tau}{\tau_{3D} \cdot SP^2})^{1/2}}\right] \tag{12}$$

By fitting the autocorrelation curves to the mentioned models we obtain several parameters, among those a characteristic number of particles PN in the detection volume and the diffusion time τ_D. Transformation of τ_D and PN into absolute parameters (diffusion coefficient D and particle concentration c) requires the knowledge of detection volume size (radii of detection volume w_0 and w_z):

$$D = \frac{w_0^2}{4\tau_D} \tag{13}$$

$$c = \frac{PN}{\pi^{3/2} SP w_0^3} \tag{14}$$

Theoretically, w_0 or SP can be obtained by measuring a reference dye of known diffusion coefficient. In praxis, several experimental pitfalls, such as optical saturation of sample, incorrect cover glass thickness correction or misaligned pinhole position, need to be controlled to get reliable size of the detection volume [74]. Moreover, w_0 determination is a critical parameter for planar systems. Lipid bilayers are only few nanometers thick (4-5 nm), compared to the size of the detection volume ($w_z \sim 1\mu m$). The diameter of the bilayer crossing the confocal volume depends on its z-position along the optical axis. The membrane positioning based on maximal fluorescence intensity along membrane normal might lead to w_0 overestimation [75]. To overcome these difficulties, several calibration-free techniques focusing on membrane diffusion were developed, e.g. z-scan FCS, 2-foci FCS or scanning FCS. In the following text, I will focus in particular on the z-scan FCS method, since this method was used in my experiments because of its robustness and availability in our laboratory.

z-scan FCS

z-scan FCS is a calibration-free method developed for measurements of lateral diffusion coefficients and average concentrations of fluorescent particles in lipid membranes [75]. Using z-scan FCS, radius of detection volume w_0 can be determined. The method is based on a set of point-scanning FCS measurements in defined intervals along the z-axis (Figure 9B). In every z-position, fluorescence intensity fluctuations are recorded, autocorrelation curve calculated and fitted to a suitable diffusion model which provides the diffusion time and the particle number. The dependence of τ_D and PN on z-position is parabolic:

$$\tau_D = \frac{w_0^2}{4D}\left(1 + \frac{\lambda^2 \Delta z^2}{\pi^2 n^2 w_0^4}\right) \tag{15}$$

$$PN = \pi c w_0^2 \left(1 + \frac{\lambda^2 \Delta z^2}{\pi^2 n^2 w_0^4}\right) \tag{16}$$

where λ is the excitation wavelength, $\Delta z = z_0 - z$ is the distance between the sample position z_0 and the position z of the focal plane, n is the refractive index of the medium. Fitting of τ_D and PN sets to these models directly provides D, c and w_0.

Anomalous diffusion

Studying of fluorophore diffusion in membranes provides a means to directly observe membrane structure. Crowded environment makes some parts of the membrane unavailable, which changes the diffusion behavior, leading to anomalous diffusion. A free lateral diffusion in planar systems is described as:

$$\langle r^2(t)\rangle = 4Dt \tag{17}$$

where $\langle r^2(t)\rangle$ is mean square displacement, D is the diffusion coefficient and t time. This equation describes mobility of freely diffusing molecules. Crowded environment slows down the diffusion and changes the power law in the diffusion equation to:

$$\langle r^2(t)\rangle = 4Dt^{\alpha} \tag{18}$$

where α is the so-called anomalous coefficient. For $0 < \alpha < 1$ the diffusion is considered as anomalous, for $\alpha = 1$ the diffusion is free. The non-linear dependence of the mean square displacement on time can be caused by several effects, for example by presence of immobile obstacles. Anomalous diffusion was observed e.g. for molecules in the cytoplasm or proteins temporarily attached to cytoskeleton. The mathematical expression for the autocorrelation function in the case of anomalous diffusion has to be modified:

$$G_{2DTrAnomalous}(\tau) = 1 + [1 - T + Texp(^{-\tau}/_{\tau_r})]\frac{1}{PN(1-T)}\frac{1}{1+(\frac{\tau}{\tau_D})^{\alpha}} \tag{19}$$

Cross-correlation function

Until now, we considered only one species of mobile fluorescently-labeled molecules and acquisition of a signal in one spectral channel. However, frequently we want to study two kinds of fluorescent molecules. In such cases, not only the autocorrelation for each fluorophore species can be analyzed, but also cross-correlation between the two species, which gave name to Fluorescent cross-correlation spectroscopy (FCCS). By the analysis of the cross-correlation curve, we can deduce whether the two fluorophore

species move independently, or together. The latter case is an indication of binding (or colocalization) between the two molecules.

Signal of two mobile molecules labeled with fluorophores of non-overlapping spectra (e.g. green and red) can be simultaneously registered. Fluorescence traces yield the cross-correlation function defined as

$$G_{RG}(\tau) = \frac{\langle F_R(t) \cdot F_G(t+\tau) \rangle}{\langle F_R(t) \rangle \cdot \langle F_G(t) \rangle} = 1 + \frac{\langle \delta F_R(t) \cdot \delta F_G(t+\tau) \rangle}{\langle F_R(t) \rangle \cdot \langle F_G(t) \rangle} \tag{20}$$

where F_R and F_G is the fluorescence intensity of red-labeled and green-labeled molecules respectively. If the green-labeled and red-labeled molecule species move independently, the cross-correlation is zero. In the other words, non-zero cross-correlation indicates partial or complete co-diffusion of the two species that can be interpreted as co-assembly or interaction of studied molecules. A fraction of co-diffusing green- and red-labeled species can be calculated from the amplitudes of the correlation curves at time zero:

$$\frac{c_{RG}}{c_{RG} + c_R} = \frac{G_{RG}(0)}{G_G(0)} \tag{21}$$

$$\frac{c_{RG}}{c_{RG} + c_G} = \frac{G_{RG}(0)}{G_R(0)} \tag{22}$$

where c_{RG} is the concentration of the co-diffusing green- and red-labeled species, c_G resp. c_R are the concentrations of unbound molecules labeled with green resp. red dye.

Application of time-resolved information for FCS/FCCS analysis

Original variants of FCS technique did not make use of time-resolved information provided by the knowledge of photon arrival time after pulse excitation. However, the time resolved information might be utilized by calculating the probability with which the photon originated from our molecule of interest [76]. Such statistical photon filtering enables us to separate fluorescence signal from the background noise or to distinguish two fluorophores with overlapping emission spectra but different excited state lifetimes. The incorporation of fluorophore lifetime patterns into FCS analysis leads to Fluorescence Lifetime Correlation Spectroscopy (FLCS) [77]. In this work,

FLCS technique was used rarely; all the detected photons were mostly considered as equal.

Comparison of FCS and FRAP

The following key advancements in technology were necessary to enable the FCS technique: detectors with a single molecule sensitivity and low noise, stable sources of light, bright and stable fluorescent dyes and confocal microscopy setup [78]. Before FCS became available, another fluorescence technique, FRAP, was used to study membrane dynamics [79,80]. It is therefore useful to write a few words on the comparison of the two methods. In FRAP, a small area of defined size and shape (typically a circle with maximally few micrometers in diameter) is photobleached by a high laser power. Consequently, a fluorescence intensity recovery, (mainly) by diffusion of fluorophores to the bleached space, is monitored with a low excitation light. A fit of the measured recovery curve provides information about diffusion coefficient of fluorescent molecules and the fractions of mobile and immobile particles.

FRAP and FCS can be considered as complementary methods. Added value of FRAP is the information about a fraction of immobile particles which is not readily available in FCS. Also, FRAP can be measured for densely labeled samples and provides information from a larger area compared to the introduced point scanning FCS approach. FRAP data acquisition is relatively fast compared to FCS, however quantitative determination of diffusion coefficients is less precise [81]. For the correct diffusion coefficient determination, both methods require a priori knowledge of the system – what type of motion the molecules are supposed to undergo, the probability of binding, differences in brightness and mobilities of the tested compounds, etc.

3.2.4 Time dependent fluorescent shift

Time dependent fluorescent shift (TDFS) is a technique enabling characterization of mobility and hydration levels of lipid membranes. It is based on a cuvette measurement of fluorescent decays of selected probes in a range of wavelengths covering probe's emission spectrum and subsequent conversion of these decays into time resolved emission spectra (TRES). TRES display the shift of emission maxima with time. The

kinetics and extent of the shift provide information about local membrane polarity and mobility.

To explain the principle of this method we shall carefully investigate Jablonski diagram (Figure 10). Absorption of light excites the molecule into the excited electronic state. Following internal conversion and vibrational relaxation cause relaxation of excited state to the lowest vibrational level of the first electronic state from which photon emission might occur (a basic principle of fluorescence). Relaxation to the lower energy state is reflected in red shifted emission of the probe compared to the excitation spectrum. The extent of the red shift is influenced by several factors, for instance solvent polarity, internal charge transfer, conformation changes or interaction with other molecules [66]. TDFS studies the effect of solvent polarity and mobility on the shift of the emission spectra.

According to the Frank-Condon principle, the electronic state excitation and the related changes in the electron charge density is much faster in comparison with movement of nuclei of molecules in the solvent. This means that the probe's charge distribution, described by a dipole moment, undergoes an ultrafast reorganization after the excitation. Consequently, surrounding polar solvent molecules redistribute towards the new energy minimum (relaxed state) to lower the energy of the excited state. This phenomenon is called time dependent fluorescence shift or solvent relaxation (Figure 10). In order to measure this process, solvent relaxation has to occur on a time scale comparable to the lifetime of the fluorescent molecules, typically in nanoseconds [62]. This is fulfilled for probes located in lipid membranes where the reorientation of solvent molecules is hindered. Solvent relaxation of polar probes in bulk water solution is typically much faster (picosecond time scale) [82,83], fluorescence from the fully relaxed excited state is detected there.

TRES can be used for determination of viscosity and polarity of the environment of the fluorescent probe. This is possible due to the fact that the rate of solvent reorientation depends on the viscosity of the sample – the reorientation of a more viscous solvent is slower. If the reorganization is slower in comparison to the fluorescence lifetime, only partial reorientation of the solvent occurs. The Stokes shift increases with solvent polarity, which allows detection of the solvent polarity by the TRES method.

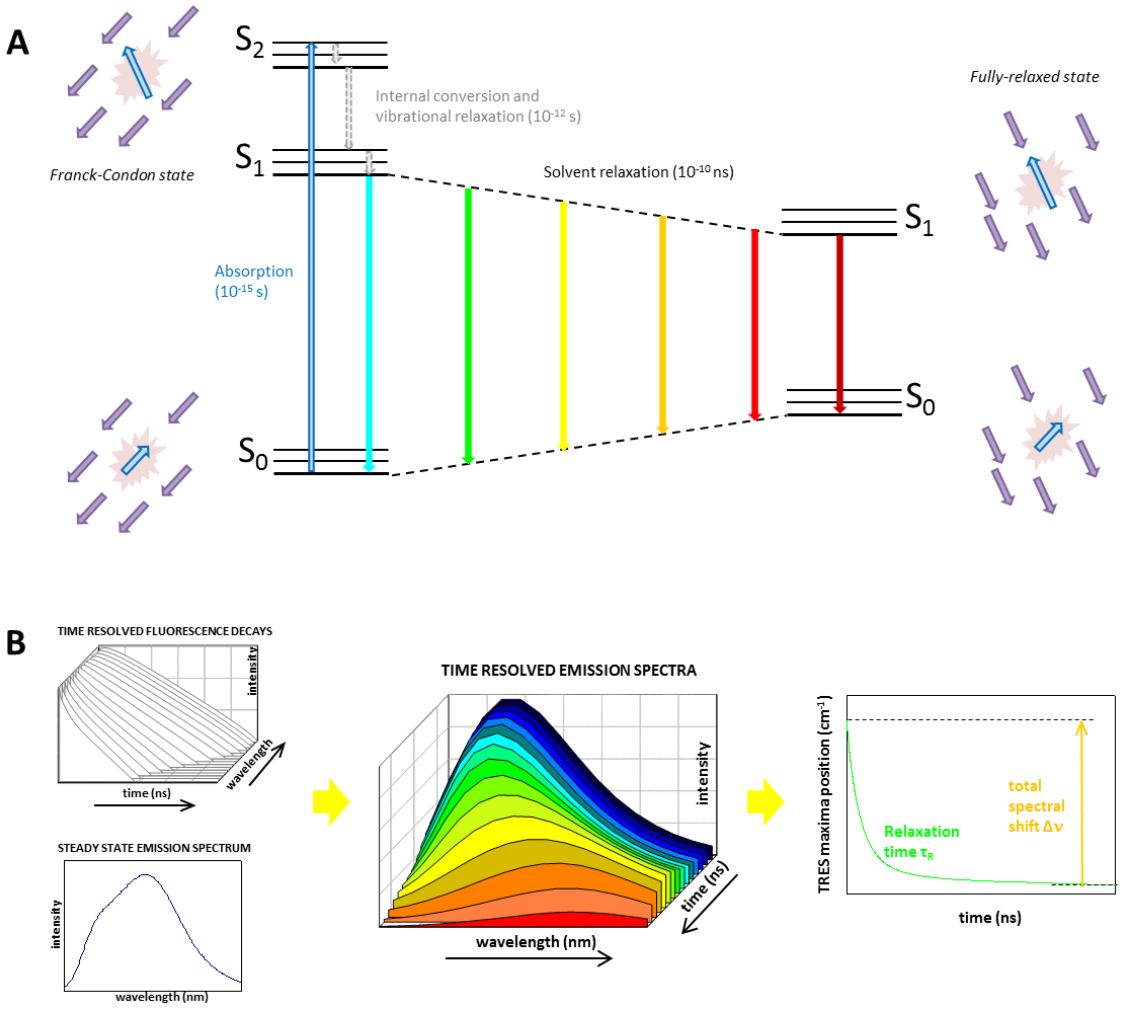

Figure 10. Illustration of time dependent fluorescent shift method – the principle and workflow. **A.** Jablonski diagram. After photon absorption, the molecule (pink spot) is excited into higher electronic singlet state. Fast non-radiative internal conversion and vibrational relaxation to the lowest vibrational level of the first excited electronic state quickly follows. From this state the molecule can emit photon (fluorescence), return non-radiatively to the ground state (not shown) or undergo intersystem crossing from excited singlet state to triplet state (not shown). The photon absorption is accompanied by enlargement of the molecule dipole moment (blue arrow located on the pink spot). According to Franck-Condon principle, response of the nuclei to electron density shift is slow and surrounding molecules of solvent (violet arrows) gradually adapt to the new situation. By their reorientation the system relaxes to the new energy minimum of the first electronic excited state (fully relaxed state). The solvent relaxation is accompanied by red-shift of fluorescence. **B.** TDFS measurement and the analysis workflow. Steady state emission spectrum and time resolved fluorescence decays measured at emission wavelengths covering the emission spectrum are required for time resolved emission spectra reconstruction. The extent and kinetics of TRES maxima shift then provides information about local polarity and viscosity.

Measuring TRES

Solvent relaxation causes red shift of emission spectra. Recording TRES spectra demonstrates such process. Direct measurement of TRES spectra is not practical, since it would require to measure full spectra for hundreds or thousands time points with picosecond resolution. The experimental approach used in praxis is based on measuring a set of fluorescent decays at various emission wavelengths D(t, λ) spanning the steady state emission spectrum of tested probes. Every decay is fitted to a sum of exponentials by an iterative reconvolution technique. The obtained parameters describe the decay shape. Parameterized decays are then normalized to the intensity of steady-state spectra at a chosen wavelength $S_0(\lambda)$. Time-resolved emission spectra S(λ,t) are then obtained by reading the values of normalized decays at specific time moments t as described by the equation:

$$S(\lambda, t) = \frac{D(t, \lambda) \cdot S_0(\lambda)}{\int_0^\infty D(t, \lambda) dt} \tag{23}$$

Analysis of time-resolved spectra provides two parameters: Total amount of fluorescence shift Δν and relaxation time τ_R. The total amount of fluorescence shift is described as a difference of spectral maxima:

$$\Delta\nu = \nu(0) - \nu(\infty) \tag{24}$$

where ν(0) is wavenumber of the initial non-relaxed (Frank-Condon) state at time t=0, ν(∞) is wavenumber of the fully relaxed state. Δν is directly related to the solvent polarity [83].

The relaxation time τ_R describes the kinetics of the solvent relaxation and is defined as

$$\tau_R = \int_0^\infty \frac{\nu(t) - \nu(\infty)}{\Delta\nu} dt \tag{25}$$

The relaxation time measures how long the solvent reorientation takes. In the context of lipid membranes, polar entities that react to changes in the probe dipole moment are water molecules that are non-covalently bound to the lipid headgroups. The solvent relaxation time of Laurdan (6-lauroyl-2-dimethylaminonaphthalene), a popular

solvatochromic probe, corresponds then to the time needed for the water molecules to rearrange [62]. Slower solvent relaxation time thus indicates reduced mobility of water molecules, which theoretically corresponds either to stronger bonding of water molecules or tighter packing of the lipid molecules.

Solvent polarity

Solvent polarity is one of the solvent properties directly experimentally accessible via TDFS technique. In the following text, more detailed description is provided. A polar solvent consists of numerous permanent dipole moments. As the charge distribution in a fluorescence molecule changes upon the excitation, the dipole moments orient along the new electric field lines which lowers the solvent energy and causes spectral shift. The described process corresponds to a dipole-dipole interaction.

Another mechanism of solvent polarization is caused by polarizability of solvent molecules. During such process, solvent molecules obtain dipole moments proportional to the local electric field of the fluorescent probe. This again leads to the lowering of energy and spectral shift.

Both mechanisms described above influence solvent polarity. There are several other phenomena contributing to the complex interplay between the solvent and the molecule, including polarizability of the molecule, solvent Stark effect, dispersion and molecule transient dipole moments [84].

In the context of fluorescent probes in lipid bilayers, the solvent polarity is frequently used to detect membrane hydration. As already mentioned, one of the most frequently used probes is Laurdan. It is stably located near the carbonyl group (*sn*-1) of phospholipids (Figure 6). This part of the membrane is intensively occupied by water molecules. The local polarity measured via Laurdan in simple lipid membranes is then related to the level of hydration of carbonyl groups in the vicinity of the probe and their propensity to move.

Generalized polarization

Simplified approach to Laurdan data acquisition and analysis utilizes dependence of Laurdan emission and excitation spectrum on the environment polarity and viscosity. Laurdan shows two distinctive emission maxima, 440 and 490 nm (excitation at 373 nm), when located in liquid-ordered resp. liquid-disordered lipid phase.

Comparison of fluorescence intensities at the mentioned emission wavelengths, I_{440} and I_{490}, provides information about Laurdan's environment. So called generalized polarization GP was introduced by Parasassi et al. [85] and is defined as

$$GP = \frac{I_{440} - I_{490}}{I_{440} + I_{490}} \tag{26}$$

Because of its simplicity, GP is frequently employed for the description of membrane order and hydration instead of calculating $\Delta\nu$ and τ_R. Because of reducing two different parameters into one, such data need to be interpreted with caution. GP values in model lipid membranes refer more on local micro-viscosity than hydration (Amaro et al. [82], Paper III).

3.2.5 Anisotropy

Anisotropy measurement is a technique based on comparison of fluorescence intensities at different polarization. It provides information about the orientation of the probe and its reorientation kinetics, which is directly related to the rotational freedom of the fluorophore. After excitation with polarized light, the emission is also polarized. If not embedded in a rigid medium, fluorophores rotate, which leads to emission light depolarization in time. Characteristic time of the depolarization caused by probe rotation is related to the size of the labeled molecule and viscosity of the environment.

The depolarization progress is obtained by measuring time-resolved anisotropy. During such measurement, the sample is excited by vertically polarized light. The emission is detected through emission polarizer placed in two orientations - vertical and horizontal. Time resolved fluorescence anisotropy decays r(t) are obtained as

$$r(t) = \frac{I_{VV}(t) - G \cdot I_{VH}(t)}{I_{VV}(t) + 2 \cdot G \cdot I_{VH}(t)} \tag{27}$$

where I_{VV} is the fluorescence decay measured with vertical orientations of excitation and emission polarizers and I_{VH} with excitation polarizer oriented vertically and emission polarizer horizontally. G is G-factor for the correction of unequal transmission efficiency of differently polarized light.

Anisotropy decays exponentially

$$r(t) = \sum_j r_{0_j} e^{-t/\varphi_j} \tag{28}$$

where $r_0 = \sum_j r_{0_j}$ is the limiting anisotropy and ϕ_j is the rotational correlation time for *j*-th component. Further analysis of rotational correlation time provides information on molecular weight and hydrodynamic radius of the rotating molecule [66]. In order to detect changes in fluorescence anisotropy, average rotational time must be on a similar timescale as the probe's fluorescent lifetime τ. If the reorientation of molecules is too slow compared to the fluorescence lifetime, we will not see any changes in anisotropy in time. On the other hand, if the reorientation of the molecules is too fast, the information about the depolarization dynamics will not be captured at the available resolution and only the average polarization will be observed.

If the probe is located in the lipid membrane, its orientation is limited by the surrounding molecules. For this reason, there is a significant direction in which the molecules tend to orient. As a result, we do not observe full depolarization, as in the case of molecules in bulk liquid. Molecular rotation might be hindered by obstacles. Then the mono-exponential anisotropy decay is given by

$$r(t) = r_\infty + (r(0) - r_\infty) \exp\left(-t/\varphi\right), \tag{29}$$

where r_∞ is residual anisotropy. This is a typical situation for DPH probe in membranes. DPH anisotropy is described by wobble-in-cone model [86,87], where DPH represents a rod wobbling in a cone with half-angle θ. Probe motion is characterized by the diffusion constant of the wobbling, dynamic parameter describing the acyl chain mobility in the perpendicular direction to the long molecular axis, and by order parameter S

$$S = \sqrt{\frac{r_\infty}{r_0}} = \frac{1}{2}\cos\theta(1 + \cos\theta) \tag{30}$$

describing the orientation constraint formed by neighboring acyl chains. Order parameter is frequently used to characterize lipid packing in membrane. The more fluid the membrane is, the lower the order parameter is.

3.2.6 Förster resonance energy transfer

Förster resonance energy transfer (FRET) enables to detect whether two fluorophores (called donor and acceptor) are in the vicinity of each other (typically <10 nm). The distance between labeled structures can indicate their interaction or colocalization at nanoscale. FRET is non-radiative energy transfer between a donor and an acceptor which occurs when acceptor molecule is in proximity of donor, donor and acceptor are in favorable mutual orientation, donor emission spectra and acceptor excitation spectra overlap and the numbers of donors and acceptors in the illuminated area are comparable, as reviewed in Piston et al. [88]. During FRET, the donor molecule returns to the electronic ground state without photon emission and the acceptor gets to the excited state and might fluoresce. The rate of energy transfer k_{FRET} is

$$k_{FRET} = \frac{1}{\tau_D}\left(\frac{R_0}{r}\right)^6 \tag{31}$$

where τ_D is the decay time of the donor in the absence of acceptor, and r is the distance between the donor and the acceptor. Förster radius, R_0, is a parameter specific for the donor-acceptor pair and describes the distance at which FRET efficiency is 50% (i.e. $k_{FRET} = \tau_D^{-1}$). FRET efficiency E is given by

$$E = \frac{k_{FRET}}{k_{FRET} + {}^1/_{\tau_D}} = \frac{R_0^6}{R_0^6 + r^6} \tag{32}$$

Thus, FRET efficiency is strongly influenced by the donor-to-acceptor distance. Förster radius can be calculated if the information about the donor emission spectrum $F_D(\lambda)$, acceptor extinction coefficient ε_A, mutual relative orientation of the donor and the acceptor transition dipoles κ^2, donor quantum yield Q_D and refractive index of the medium n are known;

$$R_0 = \frac{9000(\ln 10)\kappa^2 Q_D}{128\pi^5 N_{Av} n^4} \int_0^\infty F_D(\lambda)\varepsilon_A(\lambda)\,\lambda^4 d\lambda \tag{33}$$

where N_{av} is Avogadro's number. FRET efficiency quantification is typically based on two approaches: 1) fluorescence intensity and 2) fluorescence lifetime measurement (called FLIM-FRET for experiments performed on microscopes).

Intensity based approach compares fluorescence intensities in the donor and the acceptor channels while exciting the donor only. If FRET occurs, the intensity in the acceptor channel increases and simultaneously intensity in the donor channel decreases. Although the idea is straightforward, a practical realization is often complicated by spectral properties of the donor and the acceptor. Moreover, the steady state approach lacks the ability to distinguish between specific distribution of donor and acceptor pairs. A detected low average FRET efficiency might be caused by longer distances between the donors and the acceptors as well as by low abundance of complete FRET pairs or low acceptor concentrations.

FLIM-FRET is the excited state lifetime based FRET that monitors changes in donor excited state lifetime in the presence and the absence of an acceptor. If FRET occurs, the donor returns to the ground state without a photon emission causing reduction of donor excited state lifetime. Comparison of the donor fluorescence lifetime in the presence and the absence of an acceptor provides information about the FRET efficiency $E_{FLIM\text{-}FRET}$.

$$E_{FLIM-FRET} = 1 - \frac{\tau_{DA}}{\tau_D} \tag{34}$$

where τ_{DA} resp. τ_D is donor lifetime in the presence, resp. the absence of the an acceptor. If the decay of the donor is not mono-exponential, then τ_{DA} resp. τ_D mean amplitude weighted average lifetimes described by:

$$\tau_{amp} = \frac{\sum_i A_i \tau_i}{\sum_i A_i} \tag{35}$$

where A_i are the amplitudes obtained from exponential fits (as described by equation (1)) and τ_i are corresponding lifetimes. The main advantage of the lifetime based approach is that it is not prone to spectral and concentration artifacts. In addition, by analysis of the donor decay we are able to distinguish whether all FRET pairs are separated by long distance or only a subset of donors have an acceptor in the vicinity. In the first case, the donor decay would be mono-exponential; in the latter case the decay would be at least bi-exponential. Therefore, in this study FRET was preferentially measured by FLIM-FRET technique.

3.2.7 Homo-FRET

Energy transfer might occur between two different molecules or between chemically identical molecules. The approaches how to detect the energy transfer between two different molecules, hetero-FRET, were described in the previous chapter. FRET between chemically identical molecules, donor-donor energy migration process or homo-FRET, is not detectable by changes in spectral or excited state lifetime properties of the sample. However, FRET depolarizes emission (Figure 11). The way how to detect the energy transfer between chemically identical molecules, is to follow the fluorescence anisotropy decay. In homo-FRET, the energy transfer might occur (once or multiple times) when one molecule is excited by polarized light which leads to photon emission from another molecule in close proximity. As the second molecule can be nearly randomly oriented in respect to the first molecule, the information about the original polarization of photons is lost. Energy transfer between two identical molecules results in a faster decay rate of anisotropy and is described by another decay component in addition to the molecular rotation in anisotropy decay. Because of diverse orientations of molecules and rotational motions, more spatial positions of emission dipole moment are covered reducing residual anisotropy (compared to the situation in the absence of transfer). Homo-FRET can typically occur for probes with small Stokes shift. As described above, homo-FRET is a tool for the detection of e.g. protein oligomerization. In this work, homo-transfer was used to investigate formation of peptide dimers or higher oligomers.

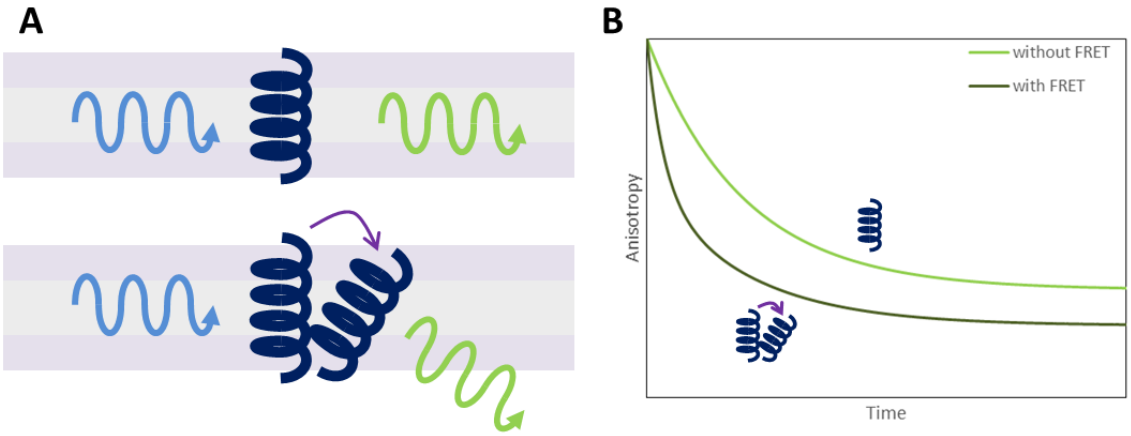

Figure 11. Simplified depiction of homo-FRET process. A. Blue, resp. green wave indicates the direction of excitation resp. emission light propagation. Energy transfer from a molecule to the chemically identical adjacent molecule is typically accompanied by depolarization of emission. **B.** Comparison of the two time-resolved anisotropy decays in the presence and absence of homo-FRET. Energy transfer is manifested by another decay component of the time-resolved anisotropy decay.

3.2.8 Quenching

Non-radiative energy transfer is one of the processes that reduce the fluorescence intensity of fluorophores. Generally, such processes are called quenching and are divided into two groups: dynamic and static quenching. Dynamic quenching can happen for example via collision between a fluorophore in the excited state and a quencher (energy transfer or charge transfer). Dynamic quenching is described by the Stern–Volmer equation:

$$\frac{F_0}{F} = 1 + K_D \cdot [Q] \tag{36}$$

where F_0 and F are fluorescence intensities in the absence and presence of a quencher, respectively, K_D is the Stern–Volmer quenching constant, and [Q] is the concentration of a quencher in the sample. Typical quenchers are oxygen, acrylamide, heavy atoms and others. Dynamic quenching reduces the excited state lifetime. It becomes more effective at higher temperatures because of increased collision rates.

Static quenching is described by formation of non-fluorescent complexes between fluorophore and quencher. Such formation happens in fluorophore ground state meaning that measured excited state lifetime of uncomplexed molecules is not changed. Increased temperature typically causes dissociation of formed complexes leading to the reduction of static quenching.

3.2.9 How to measure membrane viscosity

The aforementioned fluorescence methods are often used to probe dynamics and organization of both cellular and model lipid membranes. In this work, we aimed to utilize directly measured parameters, such as diffusion coefficient, fluorophore lifetime and order parameter, to explore physical properties of tested membranes with a focus on viscosity. In this section, we aim to clarify the terms membrane viscosity and fluidity and introduce several models connecting the membrane viscosity to the mentioned measurable parameters.

Viscosity is a macroscopic parameter describing frictional resistance of a fluid to flow. Viscosity was first described by Newton "as the proportionality factor between the velocity gradient dv/dx in the direction perpendicular to the flow direction (shear rate) and the force per unit area F/S required to maintain the flow (shear stress)" [84]. Importantly, viscosity is defined for bulk fluids. Its meaning in nanoscopic systems, such as lipid membranes, is not precisely defined and should be used with care ([84], Paper I). The term 'membrane viscosity' is frequently used in studies of mobility of membrane molecules. The more mobile the molecules are, the less viscous the membranes are. Viscosity is inversely proportional to fluidity, a term that is also connected with mobility of membrane components. Membrane mobility is typically expressed in terms of lateral diffusivity of membrane molecules. Another modified term related to viscosity is microviscosity that describes mobility of specific functional groups of the membrane molecules. This term is frequently used in TDFS studies. Other usage of the term membrane viscosity is in studies of lipid packing, which is typically investigated by measurements of rotational diffusion or employment of molecular rotors. More details about lateral and rotational diffusion and viscosity-sensing probes and their relation to membrane viscosity follow.

Rotational diffusion

Rotational diffusion describes the freedom of a molecule to rotate and is directly related to lipid packing. Rotational diffusion coefficients of probes in membranes are obtainable by time-resolved polarization measurement. The assumption is that higher values of the rotational coefficient imply a lower membrane viscosity and *vice versa*. In the literature, diphenylhexatriene (DPH) is a commonly used fluorescent probe for

viscosity measurements providing information about acyl chain mobility and acyl chain arrangement.

Lateral diffusion

Lateral diffusion describes the planar (2D) mobility of membrane components. The measurements typically provide one or more of interrelated parameters (equation (17)): diffusion coefficient, mean square displacement and characteristic time that molecules spend within a specific area. Variants of FCS, FRAP and single particle tracking are frequently used methods for diffusion measurement.

There are two main models describing diffusion of membrane components which take into account the size of the diffusing molecule compared to a solvent [89]. In case of membranes, solvent is formed by bulk lipids in a lipid bilayer. When a moving molecule has a size comparable to the lipids, free area theory [90] is applicable. This theory describes molecular diffusion as a two-dimensional random walk, where a molecule moves to a free area devoid of other molecules. The movement to a free area happens only if the moving molecule has a certain activation energy required for overcoming the frictional coupling between diffusing molecules and lipids [91]. In addition to the activation energy, the diffusion coefficient depends on the free area size, the area per diffusing molecule and temperature. This model predicts the same diffusion coefficients for all molecules of a comparable size.

The second case is applicable when a diffusing molecule is larger than surrounding lipids. This theory is frequently used for description of protein diffusion in membranes and was introduced by Saffman and Delbrück (SD model) [92]. Their theory describes diffusion of a cylinder (protein) in an infinite plane sheet of a viscous fluid (lipids, viscosity μ) surrounded by infinite regions of less viscous liquid (water or buffer, μ'). The SD model predicts a logarithmic dependence of the diffusion coefficient D on protein radius R.

$$D = \frac{k_B T}{4\pi\mu h}\left(ln\frac{\mu h}{\mu' R} - \gamma\right) \tag{37}$$

where k_B is Boltzmann constant, T is temperature, h is the thickness of the bilayer and γ is Euler's constant. *The Saffman-Delbrück model* relates the membrane viscosity to diffusion coefficient of large objects in the membrane and was confirmed by several experimental studies of proteins embedded in lipid membranes. [93,94].

Viscosity-sensitive probes

Another approach to determine viscosity of membranes is to employ environment-sensitive dyes such as molecular rotors or solvatochromic dyes. Solvatochromic fluorescent dyes report on the time required for solvent relaxation which is connected to the viscosity of the solvent. Fluorescent molecular rotors were designed to provide the most direct measurement of membrane viscosity as the rotor's quantum yield Φ (and excited state lifetime τ) directly correlates with solvent viscosity μ (Förster–Hoffmann equation) [95].

$$\Phi = z\mu^{\alpha} \quad \text{or} \quad \tau = zk_r^{-1}\mu^{\alpha} \tag{38}$$

where z and α are constants and k_r is the radiative decay constant. However, a study of physical properties of molecular rotors in bulk fluids showed that molecular rotors report more on solvent porosity than its viscosity [96]. More detailed characterization of these probes is needed to understand which property is sensed by these probes (Paper I).

3.2.10 How to measure clustering of membrane components

The resolution of standard optical microscopes does not allow observing small molecular assemblies. However, fluorescent methods mentioned above can provide information on the proximity of two compounds even in case a direct visualization of a structure is unreachable. FRET is a technique which is used to study proximity of two molecules. FRET occurs only over short distances (typically < 10 nm) because of the sixth power dependence of the transfer efficiency on the distance. Such a short distance typically ensures reliable information about the closeness of two molecules. FRET does not indicate only the proximity of molecules, it can uncover their segregation. For example, in a lipid membrane containing both donors and acceptors, segregation of donors from acceptors would be indicated by a lower FRET efficiency compared to the random distribution of the two molecular species.

Two-color FCCS is another type of method that provides information about clustering by positive cross-correlation between two species labeled with spectrally different probes. It is worth mentioning that a simple point scanning single-color FCS is unable to distinguish between monomers and dimers or other small oligomers due to a

weak dependence of the diffusion coefficient on cluster radius (SD model). Therefore, FCCS is a valuable alternative.

Mentioned approaches were used in this thesis, but they represent only a fraction of methods that are used to detect formation of clusters. For example, fluorescence antibunching, a version of FCS method, is able to determine the number of fluorophores in a cluster [97]. Similar information can be obtained with TOCCSL method (Thinning Out Clusters while Conserving the Stoichiometry of Labeling [98]).

3.3 Experimental procedures

3.3.1 Instrumentation

Time-resolved confocal fluorescence microscope Microtime 200

FCS, FLIM, FLIM-FRET and other time-resolved microscopy experiments were performed on an inverted confocal fluorescence microscope, Olympus IX71 (Olympus, Hamburg, Germany), equipped with single-photon counting unit MicroTime 200 (PicoQuant, Berlin, Germany). Fiber coupled pulsed laser diodes (405, 470, 532, 640 nm) illuminated a sample through the water-immersion objective (1.2 NA, 60x; Olympus). In experiments with two-channel acquisition, the lasers were pulsing in alternating mode in order to avoid artifacts caused by signal bleed-through. Fluorescence signal was gathered through the main dichroic mirror and (typically) 50 μm pinhole and guided to the emission dichroic mirror which splits the signal between the two single photon avalanche diodes using band pass filters. The specific selection of filters depended on spectral properties of the used dyes. In case of anisotropy experiments, polarizer and polarizing beamsplitter were part of the optical setup. All measurements were performed at room temperature.

FCS correlations curves (Papers II, IV) were calculated and fitted to different models (equations (5)-(19)) by in-house routine implemented in OriginPro 8 (OriginLab Corporation, Massachusetts, USA, http://www.originlab.com/). A fitting procedure is described in works of Benda et al. [75,77]. Similarly, diffusion coefficient and surface concentration was obtained by fitting the parameters (diffusion times or particle numbers at various z-positions) to equations (15) and (16). Fluorescence decays obtained by FLIM(-FRET) technique (Paper I, II) were fitted by tail fitting approach in Symphotime (PicoQuant, Germany, https://www.picoquant.com/) or analyzed by phasor

plot approach by in-house routine implemented in Matlab (MathWorks, Massachusetts, USA, www.mathworks.com). FLIM-FRET donor decays were further fitted to Baumann-Fayer model [99] by my colleague Radek Šachl to obtain distances between donors and acceptors in membrane and used for Monte Carlo simulations to calculate size of nanodomains (Paper II). Matlab routine for the analysis of anisotropy ASCII images (Paper I), written by Piotr Jurkiewicz, can be found in Supplementary Information of Paper I
(http://www.rsc.org/suppdata/cp/c4/c4cp00888j/c4cp00888j2.pdf).

Time resolved fluorescence spectrometer IBH 5000 U

Time resolved fluorescence decays for TDFS and time resolved anisotropy decays were recorded by IBH 5000 U SPC equipment (IBH, Glasgow, UK) using a picosecond diode laser and Hamamatsu R3809U-50 microchannel plate photomultiplier. Fluorescence decays for TDFS method were recorded at series of wavelengths spanning the steady-state emission spectrum of used fluorescent probe in 10 nm steps. To eliminate scattered light, an appropriate cut-off filter was applied. The signal was kept below 2% of the light source repetition rate, and the data were typically collected in 8192 channels (0.014 ns per channel) until the peak value reached required number of counts (typically 5000 photon counts for Laurdan TDFS measurements). In case of anisotropy measurements, linear polarizers were inserted into the optical path. The temperature was maintained by using a water-circulating thermostat. IRF of instrument was measured on highly scattering suspension of colloidal silica in water (Ludox, Sigma Aldrich).

Fluorescence decays of Laurdan (Papers III and IV) were fitted to three-exponential model by iterative reconvolution method in IBH DAS 6 software (IBH, UK). Parameters obtained from fluorescence decay fitting and steady state emission spectra were employed to reconstruct TRES by in-house routine implemented in Matlab. Fitting of DPH time resolved anisotropy decays (Paper IV) was performed in FluoFit v.4.5 (PicoQuant, Germany).

Fluorolog-3 spectrofluorimeter

Steady-state fluorescence excitation and emission spectra were recorded using Fluorolog-3 spectrofluorimeter (model FL3-11, JobinYvon Inc., Edison, NJ, USA)

equipped with a Xenon-arc lamp. Temperature was maintained using a water-circulating thermostat.

3.3.2 Sample preparation

LUV preparation

For vesicle preparation, lipids were dissolved in chloroform, fluorescent probes in methanol and peptides in 2,2,2-trifluoroethanol. Lipids, fluorescent probes and peptides were mixed to a desired ratio in a glass tube. Organic solvents were evaporated under a stream of nitrogen while continuously incubated in a water bath (ambient temperature) and then kept under vacuum for at least 1 hour. The dry lipid film was hydrated in heated buffer (typically to 40°C) and vortexed for 5 minutes. Buffer used in Paper II was 10 mM HEPES buffer (pH = 7.4, 150 mM NaCl); 100 mM phosphate buffer of pH 8, 4.5 or 7.4 in Paper III and 105 mOsm/kg glucose buffer (40°C,~75 mM glucose, 10 mM HEPES, 10 mM NaCl and pH = 7.4) in Paper IV. The cycles of heating and vortexing were repeated until the lipids and peptides were resuspended in the solution. The detachment of peptides and lipids from the surface could be facilitated by addition of clean glass beads (2 mm in diameter) into the tube. LUVs were obtained by extrusion of lipid and peptide suspension through a polycarbonate membrane with a typical effective pore diameter of 100 nm (Avestin, Ottawa, Canada) by 51 passages at ambient temperature.

GUV preparation – electroformation

GUVs were prepared in analogy to LUVs by mixing lipids, peptides and probes in a desired ratio in a glass vial (2 ml). Altogether 100 nmol of all species were mixed. 2 mol% biotinylated-DPPE was always included for the immobilization of vesicles at the BSA-biotin/streptavidin-coated glass coverslips. Glass coverslips were coated freshly before the adding of GUVs. The coating comprised of 15 minutes incubation with 200 μl of 0.1 mg/ml BSA-biotin solution, washing the chamber with water, 15 minutes incubation with 200 μl of 20 μg/ml streptavidin solution and final washing. GUVs were prepared by electroformation according to Stockl and co-workers [100]. Lipids, peptides and fluorescent probes in organic solvents were spread on two preheated titanium slides. The slides were kept for 1 hour under vacuum to evaporate any residual solvent. The slides were then stuck together by melting Parafilm. The

formed chamber was filled with 105 mOsm/kg sucrose in water and heated to 40°C. The process of vesicle formation was induced by applying a sinusoidal altering voltage (10 Hz) starting at 150 mV (peak-to-peak amplitude) and gradually increasing every 2.5 min with a step of 50 mV up to 1.1 V; this voltage was kept for another 100 minutes. At the end, a frequency of 4 Hz and voltage of 1.3 V were applied for 30 minutes for the detachment of vesicles. Prepared GUVs were transferred into a LabTek 8-well chamber slide (ThermoScientific, Waltham, USA) coated with BSA-biotin/streptavidin (see above). Landing of GUVs on the optical surface was enabled by changing the buffer in the chamber for 105 mOsm/kg glucose buffer. The glucose buffer had the same osmolality as sucrose buffer but higher density and was composed of (approximately) 75 mM glucose solution, 10 mM HEPES, 10 mM NaCl; pH = 7.4. Within one hour, GUVs were firmly attached to the coated glass surface and ready for imaging. This method was set up in our laboratory during the second year of my Ph.D. studies. Before, the gentle hydration described in the following chapter was used. The electroformation method was preferred to gentle hydration because of higher yields of formed vesicles.

GUV preparation – gentle hydration

GUVs were prepared by a gentle hydration approach described by Akahashi and co-workers [37]. 1 mL of lipid mixture in chloroform containing 1 mg of lipids was dried with a rotary evaporator and kept for an additional 2 h under vacuum. Thin lipid film was hydrated with 3 mL of prewarmed buffer (10 mM HEPES, 150 mM NaCl, 1 mM $CaCl_2$, 0.1 M sucrose, pH 7) saturated with nitrogen. The tube was then sealed, heated to 60°C, kept overnight at this temperature, and slowly cooled. White cloud containing liposomes was gently vortexed before further use. All the prepared lipid mixtures contained 5 mol% of DOPG, negatively charged lipid necessary for the given preparation technique and 4 mol% of biotinyl Cap PE necessary for attaching GUVs to BSA-biotin/streptavidin-coated glass. The measurements on GUVs prepared by gentle hydration method were performed in a FCS2 chamber (Bioptechs, Butler, PA). The chamber with a coated coverslip was filled up with 200 μL of buffer solution (10 mM HEPES, 150 mM NaCl, 1 mM $CaCl_2$, 0.1 M glucose, pH 7), 20 μL of the solution containing GUVs was added and after 30 min when enough liposomes were attached to the coverslip, the chamber was carefully flushed with the excess of buffer solution.

Chemicals and peptides

All chemicals and organic solvents were purchased from Sigma-Aldrich and Merck, or otherwise stated. All lipids were purchased from Avanti Polar Lipids, Inc. (Alabaster, AL) or otherwise stated. The headgroup labeled phospholipid N-(4,4-difluoro-5,7-dimethyl-4-bora-3a,4a-diaza-s-indacene-3-propionyl)-1,2-dihexadecanoyl-sn-glycero-3-phosphoethanolamine (BODIPY FL DHPE), Alexa Fluor 488 C5 maleimide (Alexa 488), DiIC18 (5)-DS (DiD), Alexa Fluor 488 and Alexa Fluor 647-labeled CTxB, 6-lauroyl-2-dimethylaminonaphthalene (Laurdan) were ordered from Invitrogen (Carlsbad, CA); streptavidin from IBA (Goettingen, Germany); 2,2,2-trifluoroethanol (TFE) from Alfa Aesar (Karlsruhe, Germany), acrylamide from Fluka (Switzerland); 1,6-diphenyl-1,3,5-hexatriene (DPH), arachidonic acid, biotin-labeled bovine serum albumin (biotin-BSA), and CTxB were purchased from Sigma-Aldrich; Atto488 maleimide and Atto633 NHS-ester from Atto-Tec (Siegen, Germany). Atto633-DOPE was prepared in our laboratory by coupling of Atto633 NHS ester to the amine of DOPE followed by size-exclusion chromatography.

Peptide LW21 (MW 4119, GLLDSKKWWLLLLLLLLALLLLLLLLWWKKFSRS), its fluorescently labeled variant Atto488-LW21 (MW 4933, Atto488-CGLLDSKKWWLLLLLLLLALLLLLLLLWWKKFSRS) and LAT peptide (MW 3236, EEAILVPSVLGLLLLPILAMALSVHSHR) were custom synthesized by VIDIA (Prague, Czech Republic). The identity and purity of the products (> 92% for batches used in Paper IV, ~ 80% for batches used in Paper III) were confirmed by mass spectrometry and analytical HPLC performed by Ján Sabó (Faculty of Science, Charles University) and Petr Novák (Institute of Microbiology of the CAS). The sequence of LW21 peptide contains 21 hydrophobic residues flanked by two lysine residues of the original LW peptide [57] and a native sequence of the N- and C-terminal membrane proximal motifs from human TCRζ (five N- and four C-terminal residues). Similarly, LAT peptide contains all residues of putative TMD of human LAT protein flanked by the membrane proximal motif (three N- and four C-terminal residues). Solutions of 100 μM LW21, 100 μM C_2-LW21, 1 μM Atto488-LW21 and 86 μM LAT peptides were freshly prepared in TFE for each experiment. Dimeric peptide C_2-LW21 (MW 8579, $(CGLLDPKKWWLLLLLLLLALLLLLLLLWWKKFSRS)_2$; Biomatik, Wilmington, USA) was obtained by cysteine oxidation of monomeric peptide. The efficiency of dimerization (> 95%) was confirmed by mass spectrometry and HPLC.

Peptides alamethicin (MW 1964, UPUAUAQUVUGLUPVUUEQF, where U stands for α-methylalanine), magainin 2 (MW 2467, GIGKFLHSAKKFGKAFVGEIMNS) and synthetic melittin (MW 2845, GIGAVLKVLTTGLPALISWIKRKRQQ) were purchased from Sigma-Aldrich. The peptide LAH_4 (MW 2777, KKALLALALHHLAHLALHLALALKKA) was synthetized in the laboratory of Prof. Burkhard Bechinger (RMN et Biophysique des Membranes, Institut de Chimie, Universite de Strasbourg, France). The identity and purity of the product (> 90%) was confirmed by MALDI mass spectrometry and analytical HPLC.

4 Aims of the study

The aim of my work summarized in this thesis was to advance our understanding of biophysical processes regulating organization of biological membranes. Detailed data are available on how, for example, lipid composition, temperature and surrounding environment influence membrane properties in the absence of proteins. Much less is known about membranes containing one or more species of proteins. Therefore, we have developed a model system in which protein and lipid properties can be easily studied, and used the obtained results for better understanding of more complex systems, such as living cells. The focus was on the effect of transmembrane peptides on lipid membranes. The experiments summarized in the following part cover three areas:

1) Development of new fluorescent probes sensitive to membrane environment serving as a tool for characterization of membrane properties (Paper I)
2) Selection of the most suitable lipid environment for the studies of transmembrane peptides (Paper II).
3) Biophysical characterization of model membranes containing transmembrane peptides (Papers III and IV).

5 Experimental part

The experimental part is based on four papers – three were published in impacted journals, the fourth one was deposited on BioRxiv and is submitted to the impacted journal at the time of the thesis submission. The papers are enclosed to this thesis as Appendix. The text is divided into four freely linked chapters containing motivation for individual topics, summary of the most important results and discussion. The main attention is paid to results relevant to the overall scope of the thesis. Materials and Method section is described in Chapter 3.3 and in enclosed papers.

Paper I

5.1 Characterization of molecular rotors based on boron dipyrromethene (BODIPY) dyes

Motivation and introduction of BODIPY-based molecular rotors

Studies of membrane properties focus on characterization of mutual interactions of molecules of interest but also on understanding of the environment in which the interactions occur. Fluorescence molecular sensors are frequently used for membrane environment testing due to their sensitivity, specificity and non-invasive character. The fluorophores (probes) used as sensors report on the membrane characteristics such as transmembrane potential, surface charge, morphology or lipid packing [60].

The molecular rotors were reported to be sensors of viscosity [101]. In this work, we aimed to design and characterize improved molecular rotors with focus on their use as fluidity sensors. A wide class of molecular rotors is described in Haidekker and Theodorakis, 2010 [102]: The molecular rotors are probes consisting of electron donor and acceptor units, which are connected by a conjugated system (Figure 12). In the electronic ground state, the donor and acceptor typically lie in one plane. After excitation, the charge is redistributed between the donor and acceptor units. In response to the charge redistribution, a molecule undergoes internal twisting motion, which reduces energy gap between ground and excited states. The resulting excited state is called twisted intramolecular charge transfer (TICT) state. As a result, the fluorescence is red-shifted, or completely disallowed. The extent of the rotation is influenced by immediate probe's neighborhood – whether there is a free volume for rotation or not. The ability to rotate is then frequently related to the local microviscosity.

However, not all molecular rotors necessarily need to satisfy all the aforementioned specifics (for example if the ground state corresponds to the planar configuration or if the charge transfer occurs). The key factors for the molecular rotor to be a sensor of local microviscosity seem to be the conformational change after excitation and the difference in fluorescence yield during conformational change (for a rotor to be detected by fluorescence methods) [103].

Among the first promising and sensitive molecular rotors employing TICT state were molecules based on aniline nitriles and julolidine malononitrile structures (Figure 12) [101,104]. However, these probes were excited with the light in the live cell-

incompatible spectral region of 300–450 nm limiting their use to non-cellular systems.[i] Development of spectrally-shifted probes introduced a group of meso-substituted BODIPY derivatives which also show dependency of excited state fluorescence lifetime on viscosity [64]. These probes composed of the BODIPY dipyrromethene framework and a phenyl group emits fluorescence only from the metastable twisted conformation, but not from the planar one (depicted in Figure 13). Temperature measurement of BODIPY based rotor incorporated into lipid vesicles showed that the fluorescence intensity decreases with increasing temperature [105]. This corresponds to the enabled rotation of phenyl group and it confirms that the fluorescence is decreased as the molecule rotates. In accordance, excited state fluorescence lifetime of BODIPY based rotors shortened significantly in solutions of glycerol with decreasing viscosity [64]. In other words, the fluorescence is quenched when the rotation motions are active. However, the incorporation of BODIPY-based molecular rotors into model lipid membranes of different lipid phases provided bi-exponential fluorescence decay which suggests that the dye encounters two different environments [105]. This indicates that the probe occupies at least two different positions/orientations in a membrane. This is probably caused by the imperfect incorporation of BODIPY rotor into the membranes. Yet, no information on the localization and orientation of BODIPY-based fluorescent molecular rotors was available.

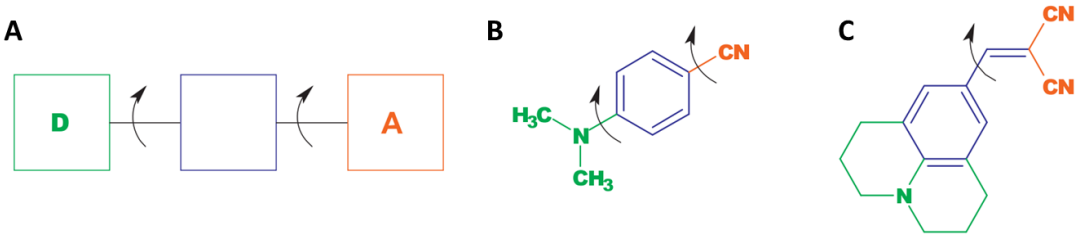

Figure 12. Molecular rotors. A The scheme of molecular rotors. Donor and acceptor of electron are depicted in green and orange, these are separated by a unit in blue. Black arrows denote the bond around which rotation is enabled. **B** Example of aniline nitrile structure: 1,4-dimethylamino benzonitrile. **C** Example of julolidine malononitriles, 9-(dicyanovinyl) julolidine. Adopted from [102].

[i] This is not entirely true for julolidine malononitriles. They have additional excitation peak at ~480 nm, which is less harmful for live-cell imaging than UV light. However, a majority of measurements with these molecular rotors were performed in the fluorescence intensity mode. To overcome a drawback of concentration dependence, ratiometric dyes were designed [158]. These probes are formed by two units – first is viscosity insensitive reporter of concentration and second one is viscosity sensor. They are placed in close vicinity so that FRET can occur. The used donor (concentration reference) is again excited by UV-light, which limits the bio-compatibility.

The defined probe location is crucial for getting reproducible and credible information about the system. The original BODIPY-based molecular rotor was mono-alkylated (compound **1**, Figure 13), whereas a majority of membrane lipids contain two acyl chains. Therefore, we hypothesized that adding one or two alkyl chains could improve the rotor localization. Synthesis of the original mono-alkylated (compound **1**) and newly proposed di- and tri-alkylated variants of the BODIPY-based rotor the compounds **2a**, **2b**, **3a** and **3b** (Figure 13) was performed in the group of Prof. Jiří Svoboda (Department of Organic Chemistry, Institute of Chemical Technology, Czech Republic). Details of the synthesis are described in the attached paper.

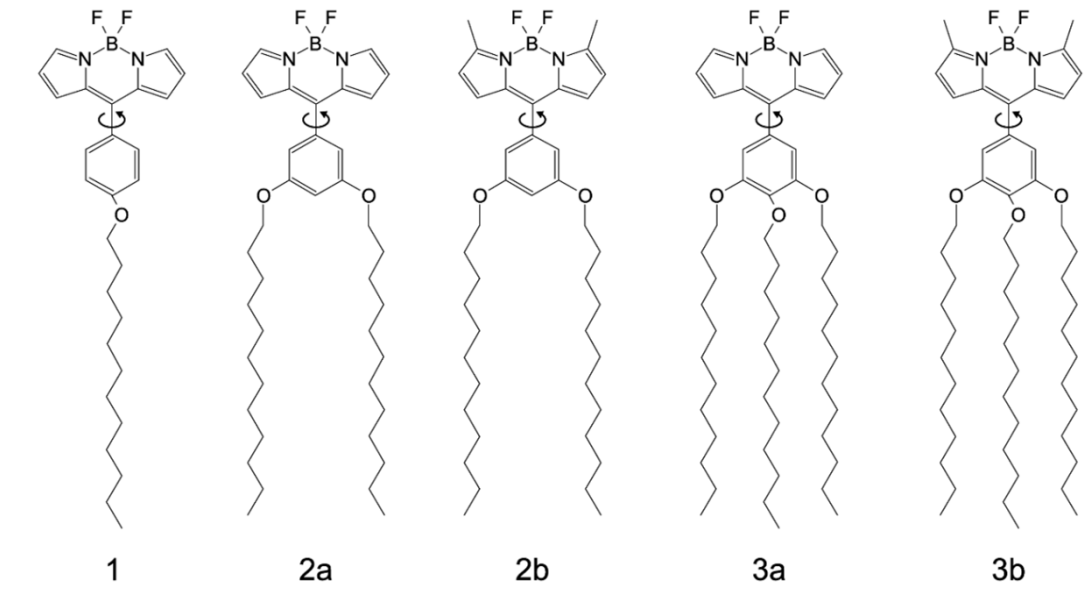

Figure 13. Structures of compounds reported in the thesis. The arrow indicates the bond around which the rotation of the molecular rotor occurs.

Results: Characterization of fluorescence properties of the probes

At first, the organic solutions of compounds were characterized spectrally to verify whether the newly synthetized compounds have potential to function as fluorescent probes. Excitation and emission spectra, extinction coefficient and fluorescence quantum yield were determined, the results are summed up in Table 1 and Figure 14. A comparison of extinction coefficients and quantum yields, main characteristics describing how easily the molecule is going to be excited and how much photons it can emit, showed the poor fluorescent properties of molecules **2a** and **3a**. Thus, these probes were excluded from further testing. On the contrary, fluorescence properties of the

newly synthesized methylated compounds **2b** and **3b** were comparable with the previously reported BODIPY-based molecular rotor (compound **1;** Table 1; [64]) providing a good basis for further characterization.

Table 1. Fluorescence properties of the studied compounds measured in solution of chloroform:methanol and in lipid vesicles.

Probe	$\lambda_{EX}/\lambda_{EM}$[a] [nm]	ε[b] [$M^{-1}\cdot cm^{-1}$]	Φ[c]	K_D[d] [M^{-1}]	F_0/F[e]
1	496/513	60 000	0.15	0.060 ± 0.020	1.7 ± 0.1
2a	501/518	11 000	0.02	n.d.	n.d.
2b	511/525	39 000	0.11	0.020 ± 0.010	3.8 ± 0.1
3a	500/517	39 000	0.01	n.d.	n.d.
3b	511/528	140 000	0.04	0.035 ± 0.020	4.5 ± 0.1

[a] Maxima of the fluorescence excitation and emission spectra. [b] Extinction coefficient. [c] Fluorescence quantum yield. [d] The Stern–Volmer quenching constant for the water-soluble acrylamide quencher. [e] The quenching ratio for 16-doxyl quencher embedded in DPPC MLVs at 60°C. F_0 and F are fluorescence intensities in the absence and presence of the quencher, respectively. n.d. not determined.

In the next step, we tested compounds **2b** and **3b** if they function as molecular rotors. Fluorescence lifetime measurements were performed in lipid vesicles composed of DMPC with embedded BODIPY rotors. DMPC is di-saturated lipid with relatively short acyl chains (14:0 PC) and transition temperature of 24°C [49]. Measurements were performed at different temperatures. Changes in temperature influence membrane lipid packing, which directly affects the ability of a probe to rotate. Fluorescence lifetimes of compounds **2b** and **3b** shortened as the membranes became more fluid. Therefore, these probes can be considered as fluorescent molecular rotors (Figure 14B). Inspection of slopes in Figure 14B indicates limited ability of all tested compounds to sense lipid phase transition.

Measurements of lifetime dependencies on membrane viscosity were preferred to the intensity-based measurements. Intensity-based measurements are susceptible to non-uniform fluorophore distribution in a sample: a higher fluorophore concentration typically means a higher fluorescence intensity falsely indicating a more viscous environment. Fluorescence lifetime is mostly independent of fluorophore concentration. Lifetime measurements were also enabled due to the exceptionally long fluorescence

lifetime of BODIPY-based rotors (1-7 ns, depending on lipid composition, compound and experimental conditions) compared to julolidene-based rotors (10-100 ps) [106].

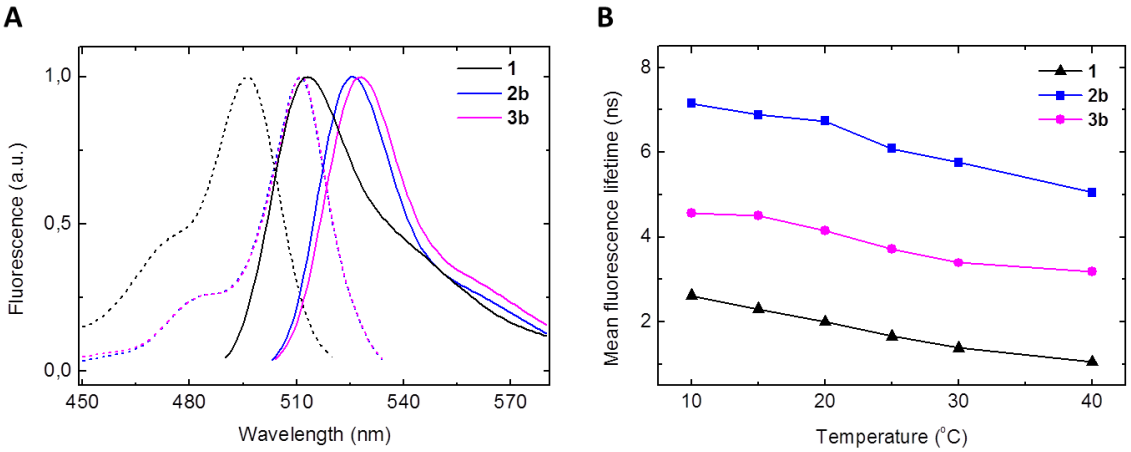

Figure 14. A. Excitation and emission spectra of the selected rotational BODIPY probes (**1**, **2b**, **3b**) in methanol/chloroform (1:1, v:v) solution at room temperature. **B.** Fluorescence lifetime of the studied rotational BODIPY probes embedded in DMPC large unilamellar vesicles as a function of temperature.

Results: Probes' location and sensitivity to the membrane viscosity

To determine whether the incorporation of di- and tri-alkyl BODIPY rotor variants to lipid membranes was improved compared to compound **1**, several quenching experiments were performed. BODIPY-rotors (compounds **1**, **2b** and **3b**) were embedded into LUVs and quenched by a water-soluble quencher – acrylamide, or by a free radical quencher – 16-doxyl (Figure 15) located in the central region of bilayers. Acrylamide was titrated against the cuvette containing the liposomal suspension, while the fluorescence intensity was continuously measured. Acrylamide quenching data were analyzed using the Stern–Volmer equation. Stern–Volmer constant was the highest for the compound **1**. In the case of second quencher, 16-doxyl, fluorescence intensities in the absence and presence of the quencher were monitored. The least efficient quenching was found for compound **1.** Both experiments showed a deeper and tighter positioning of compounds **2b** and **3b** in membranes compared to compound **1** (Table 1).

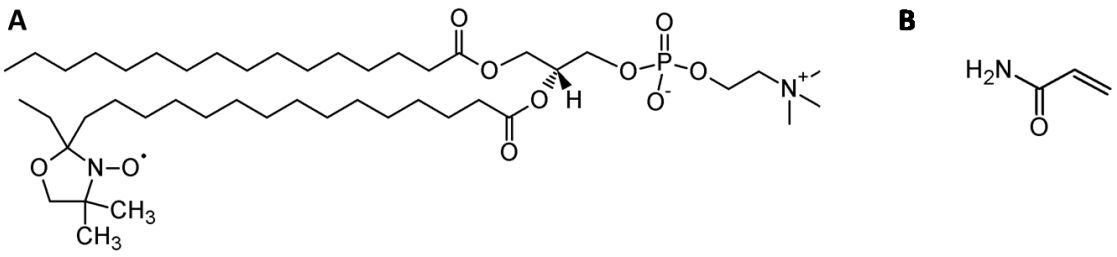

Figure 15. Structures of quenchers used in the chapter. A 1-palmitoyl-2-stearoyl-(16-doxyl)-*sn*-glycero-3-phosphocholine (16-doxyl), **B** Acrylamide.

This result was supported by additional measurements of the average distance between the probe and a membrane positioning marker, DiD, using FLIM-FRET method (Figure 16). Compound **1** (donor) exhibited the most distant positions from the marker DiD (acceptor). The plane to plane distance d_B of 36 Å for compound **1** or 33 Å for compounds **2b** and **3b**, respectively, was obtained by fitting of donor time-resolved fluorescent decays (performed by Radek Šachl). Both the FRET and quenching data indicate that addition of alkyl chains facilitates a deeper incorporation of compounds in the lipid bilayer compared to those with one alkyl chain only.

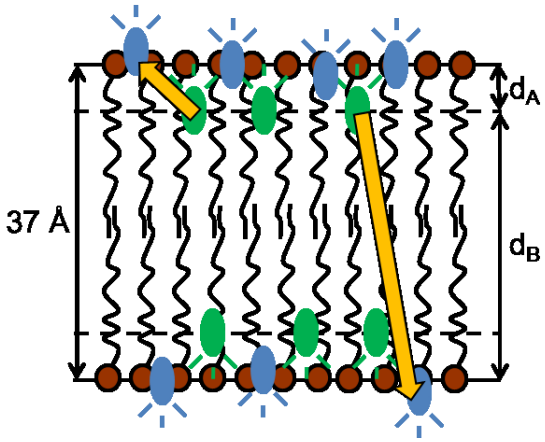

Figure 16. An illustration of the experiment detecting the localization of the probes in a lipid bilayer containing donor (compounds **1**, **2b** or **3b**; green ellipsoids) and acceptor (DiD; blue ellipsoids) molecules. The yellow arrows indicate possible energy transfer events from donors to acceptors. The plane to plane distance d_A corresponds to FRET from donors to acceptors localized in the same leaflet whereas the distance d_B corresponds to FRET from the donors to the acceptors residing in the opposite leaflet.

In the following step, we tested the BODIPY based rotors in lipids membranes of different compositions to characterize their capacity to sense diverse lipid membrane

environments. FLIM measurements of compounds **1**, **2b** and **3b** were performed in GUVs composed of DOPC (Ld phase), DPPC:cholesterol (2.2:1; Lo phase), and DPPC (So phase) at room temperature. In contrast to the original BODIPY-based molecular rotor (compound **1**), compounds **2b** and **3b** exhibited only weak bi-exponential fluorescence decay irrespective of the studied lipid phase indicating more defined location of these probes. The unexpected concomitant result was that compounds **2b** and **3b** lost their ability to distinguish between Ld and Lo phases. Mean excited state fluorescence lifetime of compounds **2b** and **3b** was nearly identical for Ld and Lo phases and only So phase could be distinguished based on these measurements (Table 2). In contrast, compound **1** showed a clear difference among all three phases (Table 2) indicating a better capacity of the probe to function as an environmental sensor in membranes compared to compounds **2b** and **3b**. However, a non-uniform membrane position of compound **1** still limits its use in more complicated systems, such as cell membranes. Lastly, we tested properties of the rotors in phase separated model membranes. The distribution of rotors between coexisting Ld and Lo phases was first determined. All tested compounds extensively preferred the Ld phase compared to Lo phase, similarly to a majority of available membrane probes. Such an observation again limits the use of all BODIPY-based molecule rotors as environment-sensitive probes in complex systems such as cellular membranes.

Table 2. Mean fluorescence lifetimes of molecular probes in different phases. Lifetimes were obtained by mono/bi-exponential tail-fitting of decays measured on GUVs by FLIM method.

Probe	τ_{Ld} [ns]	τ_{Lo} [ns]	τ_{So} [ns]
1	1.8 ± 0.1	2.9 ± 0.1	4.5 ± 0.2
2b	5.7 ± 0.1	5.7 ± 0.1	7.0 ± 0.2
3b	5.1 ± 0.1	5.4 ± 0.2	6.9 ± 0.1

The propensity of compounds **2b** and **3d** to distinguish Ld from So phases is not based only on lifetime differences but, interestingly, it is also accompanied by phase-specific fluorescence pattern. The distribution of fluorescence intensity was uneven along a GUV and the intensity pattern differed mainly between Ld and So phase. Such an observation implies that the fluorescence of the dye depends on its orientation with respect to the polarization of the excitation light; i.e. it indicates a preferential

orientation of the chromophore in membranes. To investigate it further, we performed simplified anisotropy measurements on GUVs containing the probes. Anisotropy XY cross-section images of the GUVs composed of DOPC (Ld phase) and DPPC (So phase) were calculated from the images measured separately for the emission light polarized parallel and perpendicular to the excitation light (polarized horizontally). The anisotropy distribution along the GUV containing compound **3b** varied between Ld and So phases implying reorientation of compound **3b** in membranes with these phases (Figure 17). The reorientation was also observable for compound **2b**. The fluorescence anisotropy pattern of So phase for compound **2b** showed several maxima along the GUV (coinciding with maxima for compounds **3b** and **1** in So phases). This suggests the existence of two populations (orientations) of compound **2b** in the So phase: one oriented perpendicular and one parallel to the membrane normal (Figure 17). The anisotropy pattern of compound **1** along GUV remained unchanged in both phases.

Changes in anisotropy do not reflect changes in the fluorophore reorientation kinetics which is uniform throughout the GUV. They rather result from the changes of the fluorophore orientation with respect to the polarization of the excitation light leading to the excitation pre-selection.

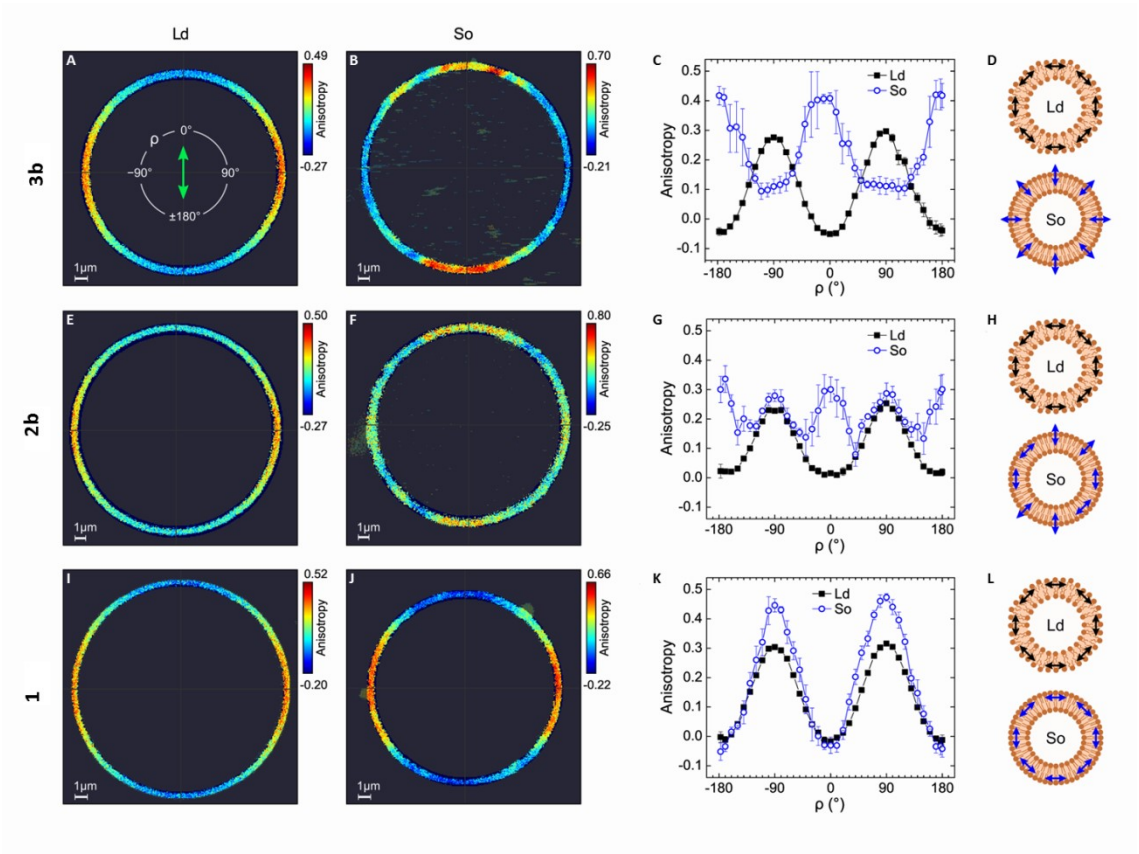

Figure 17. Fluorescence anisotropy confocal imaging of compounds 3b (A, B, C, D), 2b (E, F, G, H), and 1 (I, J, K, L). BODIPY-based molecular rotors embedded in GUVs composed of either DOPC (A, E, and I; Ld phase) or DPPC (B, F, and J; So phase) were measured at room temperature. Excitation light was polarized along the Y axis (see the green arrow in panel A). Presented pseudo-color anisotropy images are examples of GUV cross sections in the X–Y middle plane. Anisotropy as a function of the ρ contour angle around the GUV cross section (C, G, K) were averaged over at least 3 different GUVs (ρ angle is defined in panel A). A schematic orientation of the electronic transition dipole moment of the fluorophores in the liposomal membrane that agrees with the obtained results is depicted in panels D, H, and L in the form of black and blue arrows.

Conclusions and Discussion

In this work, we designed the BODIPY-based molecular rotors with improved membrane localization. Deeper rotor positioning was achieved by increasing the number of alkyl chains attached to the fluorophore body. Newly synthetized molecules proved the ability to function as molecular rotors but revealed a complex orientation of all tested probes within membranes with different lipid compositions. This means that BODIPY-based molecular rotors are suitable for measurements of lipid packing in membranes with simple and well-defined composition. In more complex membranes,

such as cellular membranes, the results could be ambiguous due to the undefined probe positioning.

Our work presents exceptionally detailed study of fluorescent molecular rotors that is typically not available for other membrane probes. Not only the fluorescent properties, such as emission and excitation spectra, quantum yield and excitation coefficient were provided, but also internal comparison of the probes and information about their location within a membrane was determined. Only such thorough characterization of fluorescent probes will enable full understanding on what they report, especially if we are interested in studies of real cell membranes.

Generally, cell membranes are the main point of interest. Our work was not focused on testing BODIPY-based rotor in cell membranes. The group of Dr. Kuimova, who developed BODIPY-based rotors, continued in research of probe compatibility with live-cell imaging. Recently, they were able to prepare the derivative that located to the plasma membrane for sufficiently long time to acquire FLIM images (several minutes) before the probe's internalization occurred [107]. However, the experimental procedure included the slowing down of cell endocytosis, which is usually the process that removes the dyes from the plasma membrane. Under these conditions, they provided images of BODIPY-based rotor separating internal and plasma membrane based on the viscosity measurements. It is worth mentioning, the new derivative used in the study was only partly characterized in terms of location and orientation in membranes. The derivative showed bi-exponential fluorescence decay in model lipid membranes in Ld or So phase [108]. This observation indicates that position/orientation of this rotor in membrane is non-uniform which again complicates interpretation of results in more complex environments.

Whether these probes will be able to produce microviscosity maps with high spatial and time resolution (by the FLIM technique) is still questionable. We demonstrated that it might work only for simple systems. Indeed, the molecular rotors characterize the membrane as a whole: As was shown here, the BODIPY based rotors are able to incorporate into more ordered lipid membranes (Lo and So phase). This was, however, enforced by the sample preparation. In the model vesicles separated into more phases, rotors strongly prefer less ordered phase which limits their use in cell membranes. Local cellular heterogeneities will probably be omitted because of rotor's preferential localization.

Another question is what exactly these dyes are probing and how it is related to the property generally called viscosity. Intuitively, membrane viscosity is related to "a frictional resistance to rotational and translational motions of molecules" [61] and so to the lipid packing. But some publications [64,105,107] relate the results measured with molecular rotors in membranes to bulk viscosity by comparison of measured lifetimes to calibration results from glycerol-methanol mixtures. It is questionable whether this is a correct interpretation of the presented data. As mentioned in the introductory chapters, viscosity is a bulk property and is poorly defined for membranes. Membrane is a heterogeneous structure providing diverse environments in the hydrophobic core and at lipid headgroups region. Both parts of membrane could affect molecular rotors. The nature of such interaction is still unknown. However, it emphasizes the need of probe location to be determined precisely. In addition, the effect of free volume has not yet been tested in membranes, but its effect was evident for bulk solutions containing molecular rotors [96]. Lastly, our fluorescence lifetime measurements showed the fluorescence lifetime dependence on lipid composition (for example see Table 2 and Figure 14B). Such observation again complicates the use of BODIPY based molecular rotors in more complex environments. It also questions the meaning of absolute viscosity values obtained by comparison of measured lifetimes to calibration experiments.

There are alternative and indirect ways how to measure lipid packing of membranes and therefore the microviscosity maps. One way is to use Laurdan and its variants [109] which have the ability to indirectly report on membrane viscosity and polarity and which incorporates well into cell membranes. Another way could be based on the measurement of probe's mobility. The map of diffusion coefficients could be obtained by imaging fluorescence correlation spectroscopy (iFCS) [110].

Paper II

5.2 Study of the formation of cross-linking-induced lipid nanodomains in model membranes

Introduction

Although the large scale phase separation is not observed in all living mammalian cells, the temporal existence of small nanodomains cannot be excluded [28] and was suggested to occur in cell-derived vesicles (GPMVs) at physiological temperatures [45,111]. This behavior is sometimes described as fluctuations of composition near critical point [112]. Lipid domains in artificial membrane systems provide a well-defined and simplified model for studying formation of domains in living cells. Attractiveness of model membranes also lies in the assumption that, nanodomain formation is expected to precede macroscopic phase separation in such systems [113].

Direct observation of nanodomains frequently fails due to the temporal and spatial resolution of optical microscopes. This limitation could be overcome by the application of super-resolution techniques or non-imaging approaches. Herein, we employed non-imaging approaches such as FCS and FLIM-FRET. For example, measurement of diffusion coefficients by FCS methods reports on the size of mobile components (SD hydrodynamic model). However this approach is only partially sensitive because the diffusion coefficient is only weakly dependent on size of domain and useful only if a probe is fully trapped inside slowly moving domain [114]. Another approach is to study typical distance between fluorescent probes via Förster resonance energy transfer studied by the FLIM-FRET method. To be able to get information about small (< ~20 nm) nanodomains, the best approach is to have donor and acceptor residing in different environments, i.e. one inside and second outside of domains [115]. The problematic part is to get a probe inside a domain. In the case of lipid phase separation, we are typically interested in separation of Lo domains from Ld domains. The list of dyes that preferentially resides in Lo phase is short [114]. In this work, we made use of a β-subunit of cholera toxin protein complex (CTxB) that binds up to five molecules of glycosphingolipid GM1 residing in Lo domains [116]. Such cross-linking induces formation of macroscopic domains in membranes containing DOPC, cholesterol, sphingomyelin and GM1 at certain ratios [117].

Summary of results

In the presented work, we studied the lipid systems prone to nanodomain formation with lipid composition close to the macroscopic phase separation. To our knowledge, it is one of the first works showing nanoscopic heterogeneities in model lipid membranes. Selected model systems were pure lipid membranes lacking transmembrane proteins and cytoskeleton. GUVs were composed of DOPC, cholesterol and increasing concentrations of sphingomyelin, physiologically relevant amounts of glycosphingolipid GM1 and DOPG (5%) required for GUV preparation by gentle hydration method (Table 3). CTxB was added to support nanodomain formation. We studied several lipid compositions under three different conditions: in the presence of low, medium and high load of CTxB. The existence of nanodomains in GUVs was studied by z-scan FCS and FLIM-FRET approach. Alexa Fluor 647-labeled CTxB was used for FCS measurement. Alexa Fluor 488-labeled CTxB was used as donor molecule positioned in putative nanodomains, and bulk lipid marker (DiD) as acceptor molecules for FLIM-FRET experiments. The amount of added CTxB depended on the used method and is described in Table 4 and in Experimental section of enclosed Paper II.

Table 3. Lipid composition (molar fractions) of GUVs used for nanodomain studies.

	DOPC	Sph	Chol	DOPG	GM1	Macroscopic phase separation
A	0.68	0	0.25	0.05	0.02	No
B	0.49	0.19	0.25	0.05	0.02	No
C	0.44	0.24	0.25	0.05	0.02	No*

* A majority of GUVs was not phase separated under our experimental conditions

In the ternary phase diagram of DOPC, sphingomyelin and cholesterol (Figure 18), there is a region in which two macroscopic phases coexist. We were interested in lipid composition in the border area of the phase diagrams that separates one-phase and two-phase region (points **B** and **C** of the diagram in Figure 18). In this area, we are close to the macroscopic phase separation and it is therefore more likely that nanodomains can be formed (Table 3, phase diagram Figure 18).

Table 4. Total amount of CTxB (both labeled and unlabeled) applied for z-scan FCS and FLIM-FRET experiments.

Method	Load	Alexa Fluor 647-labeled CTxB [μg]	Alexa Fluor 488-labeled CTxB [μg]	Non-labeled CTxB [μg]
z-scan FCS	Low	0.01	0	0
	Medium	0.04	0	0
	High	0.08	0	0
FLIM-FRET	Low	0	0.02	0
	High	0	0.02	20

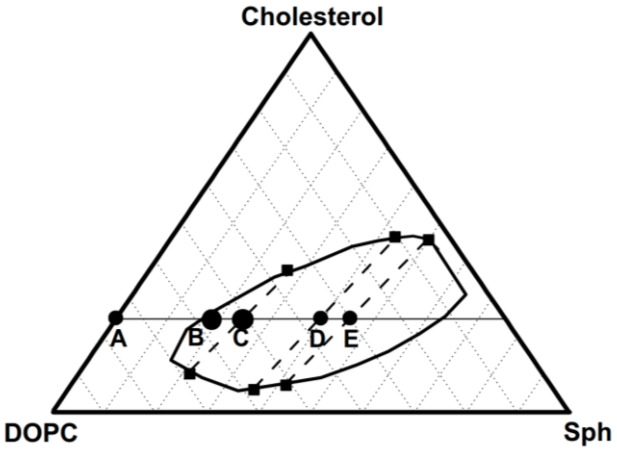

Figure 18. Ternary phase diagram for DOPC/Sph/Cholesterol lipids according to Smith and Freed [118]. The line connecting points **A** to **E** denotes constant cholesterol content. All measurements were done in marked points **A** to **C** corresponding to the lipid compositions given in Table 3. Compositions **D** and **E** formed phase separated GUVs and are not discussed in the text of thesis.

Reference composition **A** lacking sphingomyelin showed no macroscopic phase separation in the presence or absence of CTxB. Increasing concentration of applied CTxB did not affect diffusion coefficients of CTxB or fluorescently labeled membrane lipid (Table 5). Similarly, decay of donor's fluorescent intensity (CTxB) in the presence of acceptor (DiD) was not affected by CTxB load, indicating random distribution of donors and acceptors.

Table 5. Mean diffusion times with standard deviations for Alexa Fluor 647-labeled CTxB bound to GM1 molecules. The values were obtained from the position where membrane was in focus (z-scan FCS). Every value was averaged over the measurements of at least three vesicles.

Composition	Mean diffusion times for CTxB load: [ms]		
	Low	Medium	High
A	6.6 ± 0.1 for all loads		
B	5.9 ± 0.2	40.3 ± 2.2	46.5 ± 10.5
C	12.8 ± 0.9	14.6 ± 2.9	12.0 ± 6.8

Phase diagram according to Smith and Freed [118] manifests that lipid composition **B** is close to the phase boundary region. Lipid composition **C** is expected to be phase separated. Presented phase diagram (Figure 18) is shown here to provide a qualitative basis for the presentation of our data, the precise position of the boundary line as well as the exact tie-line field were beyond the scope of this publication. Prepared GUVs for both compositions did not exhibit optically resolvable phase-separated GUVs (composition **B** shown uniform distribution of lipids, composition **C** contained only low fraction of phase separated GUVs – these were not used for further studies). Both compositions were considered to be prone to nanodomain formation, because their composition is close to the boundary of macroscopic phase separation. In this study, we proved by elegant use of advanced fluorescent techniques that nanodomains are indeed formed after addition of cross-linker in both compositions. Moreover, detailed analysis of FCS and FLIM-FRET data revealed two distinct ways of nanodomain formation:

For the composition **B**, nanodomain formation was induced by the cross-linker. FCS data showed dependence of diffusion times on CTxB load indicating a formation of larger and slowly moving objects (Table 5). Correspondingly, donor (labeled CTxB) lifetime in FRET experiments prolonged with increasing concentration of unlabeled CTxB due to the separation of donor (labeled CTxB, localized in domains) and acceptor (DiD, location outside of domains) by domain formation (Figure 19). Using a combination of FLIM-FRET data with Monte Carlo modeling of the donor decay response, the diameters of nanodomains were predicted to be 5 nm (low load of CTxB) and 8 nm (high load of CTxB). Monte Carlo simulations were performed by Radek Šachl. Because of the dependence of results on CTxB load, we proposed that the

starting lipid mixture with the composition **B** lacks heterogeneities and the domains are formed or enlarged by increased cross-linker levels.

For the composition **C**, the mechanism of domain formation is expected to be different. FCS and FLIM-FRET data show no dependence of diffusion times on CTxB load (Table 5). Yet, the diffusion time of labeled CTxB was slower and fluorescent decay was prolonged compared to the composition **A** indicating the presence of nanodomains. The size of nanodomains for the composition **C** was estimated to be 24 nm. Based on our results, we proposed that sphingolipid/GM1/cholesterol nanodomains were formed before the addition of the cross-linker.

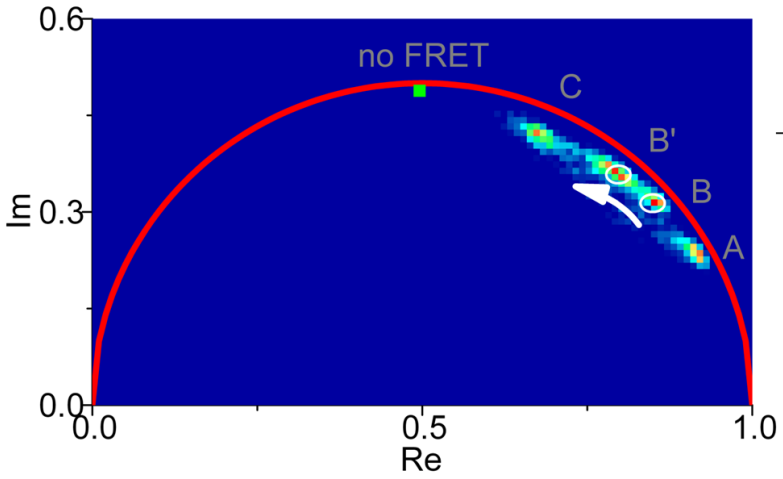

Composition	Domain sizes (nm)
A	No domain formation proved
B	5 – 5.4
B'	8
C	24

Figure 19. FLIM-FRET phasor diagram displaying shift of the Alexa Fluor 488-labeled CTxB decay functions towards a lower FRET efficiency (FRET efficiency decreases in the order **A** > **B** > **B'** > **C**) and when excess of a non-labeled crosslinker is added (**B** > **B'**). FRET efficiency did not change for compositions **A** and **C** in the presence of higher CTxB loads. Inserted table shows calculated size of domain radius based on Monte Carlo simulations of FLIM-FRET data.

Conclusions

This work presented a detailed dynamic and structural study of a cross-linker-triggered formation of nanodomains. This work belongs to the first studies that provided evidence of the existence of lipid nanodomains which are not visible using standard microscopy techniques. Importantly, we were able to characterize partially the properties and size of such nanodomains. Further, the study highlights the usability of advanced fluorescence techniques, such as z-scan FCS or FLIM-FRET for the characterization of membrane entities at nanoscale range. During this work, I also learned how to use these techniques, which were necessary for the follow-up studies.

Related discussion in the scope of the thesis: Relevance of the used model systems for the characterization of proteo-lipid membranes

The conclusions above (and in the paper) focuses primarily on the characterization of the nanodomain formation. The model system was chosen directly for this purpose. However, it also bears relevance for the discussion on characterization of proteo-lipid membranes discussed in the following chapters.

The herein studied model membrane systems containing nanoheterogeneities are considered to be more relevant to the real state of cell membranes than a large scale phase separation observed in model lipid systems with different composition. [45,111,119]. On the other hand, the question remains whether transmembrane peptides (proteins) would interact with nanodomains of the more ordered membrane environment. There are some studies supporting this idea: Using coarse grain molecular dynamics simulations, authors predicted that GM1 molecules mediate transport of transmembrane peptides from Ld to Lo phase [120]. Moreover, the experiments on plasma membrane spheres showed that transmembrane proteins could partition into more ordered phases induced by GM1 crosslinking [45,47]. However, in these type of experiments, the effect of formation of vesicles (PMS and GPMVs) in the presence of chemical cross-linkers has to be taken into account as an factor potentially influencing membrane organization [46,121]. On the contrary, several papers [47,122,123] using phase separated model membranes demonstrated the exclusion of transmembrane peptides from Lo phase due to the energetic constraints of tight lipid packing of this phase. Based on these studies and observed energetic penalty accompanying Lo partitioning of transmembrane peptides [122], it is difficult to imagine that the peptide would fit into tightly packed lipid nano-assemblies, unless the peptide has an increased affinity for the lipids of the Lo phase, for example due to specific interactions. Taking into account the aforementioned arguments, we used only simple lipid compositions forming Ld phase in our following studies focused on peptide effect on model membranes.

An interesting fact worth mentioning is that the exclusion of peptides from Lo phase could be perceived as an enrichment of peptides in Ld phases [124]. If the suggested approach indeed leads to enrichment of peptides in the Ld phases, it could enable studies of model membranes crowded with peptides that would otherwise be typically limited by poor incorporation of peptides into model membranes.

Paper III

5.3 Determination of peptide orientation in membranes

Introduction

Previous studies were focused on characterization of pure lipid membranes. However, cellular membranes are densely populated by proteins. Proteins associate with membranes peripherally via protein-protein and protein-lipid interactions, use lipid anchors for a more stable attachment, but can be also fully integrated in a membrane. Such integration requires the presence of one or multiple transmembrane domains (TMDs) in protein structure.

To be able to study protein-lipid interactions, we need to choose a proper model system. Generally, two-component system is sufficient – just the lipids and proteins. First, a model system needs to be characterized. Not only proper choice of proteins and lipids is important, but also parameters such as fluidity of membrane, protein membrane orientation and its tendency to cluster, propensity to domain formation, extent of protein incorporation and many more must be verified. The parameters need to be tested experimentally or, at least, verified in literature. In this context, we would like to introduce a new approach how to study the orientation of small proteins in membranes.

The orientation of peptide with respect to a lipid bilayer can be investigated by several methods including solid state nuclear magnetic resonance [125], X-ray diffraction [126], oriented circular dichroism spectroscopies [127] or attenuated total reflection Fourier-transform IR spectroscopy [128]. However, in order to maintain the form of a model membrane, its composition and level of hydration comparable to samples that are typically used for fluorescence microscopy/spectroscopy, the use of fully hydrated lipid unilamellar vesicles is preferred for the determination of peptide orientation with regard to membrane normal. Previously, FRET approach [129] and monitoring emission properties of tryptophan amino acid [130] were reported. The disadvantage of these methods is a necessity of specific peptide composition or several modifications of peptides. For example, to observe a polarity dependent shift of tryptophan emission requires a tryptophan residue positioned in the hydrophobic part of peptide/membrane structure. Herein (Paper III), we investigated capabilities of TDFS for the determination of peptide orientation in lipid membranes. A TDFS method is remarkably sensitive to the membrane polarity and microviscosity, both parameters

potentially sensitive to the presence of a rigid body of peptide and its polar amino acids. There are no requirements on peptide composition and labeling with fluorescent dyes is also not needed.

Membrane polarity and microviscosity differ significantly along the bilayer normal, therefore position of solvatochromic dyes is crucial for the determination of these parameters. Laurdan probe was selected due to the lack of charge and its well-defined position at water-membrane interface: Laurdan is located at the level of *sn*-1 carbonyls of phospholipids [131]. In the literature, membrane polarity acquired from TDFS measurements using Laurdan probe is typically interpreted as the level of membrane hydration at this membrane depth. TDFS method also provides information on local membrane microviscosity which is expressed as a relaxation time needed for rearrangement of hydrated carbonyls.

The peptides selected for this study were of two types – i) antimicrobial peptides and ii) transmembrane peptides (a list of selected peptides is in the Table 6). Transmembrane peptides are represented by model transmembrane peptide LW21 and LAT peptide derived from the transmembrane domain of signaling adaptor protein LAT present at the plasma membrane of T lymphocytes. The design of transmembrane peptide LW21 was adapted from Kaiser et al. [57], (Table 6): 21 hydrophobic residues surrounded by two lysines at both ends. Another 4-5 residues from CD247 molecule were added at both ends to further stabilize the transbilayer orientation of the peptide. Expected orientation of these peptides inserted in model lipid bilayers is transmembrane.

Antimicrobial peptides belong to the large family of peptides that are involved in the innate immunity. A common feature of these peptides is the amphipathic distribution of polar and hydrophobic residues along their α-helical structure. Amphipathicity determines their capacity to interact with and insert into phospholipid membranes. In this work, three linear peptides were tested: magainin 2, alamethicin and LAH_4. LAH_4, is a model antimicrobial peptide designed by Bechinger et al. [132] to control peptide membrane orientation. Its four histidines allow manipulation of the net charge and hydrophobic moment of the helix by changing pH. It has been shown on supported bilayers that LAH_4 helices are oriented parallel to the membrane surface at $pH < 6$, when the histidines carry net positive charge. The LAH_4 peptide adopts transmembrane orientation at neutral and basic pH [132]. The other two peptides, alamethicin and

magainin 2, are known to bind membranes in transmembrane and peripheral manner, respectively, and provide excellent controls for our method.

Table 6. Selected peptides used in this work and their expected orientation in POPC lipid bilayer.

Peptide	MW [g mol^{-1}]	Amino acid sequence	Peptide orientation
Alamethicin	1964	UPUAUAQUVUGLUPVUUE QF*	Transmembrane at pH 7.4
Magainin 2	2467	GIGKFLHSAKKFGKAFVGE IMNS	Peripheral at pH 7.4
LAH_4	2777	KKALLALALHHLAHLALH LALALKKA	Transmembrane at pH 8 Peripheral at pH 4.5
LW21	4119	GLLDSKKWWLLLLLLLLA LLLLLLLLWWKKFSRS	Expected: Transmembrane at pH 7.4
LAT	3236	EEAILVPSVLGLLLLPILAM ALSVHSHR	Expected: Transmembrane at pH 7.4

**U: α-methylalanine – proteinogenic amino acid inserted to proteins biosynthetically*

Results

TDFS measurements of Laurdan embedded into the LUVs composed of the lipid POPC[ii], and selected peptides provided information on the polarity and mobility of the dye environment at the glycerol level of the bilayer (spectral shift Δν and relaxation time τ_r; Table 7). Several peptide:lipid ratios were tested: 0, 1:100 (i.e. 1 mol% of peptide), 1:10 (i.e. 10 mol%) as well as 1:50 (i.e. 2 mol%) for LW21 and LAT peptides. LAH_4 orientation was tested at acidic and basic pH. Considering the widespread use of Laurdan generalized polarization (GP), we added also the corresponding values.

[ii] For the scope of the thesis, the mobility and polarity measurements were the main goal. The selection of POPC lipid, however, played role in another part of the paper, describing lipid bilayer stability in the presence of antimicrobial peptide LAH_4.

Table 7. Polarity (Δν), mobility (τ_r), and generalized polarization (GP) detected by Laurdan located at the glycerol level of zwitterionic POPC LUVs (1:100 dye/lipid mol/mol ratio).

			Laurdan		
Peptide	pH	Peptide/Lipid	Δν [cm^{-1}]	τ_r [ns]	GP
−	4.5	0	3980 ± 60	1.86 ± 0.04	−0.127 ± 0.017
LAH_4	4.5	1:100	3980 ± 60	1.83 ± 0.04	−0.138 ± 0.018
LAH_4	4.5	1:10	3960 ± 50	1.86 ± 0.02	−0.126 ± 0.017
−	8.0	0	4040 ± 60	1.62 ± 0.07	−0.161 ± 0.021
LAH_4	8.0	1:100	4010 ± 50	1.70 ± 0.02	−0.152 ± 0.020
LAH_4	8.0	1:10	4060 ± 50	2.35 ± 0.03	−0.073 ± 0.021
−	7.4	0	4067 ± 50	1.59 ± 0.05	−0.159 ± 0.021
Magainin 2	7.4	1:100	4060 ± 50	1.57 ± 0.05	−0.188 ± 0.024
Magainin 2	7.4	1:10	4020 ± 50	1.66 ± 0.05	−0.154 ± 0.020
Alamethicin	7.4	1:100	4040 ± 50	1.81 ± 0.05	−0.142 ± 0.019
Alamethicin	7.4	1:10	4020 ± 50	2.82 ± 0.05	−0.018 ± 0.020
LAT	7.4	1:100	4090 ± 50	1.72 ± 0.05	−0.126 ± 0.017
LAT	7.4	1:50	4120 ± 50	1.78 ± 0.05	−0.125 ± 0.017
LAT	7.4	1:10	4110 ± 50	1.88 ± 0.05	−0.096 ± 0.013
LW21	7.4	1:100	4190 ± 50	1.58 ± 0.05	−0.158 ± 0.021
LW21	7.4	1:50	4150 ± 50	1.75 ± 0.05	−0.119 ± 0.016
LW21	7.4	1:10	4180 ± 50	2.77 ± 0.05	−0.020 ± 0.020

Based on the measured data, several conclusions have been drawn: Firstly, the relaxation time of Laurdan is prolonging with the increasing concentration of peptides with expected transbilayer orientation (alamethicin and LAH_4 at pH 8). Increase in relaxation time is well detectable also for LAT and LW21 transmembrane peptides. A prolongation of Laurdan relaxation time is the most significant in membranes containing alamethicin, LAH_4 and LW21 at the highest measured concentrations. The relaxation time prolongation is weaker in the case of LAT peptide, but the difference is still evident. Membranes containing peripheral peptides and control lipid membranes

provide comparable relaxation times indicating that the degree of mobility of carbonyl groups is not influenced by the peripherally bound peptide. Secondly, the spectral shift appears to be constant (Δν values within experimental error) for all tested cases except a small deviation of LW21 peptide.

Discussion

Measured Laurdan values for alamethicin and LAH_4 peptides (transmembrane orientation) and our newly designed LW21 and LAT peptides exhibited similar trend: Prolongation of relaxation time and constant or slightly increased spectral shift with increasing content of peptides. These data confirmed expected transmembrane orientation of LW21 and LAT peptides. Prolonged relaxation time observed for membranes containing peptides with transmembrane orientation reports on a direct interaction between peptides and lipids at glycerol level. The mobility of acyl groups is slowed down due to the presence of integral peptides. As will be discussed in detail in section corresponding to Paper IV, the mobility is lowered due to temporal trapping of lipids on rough surface of the peptide. On the other hand, no change of relaxation time τ_r for membranes containing peripheral peptides indicates that the lipid carbonyl groups being about 1 nm below the external surface of the bilayer are not influenced by tested peripherally bound peptides.

Surprisingly, the effect of LAT peptide on Laurdan relaxation time was weaker compared to all other tested transmembrane peptides. We speculate that this is caused by the presence of helix-breaker-amino acids, proline and glycine, that kink its helical structure. Helix kink allows rocking of individual peptide segments. Such movement, absent from the rigid helix of the LW21 peptide, could weaken the direct interaction between carbonyl groups of the lipids and the polar groups of the peptide.

Remarks on the interpretation of GP and Δν values

The examination of phase transitions in lipid membranes showed correlation between decreased level of hydration (smaller spectral shift Δν) and reduced mobility of hydrated carbonyls (longer relaxation time τ_r) [133]. However, this is not a general property of all systems. The studies investigating the effect of ions or heavy water on membrane mobility and hydration showed only small changes in the polarity parameter Δν compared to the changes of mobility parameter τ_r [134,135]. For example in the

"ions case", this can be interpreted so that the network of hydrogen bonds in the lipid carbonyl region is strengthened by the presence of the ions, but the amount of water molecules does not change. Our results from membranes containing peptides are similar to the mentioned studies. The hindered rotational and translational freedom of the acyl groups (longer relaxation time) is accompanied with the unchanged (compared to peptide-free membranes) or slightly increased polarity. Such results indicate that the level of hydration is not changed significantly and that the peptide does not disrupt membrane integrity.

GP value is sometimes interpreted as an indicator of "extent of water penetration" [136]. This interpretation assumes: A lower the GP value is more water molecules are located at the carbonyl level of phospholipids and, as a consequence, membrane components are supposed to be more mobile. Our results show increasing GP values with increasing content of integral peptides. Based on the interpretation mentioned above, such result would indicate a lower amount of water molecules inside the lipid membranes containing peptides compared to pure lipid membranes. However, polarity ($\Delta\nu$) is not affected in tested proteo-lipid membranes or is increased for the case of LW21 peptide. This is a contradiction implying that Laurdan GP cannot be generally considered as an indicator of "extent of water penetration". Such interpretation is typically valid only if an increase of τ_r is accompanied with a decrease in $\Delta\nu$ (or *vice versa*). We, therefore, prefer TDFS measurements instead of standard GP evaluation by spectral demixing.

An example of alternative GP interpretation was reviewed in [82]. The dependence of Laurdan $\Delta\nu$, τ_r and GP on temperature in DMPC vesicles was investigated in this work. Results demonstrate that GP values followed closely the trend of decreasing τ_r with increasing temperature. The polarity parameter $\Delta\nu$ increased slightly with increasing temperature. Those results and results from Paper III indicate the important conclusion that GP reflects more the membrane mobility than membrane hydration at the depth of lipid carbonyl groups.

The attached Paper III further addresses the question of membrane penetration efficiency of antimicrobial peptide LAH_4. This part was of primary interest of my colleagues and I was not involved in FCS-based dye leakage assays. Therefore, this part is not further discussed in this thesis.

Paper IV

5.4 The impact of transmembrane peptides on lipid membrane properties

Motivation

The studies described in the previous chapters were necessary pre-requisites for our research described in this section. In my opinion, this chapter describes the most interesting results of my work. For this reason, some parts are longer than in previous studies to provide sufficient evidence for our findings.

Cellular membranes are formed largely by lipids but proteins can constitute up to 50% of their total mass [137]. This opens a question how integral proteins influence the structure and dynamics of lipid membranes. Integral proteins span membrane via one or multiple transmembrane domains (TMDs) to deal with the hydrophobicity of lipid membranes. TMDs are in direct contact with lipids which allows for many possible interactions between the TMD and the lipids. Although these facts are generally known, the precise effect of proteins on lipid organization is not clear.

Lipids in the first shell that are surrounding protein TMD are called annular lipids. Annular lipids behave differently compared to bulk lipids which are not in a direct contact with proteins. The existence of annular lipids was confirmed by EPR studies by observing a different level of mobility of annular and bulk lipids [138,139]. Interaction of proteins and annular lipids is expected to follow the mattress model, which predicts that length of annular lipids adapts to the length of hydrophobic part of protein to cope with hydrophobic mismatch. This was demonstrated in model systems [140], where the hydrophobic mismatch between transmembrane peptide and surrounding lipids caused systematic changes in average membrane thickness. Thus, the ability of proteins to change local environment might have an effect on lipid organization. If e.g. length of protein TMD is larger than average thickness of the surrounding membrane, annular lipids might react in the way, that they straighten their acyls chains. It could also lead to lateral sorting – specific lipids might be attracted to protein surfaces. Locally the thickness of bilayer would be bigger which might further attract other lipids with long acyl chains or repel lipids with short acyl chains.

Lipid acyl chain length adaptation is not the only way how to cope with hydrophobic mismatch. It was shown that in case of positive hydrophobic mismatch (lipid bilayer is thin compared to peptide length) model transmembrane peptides might

avoid incorporation into lipid membranes and prefer extramembranous aggregates, the extent of such incorporation is also influenced by flanking residues and lipid membrane composition [141]. In addition, long transmembrane peptides can tilt in a bilayer; however the measured tilt angles were typically insufficient to match differences in membrane thickness and the peptide length. Therefore, a combined effect of tilt and other adaptations is expected [142]. Another way is to form peptide clusters to minimize contact with non-matching lipids [130,143]. The adaption of lipids or peptides to negative hydrophobic mismatch is analogous. Lipid acyl chains can shorten their lengths by disordering [140], peptides can self-associate [144], non-lamellar phase formation can be induced [145]. The incorporation of such peptides into thick membranes is generally poor [57]. Peptide backbone distortion was also suggested as a response to hydrophobic mismatch, but so far it has not been observed experimentally.

We have discussed local membrane changes, but proteins may influence also global membrane dynamics. It was shown that membrane dynamics is reduced in the presence of large proteins. Ramadurai and colleagues measured lateral diffusion of several purified proteins embedded in fully hydrated lipid membranes using fluorescence techniques. They found that protein diffusion linearly decreased with increasing protein content provided the concentrations were above a certain threshold [93]. The interpretation was that this is an impact of protein crowding, which agreed well with the existing theoretical predictions [146]. The focus was on large, multispanning membrane proteins. However, the most of proteins in cellular membranes are small (single-spanners) and mobile, and the interpretation of their results as the impact of obstacles is questionable. We were therefore interested whether a small and highly mobile model of a simple transmembrane protein can influence membrane dynamics and what is the mechanism responsible for this effect. To distinguish the pure effect of protein on membrane properties we decided to study the effect of small transmembrane peptide on membrane dynamics under matching conditions.

Results: Introduction of experimental system

Therefore, a model system of choice is important. As mentioned in previous paragraphs, we wanted to focus on highly fluid environment so that the peptide fits well in a membrane and its hydrophobic length matches the thickness of the lipid bilayer. To see the effect of a single peptide helix, we preferred to avoid peptide oligomerization. And finally, even after addition of third component, cholesterol, phase separation or

nanodomain formation would be undesired. Cholesterol was added to better mimic real plasma membrane.

To fulfill all mentioned conditions we selected and tested the following system: DOPC glycerophospholipid in combination with already introduced transmembrane peptide LW21. Its primary structure is:

LW21: GLLDSKKWWLLLLLLLLALLLLLLLLWWKKFSRS

The identity and purity of the synthetic LW21 peptide (> 92%) was confirmed by mass spectrometry and analytical HPLC. It was shown previously that the peptide possesses predominantly α-helical structure in a lipid bilayer [57] .

To verify appropriateness of our model system, we performed several tests. First, the incorporation of our modified and freshly synthesized LW21 peptide in lipid membranes was tested based on a comparison of average fluorescence intensities of labeled peptides (Atto488-LW21) in lipid bilayers of different thicknesses (different acyl chain length: di-14:1 PC, di-18:1 PC, i.e. DOPC, and di-22:1 PC). The test confirmed the most efficient incorporation of LW21 into di-18:1 PC and di-22:1 PC in the absence of cholesterol (Figure 20).

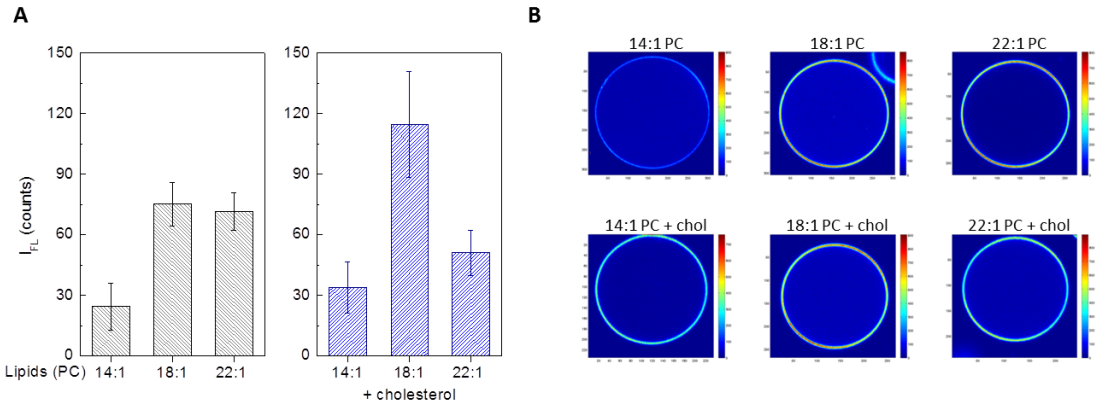

Figure 20. Incorporation of the LW21 peptide into membranes with different thickness. A. An average fluorescence intensity of fluorescently labeled peptide incorporated into GUVs composed of phospholipids with varying acyl chain length was determined in the absence (left panel) or presence (right panel) of 25 mol% cholesterol. The same amount of labeled peptide was used for the preparation of GUVs of various thicknesses. **B.** Representative examples of homogeneous peptide distribution along GUVs of different membrane thickness.

In the presence of cholesterol, maximum incorporation of the peptide was observed for di-18:1 PC membranes (Figure 20). These results are in agreement with previously published data [57]. Glycerophospholipid DOPC with and without cholesterol was therefore selected for further studies. Such system also fulfills another requirement: the absence of lipid nanodomains as confirmed in Paper II.

Monomeric character of LW21 peptide was tested by time-resolved anisotropy decays of tryptophan residues present in peptides. Anisotropy decays were recorded for LUVs containing up to 5 mol% of LW21 peptide, as well as dimeric and monomeric control samples. We used peptide C_2-LW21 as a dimeric control (MW 8579, $(CGLLDPKKWWLLLLLLLLALLLLLLLLWWKKFSRS)_2$. The dimer was obtained by cysteine oxidation of monomeric peptide. The antimicrobial peptide mellitin served as a monomeric control. All compositions containing LW21 peptide resulted in anisotropic decays following the shape of monomeric control suggesting a monomeric state of our LW21 peptides (Figure 21). In addition, studies of similar systems with WALP family peptides (i.e. peptides with alternating Leu and Ala sequence flanked by Trp, e.g. $WW(LA)_8LWW$) confirmed no or limited aggregation of peptides in DOPC membranes at concentrations tested herein [143].

One of the requirements, the transbilayer orientation of LW21 peptides in glycerophospholipid membranes was confirmed by a novel application of TDFS. More details were described in the previous chapter (Paper III).

To conclude this part: the system of LW21 peptide incorporated in DOPC with and without cholesterol was properly selected for further testing in the absence of: phase transition, bulky structures causing crowding (e.g. by extracellular domains of proteins), peptide aggregation and hydrophobic mismatch.

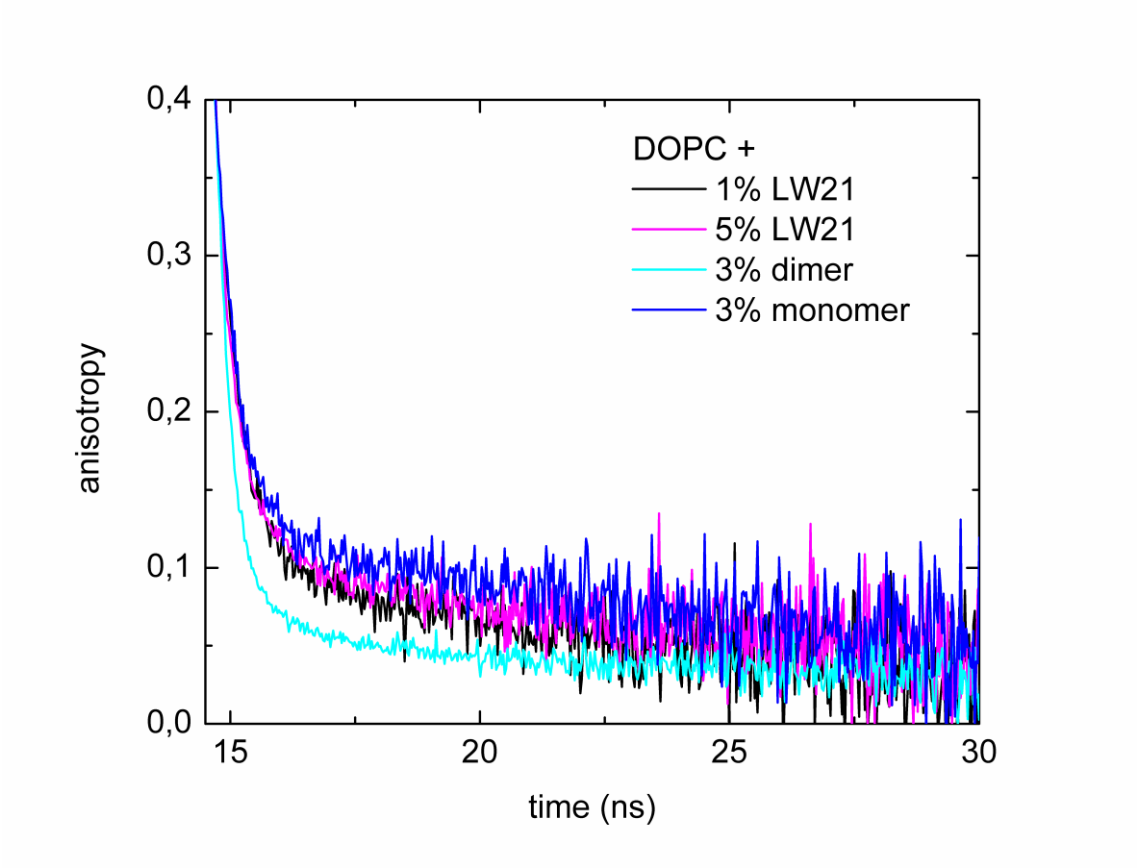

Figure 21. LW21 peptide is monomeric and non-aggregated in tested membranes. Time resolved fluorescence anisotropy decays of LW21, C_2-LW21 and melittin peptides in DOPC membranes demonstrate the monomeric state of LW21 peptide at both concentrations, 1 and 5 mol%. Melittin represents a monomeric control, whereas C_2-LW21 dimerizes due to the presence of free cysteine in its N terminus.

Results: The impact of a simple α-helical transmembrane peptide on lipid membrane dynamics

Proper choice and characterization of the model system allowed us to compare the dynamics of peptides and lipids in GUVs containing 0-3 mol% LW21 in the presence and absence of 25 mol% of cholesterol. Diffusion of fluorescently labeled peptide Atto488-LW21 and lipid marker DiD was measured by z-scan FCS technique at the top of GUVs. We observed reduced mobility of both peptides and lipid markers with increasing peptide concentration (Figure 22A). At the highest tested peptide concentration, 3 mol%, diffusivity of both molecules was reduced by approximately 35% in DOPC membranes. In agreement with the literature [147], lipid molecules diffused somewhat faster than peptides at all tested peptide concentrations. The mobility reduction was intensified in the presence of cholesterol (Figure 22A). At the highest

peptide concentration, 3 mol%, we observed 2-3 fold decrease in the diffusion coefficients for both tested molecules. Importantly, lateral diffusion of lipids and peptides was indistinguishable in membranes with cholesterol (Figure 22A).

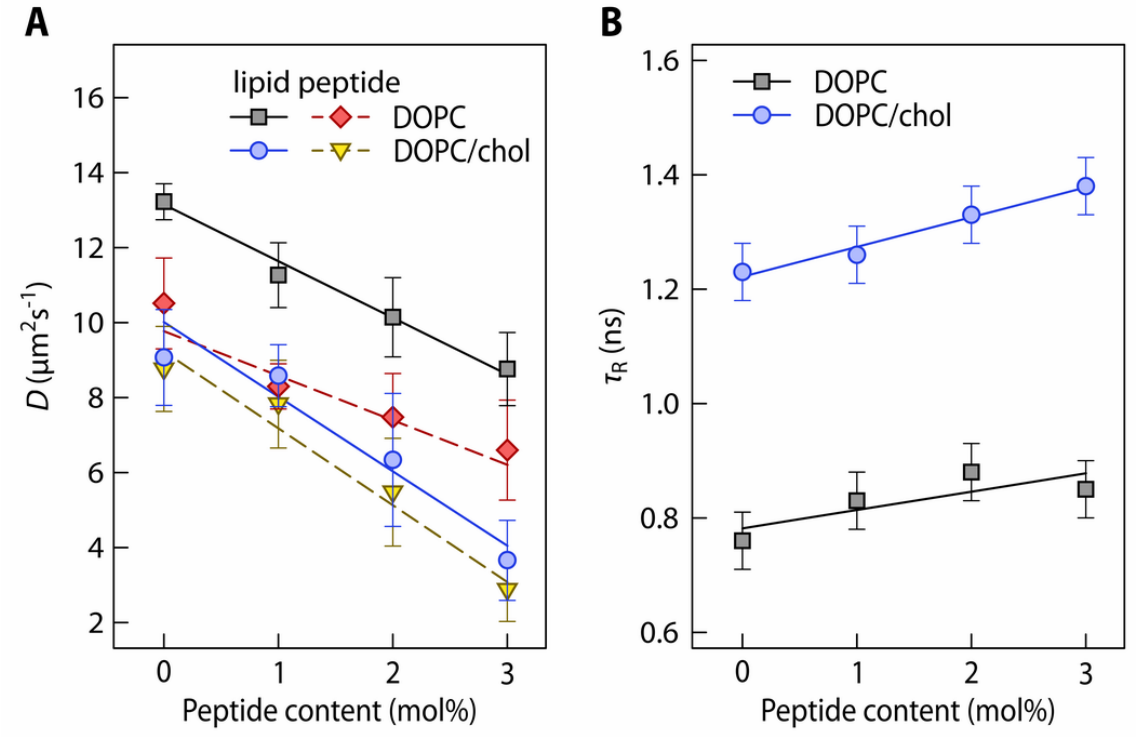

Figure 22. **Impeded local viscosity and lateral diffusion in membranes with peptide. A.** Lateral diffusion coefficients of lipid tracer (DiD; full lines) and fluorescently labeled LW21 peptide (dashed lines) were measured in GUVs composed of DOPC (black and red lines) and DOPC:cholesterol (3:1; blue and yellow lines), in the presence of increasing concentration of unlabeled peptide. Each presented diffusion coefficient (*D*) was measured for at least 10 vesicles in three independent experiments using calibration-free *z*-scan FCS technique. Error bars indicate standard deviations (SD). **B.** Local lipid mobility (viscosity) as a function of increasing peptide concentration was determined in the absence (black squares) or presence (blue circles) of 25 mol% cholesterol using Laurdan fluorescent probe by TRES. The relaxation time τ_R reports on the local lipid mobility. Error bars represent intrinsic uncertainty of the method.

The diffusion of lipid marker was free for all tested membrane compositions as indicated by anomalous coefficient equal to one (Table 8). Therefore, the peptides cannot be considered as obstacles for diffusing lipids. Lipid markers and peptides moved independently as indicated by zero amplitude of cross-correlation between peptide and lipid fluorescence signals (Figure 23).

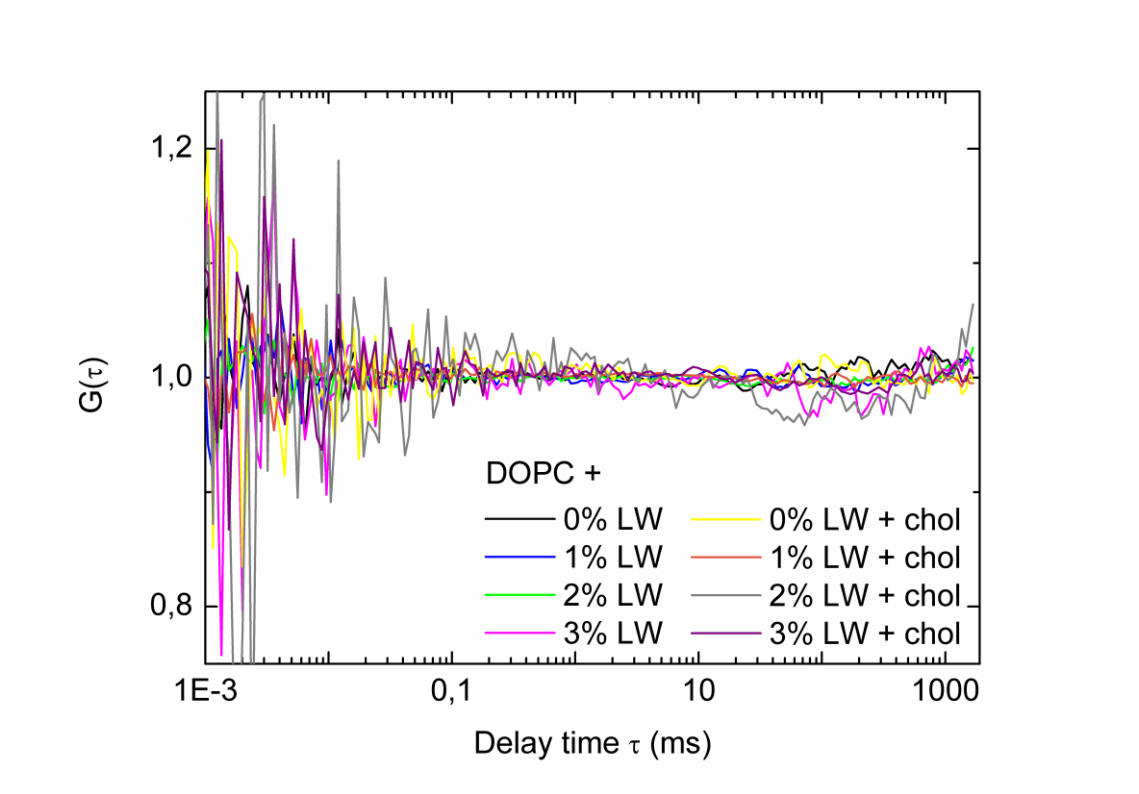

Figure 23. No cross-correlation between lipid marker DiD and fluorescently labeled peptide indicates independent movement of peptides and lipid markers. Depicted curves show a typical shape of cross-correlation between the two channels at the z-plane, where the membrane was in focus.

Table 8. Average anomalous coefficients and standard deviations for DiD dye in DOPC and DOPC+cholesterol membranes. Anomalous coefficients were obtained by fitting of autocorrelation curves to a model of anomalous diffusion in 2D. Autocorrelation curves were calculated for the z-position where the membrane was in focus.

Peptide content [%]	Anomalous coefficient	
	DOPC	DOPC + chol
0	0.99 ± 0.02	0.99 ± 0.02
1	0.99 ± 0.01	0.99 ± 0.01
2	0.99 ± 0.01	0.99 ± 0.01
3	0.99 ± 0.01	0.99 ± 0.01

The reduction of membrane dynamics was supported by z-scan FCS measurements performed using LW21 peptides of different batch. These peptides were synthetized by U.S. company Biomatik. We measured diffusion coefficients of BODIPY-FL-DHPE lipid marker in DOPC membranes with increasing concentrations of the peptide (Figure

24). In agreement with previous results, the lipid marker diffusion was reduced with increasing concentration of peptides. The addition of various concentrations of cholesterol further reduced the diffusion of lipid markers. The mass spectrometry analysis kindly provided by Ján Sabó (J. Heyrovsky Institute of Physical Chemistry of the CAS) and Petr Novák (Institute of Microbiology of the CAS) revealed limited purity and stability of this batch of peptide. Therefore, these results were not used in the submitted manuscript. However, those experiments confirmed reduced lipid mobility in the presence of peptides under different experimental conditions.

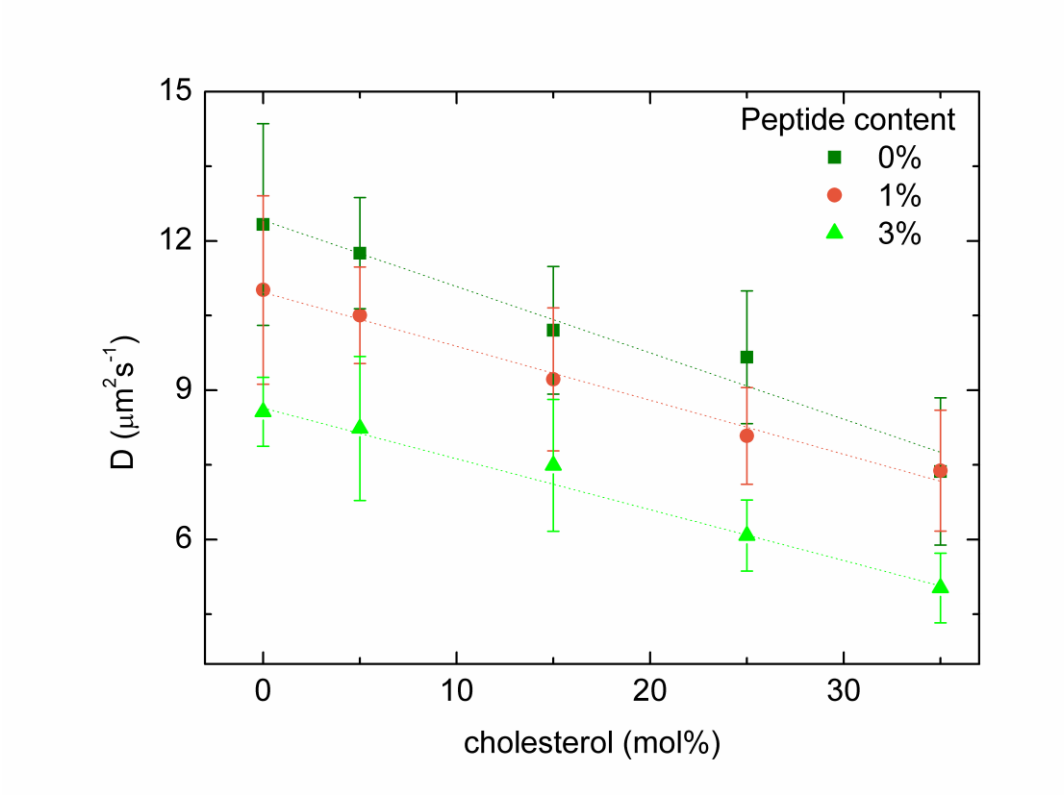

Figure 24. **Reduced mobility of lipids in the presence of peptides and cholesterol.** Diffusion coefficients of lipid marker BODIPY-DHPE in GUVs composed of DOPC, cholesterol (0-35 mol%) and unlabeled transmembrane peptide LW21 (0-3 mol%; a batch synthetized by Biomatik, US). Measurements were performed at room temperature. Mean and standard deviation were obtained from at least seven GUVs and at least two independent sets of measurements.

Furthermore, we evaluated membrane dynamics at the nanoscale using environment-sensitive fluorescent probes. We performed TDFS of Laurdan experiments, this time 0-3 mol% LW21 peptide was embedded in DOPC resp. DOPC with 25 mol% cholesterol LUVs. In agreement with previous results in POPC membranes, relaxation time τ_r prolonged with increasing peptide concentration indicating restricted movement of lipid

carbonyl groups in the presence of peptides (Figure 22B). Significant increase of τ_r as a function of peptide content in DOPC membranes entails that LW21 hinders mobility of lipids. The impact of peptides was slightly stronger in the presence of cholesterol compared to its absence (linear regression slope of 0.05 versus 0.03, respectively). The second TDFS parameter, polarity, was constant irrespective of peptide concentration suggesting that peptides do not disturb the structural integrity of lipid bilayer and fluid lipids adapt to the presence of this 'imperfect' membrane components. TDFS measurements of Laurdan probe provide information about the movement of lipid carbonyl groups. To gain also the information about lipid acyl chain ordering, we performed time-resolved anisotropy measurements of DPH probe in LUVs of analogous compositions. The obtained order parameter increased with increasing concentration of peptides indicating restricted movement of lipid acyl chains in the presence of peptides. Experimental results pointed to the increased viscosity caused by the presence of peptides.

Table 9. Order parameter *S* of DPH in membranes with the LW21 peptide.

Membrane (LUV)	*S* (DOPC)	*S* (DOPC/cholesterol)
DOPC	0.19 ± 0.06	0.43 ± 0.01
DOPC + 3% LW21	0.28 ± 0.04	0.51 ± 0.05
DOPC + 10% LW21	0.39 ± 0.02	0.55 ± 0.08

Results: Mechanism behind reduced mobility of membrane molecules in the presence of LW21 peptide

To get more molecular insight into our experimental data we used all-atom MD simulations. All MD simulations were performed by Lukasz Cwiklik. LW21 peptide in the form of an ideal α-helix was inserted into the membrane in transbilayer manner. MD simulations were carried out in the absence or presence of 25 mol% cholesterol for 500 ns at the temperature of 293 K. MD simulations confirmed considerably impeded mobility of lipids close to the peptide (Figure 25). Interestingly, we observed that this is caused by the rough surface of the peptide and trapping of acyl chains of annular lipids in the grooves therein (Figure 26). Contacts between peptide and lipids were found to be

rather stable and non-specific. Statistical analysis of simulated data confirmed retarded movement of lipids in the proximity of the peptide (in both types of membranes: DOPC +/- cholesterol) and a limited number of contacts between cholesterol and peptide molecules indicating the exclusion of cholesterol away from the peptide surface (Figure 26). This is probably caused by the incompatibility between the planar shape of cholesterol molecule and the roughness of transmembrane peptides. Our findings demonstrate that the mobility of lipids is affected by a single transmembrane domain due to its rough surface. Rough surface is an intrinsic property of probably all stable helical peptides formed by native amino acids and is not limited to poly-leucine segment studied herein. A rough surface decorates all TMDs of proteins characterized so far by crystallography or NMR at sufficient resolution (< 4.5 Å; PDBTM database - pdbtm.enzym.hu [148]).

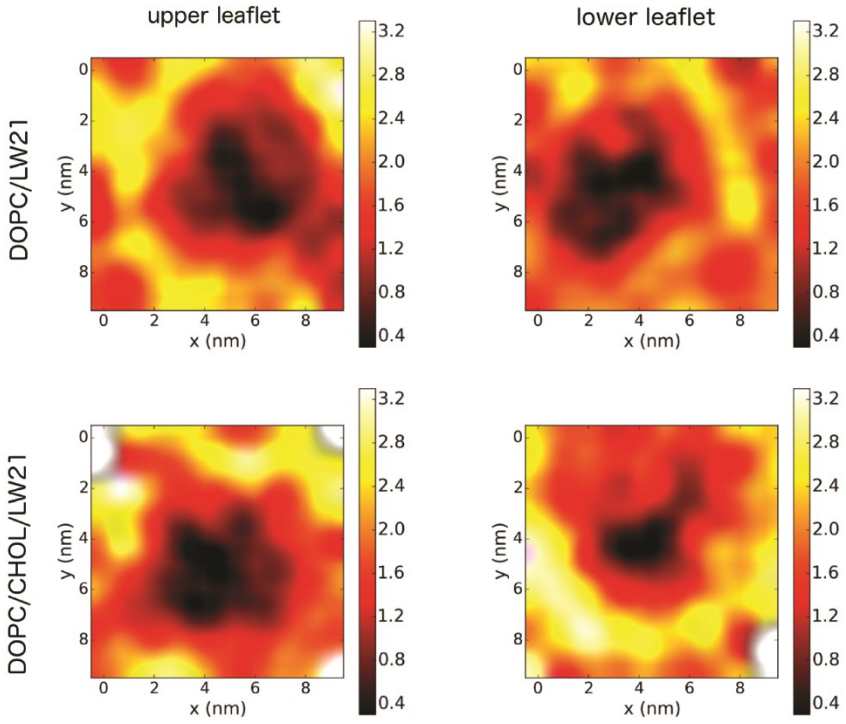

Figure 25. **Retardation of phospholipids in the vicinity of the LW21 peptide surface – maps for both leaflets presented.** Lateral diffusion maps of lipids as resolved by all-atom MD simulations in the absence (upper row) and presence of cholesterol (bottom row) for the individual membrane leaflets (left/right column). The maps are centered to an average position of the LW21 peptide. The plots show the average distance travelled by a lipid starting at a particular lateral position in a bilayer over 100 ns time.

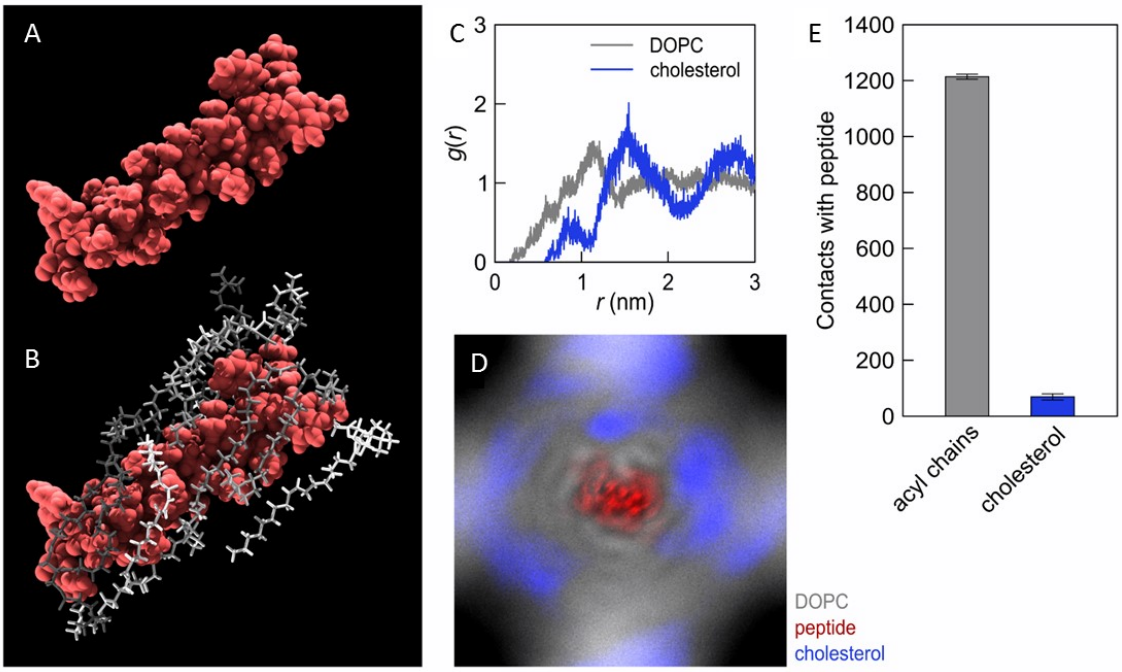

Figure 26. **Non-specific lipid acyl chain trapping on the rough surface of LW21 peptide and cholesterol segregation – MD simulations. A and B.** A typical snapshot from MD simulation of the peptide in DOPC bilayer indicating trapping of lipid acyl chains in the grooves formed by peptide amino acid side chains. Peptide surface (A) is shown in red. Interacting lipids are shown in different shades of grey using licorice representation (B). Non-interacting lipids and water were removed for clarity. **C.** Pair correlation function [g(r)] of phospholipids and cholesterol from the center of mass of the peptide. This function quantifies the probability of intermolecular distances between the peptide and lipids with respect to those in an ideally mixed system. **D**. Distribution map of cholesterol (blue) and phospholipids (grey) in membrane with peptide (red). The peptide was centered and rotations were removed by data postprocessing. **E.** Quantification of phospholipid and cholesterol contacts with the peptide calculated in MD simulations. Error bars represent error of the mean estimated by the block averaging method.

The data acquired using LW21 peptide could not be compared with a smooth variant since all α-helix-forming amino acids intrinsically form structures with a rough surface. Therefore, we generated the coarse grain toy models of cylinder-like objects with varying surface roughness (M1-M3; Figure 27A) which were embedded in DOPC membranes. The autocorrelation data acquired from MD simulations indicate longer lipid contacts with the rougher models (M3 > M2 > M1; Figure 27B). The acyl chains are entrapped in the grooves of the rough models (M2 and M3) which hinders their mobility. Virtually no trapping was observed at the smooth surface of model M1. The results from MD simulations provide proof that roughness is a unique property of peptides influencing membrane dynamics.

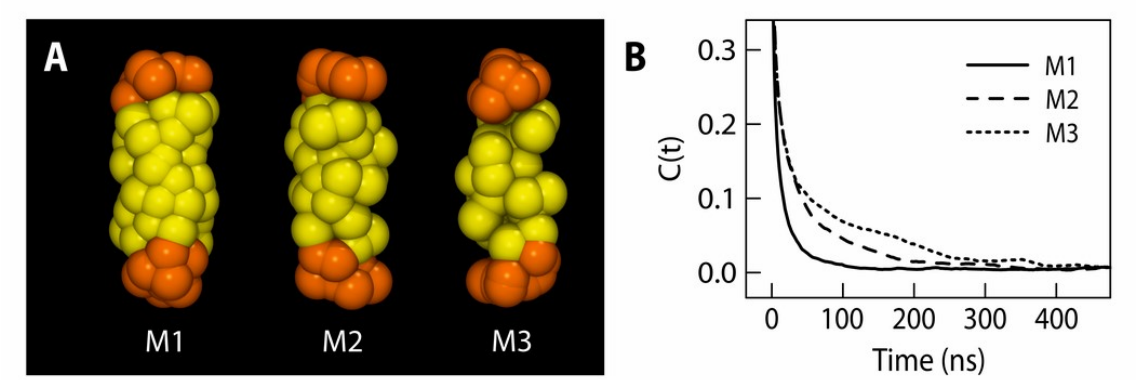

Figure 27. Rough surface interferes with membrane dynamics. A. Toy models (M1-M3) of cylindric-like structures generated using coarse grain force field. **B.** The autocorrelation curves for contacts between lipid tails and the surface of model structures M1-M3 with increasing roughness embedded in DOPC membrane indicating trapping of acyl chains at the rough surface of M2 and M3.

Discussion: Presence of α-helical transmembrane peptide in lipid membranes reduces mobility of membrane components

In this work, we have investigated how a small and highly mobile transmembrane protein can influence membrane dynamics and organization under well-controlled conditions in synthetic model membranes. Our model system was selected to avoid impact of factors which were previously shown to influence membrane dynamics, e.g. hydrophobic mismatch, crowding and molecular clustering (aggregation). In summary, our experimental and computational data provide the evidence that lipids non-specifically and transiently interact with the rough surface of α-helical transmembrane peptides which leads to increased local viscosity and reduced lateral diffusion of membrane components. Rough surface is an intrinsic property of all transmembrane peptides due to the fact that amino acid residues point outward of the central helix. Residues naturally form grooves and peaks where the subtle acyl chains can be temporarily trapped. The only exception to this rule is amino acid glycine, whose side chain is a single hydrogen atom. As a consequence, poly-Gly helix would have a smooth surface. However, such situation is highly improbable due to glycine preference for β-sheet secondary structure. Therefore, the reduction of membrane components' mobility is expected by probably all transmembrane protein structures. Indeed, the theory of lipid trapping on rough surface of peptides and slowing down of membrane

dynamics is also supported by other experimental works performed with large transmembrane proteins spanning the membrane via several α-helices. For example, the crystallographic studies of transmembrane protein aquaporin were able to resolve structures of annular lipids indicating that these lipids were strongly bound (i.e. trapped at the surface) [149]. Also, inverse correlation between protein density and lateral diffusion has been observed in both model and cell membranes [79,93,150]. In addition, a computational study showed collective lateral diffusion of annular lipids with large proteins [151]. Our study for the first time shows that even small peptides with their rough surface have large impact on membrane dynamics.

Discussion: The effect of cholesterol on proteo-lipid membrane organization

Experimental data for both types of membranes, in the presence and absence of cholesterol showed the equal trends – slowing down of membrane components in the presence of peptides. Nevertheless, the magnitude of such change was different in the presence and absence of physiological levels of cholesterol. FCS and TDFS data showed stronger mobility reduction in the presence of cholesterol, whereas the change in order parameter (DPH anisotropy) was more pronounced in the absence of cholesterol. This probably happens due to the cholesterol ability to alter the interior of membranes and parts closer to the water interface differently. Cholesterol stabilizes a lipid membrane by ordering its hydrophobic interior, increasing lipid packing and sealing it against water-soluble molecules [152]. The highly ordered interior of cholesterol-containing membranes is thus less susceptible to further ordering but the presence of peptide is still causing an increase in order as measured by DPH. This increase was smaller than the one obtained in pure DOPC membrane. Cholesterol impact on headgroup parts is weaker, but not negligible. Our TDFS results show that mobility of DOPC lipid carbonyls, which is hindered by cholesterol, is further reduced by the peptide. In fact the change in this local viscosity caused by the peptide is slightly larger in the presence of cholesterol. This synergic action of peptide and cholesterol is also manifested in two-three-fold slowdown of lipid diffusion upon addition of peptide, which outperforms the changes induced by the peptide in pure DOPC.

In silico experiments revealed segregation of cholesterol away from peptide surface. This finding is supported by similar protein-lipid simulations [153,154]. The main reason for cholesterol segregation could be probably found in the rigid body of

cholesterol that is unable to adapt to the rough surface of peptides. As a result, cholesterol is excluded from the peptide surface and more flexible lipid acyl chains preferentially occupy this space.

Cholesterol exclusion from peptide surface could have far-reaching consequences for cell membrane organization. We speculate that unless there is a specific interaction between cholesterol and a protein, or the protein surface is shaped to fit cholesterol structure, the probability of finding protein and cholesterol molecules in close proximity is very low. This, in principle, could lead to a segregation of the two molecules into different membrane domains or areas. The segregation of cholesterol from proteins could cause formation of high cholesterol content area free of transmembrane proteins, as was recently suggested in the literature [155]. It could also lead to preferential positioning of peptides and proteins to more fluid lipid environment with more favorable lipid packing.

6 Summary

In the thesis, we investigated properties of lipid membranes and influence of peptides on membrane dynamics. We covered several topics, which all pointed towards characterization of proteo-lipid membranes. Initially, we characterized fluorescence probes reporting on membrane viscosity. Further, we detected lipid inhomogeneities in membranes and studied their properties. We utilized a sensitive fluorescence technique for determination of membrane protein orientation. With help of the achieved results, we were able to propose an optimal model system for studies of protein-lipid interactions and we discovered that even small single-spanning proteins can affect membrane properties. They do so by slowing the membrane dynamics due to a nonspecific temporary trapping of lipids at the rough surface of peptide.

More specifically, we reached the following conclusions:

- Molecular rotors based on BODIPY structure are used as viscosity sensors, but their membrane localization is poorly characterized. We designed new molecular rotors with a deeper localization within membrane by increasing the number of C12 alkyl chains linked to the fluorophore moiety. Detailed characterization of original and newly synthetized BODIPY-based molecular rotors by various fluorescence techniques revealed complex positioning and orientation of probes depending on composition and the rigidity of the membrane. The use of such molecular probes is, therefore, limited to membranes with simple composition.
- Formation of nanodomains triggered by the presence of cross-linker in model membranes at lipid compositions close to the optically resolvable phase separation boundary was observed. For the first time, the formation of two different types of sub-resolution domains was presented, including the estimation of their size. The work provided tools how to study nanodomain formation which remains elusive for conventional microscopy imaging.
- The TDFS method was introduced to identify the mode of peptide orientation in lipid membranes and to characterize the effect of transmembrane peptides on the bilayer organization. The main advantage of this approach is that no peptide modification or peptide labeling is necessary to gain the information about its membrane orientation. TDFS sensed by Laurdan in POPC bilayers in the presence

of transmembrane proteins indicates that there is a direct interaction between the peptide and lipids in the bilayer.

- Single transmembrane peptides change the model membrane properties by non-specific and transient interactions of annular lipids with the rough surface of α-helical transmembrane peptides. Trapping of acyls chains leads to increased local viscosity and reduced lateral diffusion of membrane components. A tendency of cholesterol to segregate from TMDs might help formation and/or stabilization of cholesterol-enriched, protein-low domains. Such changes will locally affect intermolecular interactions or reaction kinetics of cellular processes associated with membranes and thus affects vital functions of living cells.

Our work on lipid membranes with proteins extends the understanding of cell membranes densely populated by proteins. The results add to the mosaic of factors influencing membrane organization and associated processes. Our results might help to interpret observations made using highly complex systems, e.g. living cells, which are not suitable for elementary studies, such as the one presented in this work.

7 Outlook

The thesis opens several possible directions of further research. Lipid acyl chain trapping on peptide rough surface raises a question whether there is preference of specific lipids to adapt to lipid surface. For example, good candidates for trapping are polyunsaturated fatty acids (PUFA) which are known to modulate membrane organization due to their flexibility [156]. The conformational flexibility is ensured by energetically undemanding rotation along single carbon bonds [157], making membranes composed of PUFA more disordered compared to membranes composed of saturated and mono-unsaturated acyl lipid chains. We speculate, whether PUFA could twist around TMD and fill in all grooves to make the surface softer and thus regulate membrane fluidity. We performed preliminary test to monitor dynamics of lipids and peptides in GUVs composed of DOPC, 3% LW21 and increasing amount of arachidonic acid (Eicosa-5Z,8Z,11Z,14Z-tetraenoic acid; PUFA) by z-scan FCS approach. The dynamics of membrane components was not significantly influenced by the presence of arachidonic acid (Figure 28). However, other comparative tests how PUFA alone change membrane dynamics are needed. Likewise, what amount of PUFA would be necessary for detectable effect on membrane organization.

Further, the effect of cholesterol would be subject of very interesting study. The cholesterol segregation from protein surface might cause its enrichment in low protein areas, i.e. unequal distribution of cholesterol in membrane. The intensity of this effect is currently not known. Cholesterol segregation from peptide surface in model membranes might be again strengthened by the presence of PUFA that are known to be sterically incompatible with cholesterol (reviewed in [156]).

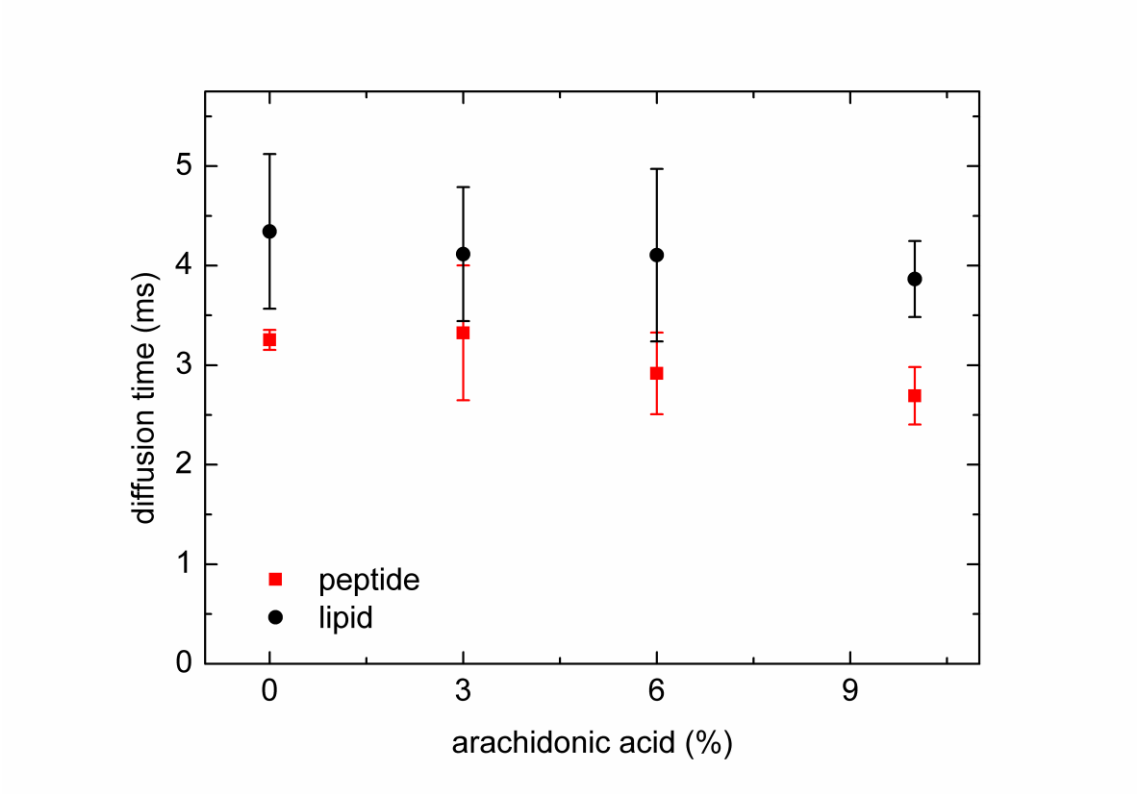

Figure 28. The effect of PUFA on model membrane dynamics. The presence of arachidonic acid (PUFA) in GUVs composed of DOPC and 3% LW21 does not significantly alter the dynamics of lipid markers (DiD) and fluorescently labeled peptides (LW21 peptide labeled with covalently linked Atto488 dye).

Finally, areas with high protein density will significantly reduce membrane dynamics. The effect in the high protein density area might be also mimicked in model lipid membranes. Biotinylated transmembrane peptides could be cross-linked by streptavidin to form clusters of defined size and conformation. The effect of such clusters on membrane dynamics and the dynamics inside the clusters could be studied by fluorescence techniques, thus providing a better insight into the behavior of such more complex systems, providing again an environment more comparable to living cells.

8 References

[1] S.J. Singer, G.L. Nicolson, The fluid mosaic model of the structure of cell membranes, Science, 175 (1972) 720–731.

[2] R. Phillips, T. Ursell, P. Wiggins, P. Sens, Emerging roles for lipids in shaping membrane-protein function, Nature, 459 (2009) 379–85.

[3] O.S. Andersen, R.E. Koeppe, Bilayer thickness and membrane protein function: an energetic perspective, Annu. Rev. Biophys. Biomol. Struct., 36 (2007) 107–30.

[4] R.G.W. Anderson, K. Jacobson, A Role for Lipid Shells in Targeting Proteins to Calveolae, Rafts, and Other Lipid Domains, Science (80-.)., 296 (2002) 1821–1826.

[5] C. Thiele, M.J. Hannah, F. Fahrenholz, W.B. Huttner, Cholesterol binds to synaptophysin and is required for biogenesis of synaptic vesicles, Nat. Cell Biol., 2 (2000) 42–9.

[6] F.-X. Contreras, A.M. Ernst, P. Haberkant, P. Björkholm, E. Lindahl, B. Gönen, C. Tischer, A. Elofsson, G. von Heijne, C. Thiele, R. Pepperkok, F. Wieland, B. Brügger, Molecular recognition of a single sphingolipid species by a protein's transmembrane domain, Nature, 481 (2012) 525–9.

[7] G. van Meer, D.R. Voelker, G.W. Feigenson, Membrane lipids: where they are and how they behave, Nat. Rev. Mol. Cell Biol., 9 (2008) 112–24.

[8] M. Caffrey, G.W. Feigenson, Fluorescence quenching in model membranes 3 Relationship between calcium adenosinetriphosphatase enzyme activity and the affinity of the protein for phosphatidylcholines with different acyl chain characteristics, Biochemistry, 20 (1981) 1949–1961.

[9] L. Yetukuri, K. Ekroos, An. Vidal-Puig, M. Orešič, Informatics and computational strategies for the study of lipids, Biochim. Biophys. Acta - Mol. Cell Biol. Lipids, 1811 (2011) 991–999.

[10] B. Alberts, A. Johnson, J. Lewis, E. Al, Membrane proteins, Mol. Biol. Cell, (2002).

[11] O.G. Mouritsen, M. Bloom, Mattress model of lipid-protein interactions in membranes, Biophys. J., 46 (1984) 141–53.

[12] M.B. Ulmschneider, M.S. Sansom, Amino acid distributions in integral membrane protein structures, Biochim. Biophys. Acta, 1512 (2001) 1–14.

[13] T.K.M. Nyholm, S. Özdirekcan, J.A. Killian, How Protein Transmembrane Segments Sense the Lipid Environment, Am. Chem. Soc., 46 (2007) 1457–65.

[14] W.P. Russ, D.M. Engelman, The GxxxG motif: A framework for transmembrane helix-helix association, J. Mol. Biol., 296 (2000) 911–919.

[15] G. von Heijne, The distribution of positively charged residues in bacterial inner membrane proteins correlates with the trans-membrane topology, EMBO J., 5 (1986) 3021–3027.

[16] J. Nilsson, B. Persson, G. von Heijne, Comparative analysis of amino acid distributions in integral membrane proteins from 107 genomes, Proteins Struct. Funct. Bioinforma., 60 (2005) 606–616.

[17] C. Buda, I. Dey, N. Balogh, L.I. Horvath, K. Maderspach, M. Juhasz, Y.K. Yeo, T. Farkas, Structural order of membranes and composition of phospholipids in fish brain cells during thermal acclimatization, Proc. Natl. Acad. Sci. U. S. A., 91 (1994) 8234–8238.

[18] D.M. Owen, K. Gaus, A.I. Magee, M. Cebecauer, Dynamic organization of lymphocyte plasma membrane: lessons from advanced imaging methods, Immunology, 131 (2010) 1–8.

[19] E. Drolle, W.F.D. Bennett, K. Hammond, E. Lyman, M. Karttunen, Z. Leonenko, Molecular dynamics simulations and Kelvin probe force microscopy to study of cholesterol-induced electrostatic nanodomains in complex lipid mixtures, Soft Matter, 13 (2017) 355–362.

[20] J. Bai, R.E. Pagano, Measurement of spontaneous transfer and transbilayer movement of BODIPY- labeled lipids in lipid vesicles, Biochemistry, 36 (1997) 8840–8848.

[21] A. Kusumi, K.G.N. Suzuki, R.S. Kasai, K. Ritchie, T.K. Fujiwara, Hierarchical mesoscale domain organization of the plasma membrane, Trends Biochem. Sci., 36 (2011) 604–15.

[22] T.S. Van Zanten, A. Cambi, M. Koopman, B. Joosten, C.G. Figdor, M.F. Garcia-parajo, Hotspots of GPI-anchored proteins and integrin nanoclusters function as nucleation sites for cell adhesion, PNAS, 106 (2009) 18557–18562.

[23] S.K. Saka, A. Honigmann, C. Eggeling, S.W. Hell, T. Lang, S.O. Rizzoli, Multi-protein assemblies underlie the mesoscale organization of the plasma membrane, Nat. Commun., 5 (2014) 1–14.

[24] T.S. van Zanten, J. Gómez, C. Manzo, A. Cambi, J. Buceta, R. Reigada, M.F. Garcia-Parajo, Direct mapping of nanoscale compositional connectivity on intact cell membranes, Proc. Natl. Acad. Sci. U. S. A., 107 (2010) 15437–42.

[25] K. Simons, E. Ikonen, Functional rafts in cell membranes, Nature, 387 (1997) 569–72.

[26] L.J. Pike, Rafts defined: a report on the Keystone Symposium on Lipid Rafts and Cell Function, J. Lipid Res., 47 (2006) 1597–8.
[27] I. Levental, S. Veatch, The Continuing Mystery of Lipid Rafts, J. Mol. Biol., 428 (2016) 4749–4764.
[28] E. Sevcsik, G.J. Schütz, With or without rafts? Alternative views on cell membranes, BioEssays, 38 (2015) 129–39.
[29] O.G. Mouritsen, M. Bloom, Models of Lipid-Protein Interactions in Membranes, Annu Rev Biophys Biomol Struct, 22 (1993) 145–71.
[30] H.J. Sharpe, T.J. Stevens, S. Munro, A comprehensive comparison of transmembrane domains reveals organelle-specific properties, Cell, 142 (2010) 158–69.
[31] K. Ritchie, R. Iino, T. Fujiwara, K. Murase, A. Kusumi, The fence and picket structure of the plasma membrane of live cells as revealed by single molecule techniques (Review), Mol. Membr. Biol., 20 (2003) 13–18.
[32] T. Fujiwara, K. Ritchie, H. Murakoshi, K. Jacobson, A. Kusumi, Phospholipids undergo hop diffusion in compartmentalized cell membrane, J. Cell Biol., 157 (2002) 1071–1081.
[33] J.B. de la Serna, G.J. Schütz, C. Eggeling, M. Cebecauer, There is no universal model of the plasma membrane organisation, Front. Cell Dev. Biol., 4 (2016).
[34] E.G. Finer, A.G. Flook, H. Hauser, Mechanism of sonication of aqueous egg yolk lecithin dispersions and nature of the resultant particles, Biochim. Biophys. Acta - Lipids Lipid Metab., 260 (1972) 49–58.
[35] F. Olson, C.A. Hunt, F.C. Szoka, W.J. Vail, D. Papahadjopoulos, Preparation of liposomes of defined size distribution by extrusion through polycarbonate membranes, Biochim. Biophys. Acta - Biomembr., 557 (1979) 9–23.
[36] E.E. Ambroggio, L.A. Bagatolli, Giant Unilamellar Vesicles, Fluorescence Microscopy and Lipid – Peptide Interactions, in: M. Castanho (Ed.), Membr. Pept. Methods Results Struct. Funct., 2009: pp. 179–200.
[37] K. Akashi, H. Miyata, H. Itoh, K. Kinosita, Preparation of giant liposomes in physiological conditions and their characterization under an optical microscope, Biophys. J., 71 (1996) 3242–50.
[38] T. Pott, H. Bouvrais, P. Méléard, Giant unilamellar vesicle formation under physiologically relevant conditions, Chem. Phys. Lipids, 154 (2008) 115–9.
[39] L.-R. Montes, A. Alonso, F.M. Goñi, L. a Bagatolli, Giant unilamellar vesicles electroformed from native membranes and organic lipid mixtures under physiological conditions, Biophys. J., 93 (2007) 3548–54.
[40] R.P. Richter, R. Bérat, A.R. Brisson, Formation of solid-supported lipid bilayers: An integrated view, Langmuir, 22 (2006) 3497–3505.
[41] M. Przybylo, J. Sýkora, J. Humpolíčková, A. Benda, A. Zan, M. Hof, Lipid diffusion in giant unilamellar vesicles is more than 2 times faster than in supported phospholipid bilayers under identical conditions, Langmuir, 22 (2006) 9096–9.
[42] M.L. Wagner, L.K. Tamm, Tethered Polymer-Supported Planar Lipid Bilayers for Reconstitution of Integral Membrane Proteins : Silane-Polyethyleneglycol-Lipid as a Cushion and Covalent Linker, 79 (2000) 1400–1414.
[43] P. Mueller, D.O. Rudin, H.T. Tien, W.C. Wescott, Methods for the Formation of Single Bimolecular Lipid Membranes in Aqueous Solution, J. Phys. Chem., 67 (1963) 534–535.
[44] E. Sezgin, P. Schwille, Model membrane platforms to study protein-membrane interactions, Mol. Membr. Biol., 29 (2012) 144–54.
[45] D. Lingwood, J. Ries, P. Schwille, K. Simons, Plasma membranes are poised for activation of raft phase coalescence at physiological temperature, Proc. Natl. Acad. Sci. U. S. A., 105 (2008) 10005–10010.
[46] I. Levental, M. Grzybek, K. Simons, Raft domains of variable properties and compositions in plasma membrane vesicles, PNAS, 108 (2011) 11411–11416.
[47] H.-J. Kaiser, D. Lingwood, I. Levental, J.L. Sampaio, L. Kalvodova, L. Rajendran, K. Simons, Order of lipid phases in model and plasma membranes, Proc. Natl. Acad. Sci. U. S. A., 106 (2009) 16645–50.
[48] R. Koynova, M. Caffrey, Phases and phase transitions of the phosphatidylcholines, Biochim. Biophys. Acta, 1376 (1998) 91–145.
[49] Phase Transition Temperatures for Glycerophospholipids, Avantilipids.com/tech-Support/physical-Properties/phase-Transition-Temps/ Accessed Novemb. 1, 2017, (n.d.).
[50] N. Kahya, P. Schwille, How phospholipid-cholesterol interactions modulate lipid lateral diffusion, as revealed by fluorescence correlation spectroscopy, J. Fluoresc., 16 (2006) 671–8.
[51] S. Veatch, S. Keller, Miscibility Phase Diagrams of Giant Vesicles Containing Sphingomyelin,

Phys. Rev. Lett., 94 (2005) 3–6.
[52] S. Veatch, S.L. Keller, Seeing spots: Complex phase behavior in simple membranes, Biochim. Biophys. Acta - Mol. Cell Res., 1746 (2005) 172–185.
[53] J.A. Killian, G. Von Heijne, How proteins adapt to a membrane-water interface, Trends Biochem. Sci., 25 (2000) 429–434.
[54] M.R.R. de Planque, B.B. Bonev, J. a a Demmers, D. V Greathouse, R.E. Koeppe, F. Separovic, A. Watts, J.A. Killian, Interfacial anchor properties of tryptophan residues in transmembrane peptides can dominate over hydrophobic matching effects in peptide-lipid interactions, Biochemistry, 42 (2003) 5341–8.
[55] M.R.R. de Planque, J.A. Killian, Protein-lipid interactions studied with designed transmembrane peptides: role of hydrophobic matching and interfacial anchoring, Mol. Membr. Biol., 20 (2003) 271–84.
[56] J.H. Davis, D.M. Clare, R.S. Hodges, M. Bloom, Interaction of a synthetic amphiphilic polypeptide and lipids in a bilayer structure, Biochemistry, 22 (1983) 5298–5305.
[57] H.-J. Kaiser, A. Orłowski, T. Róg, T.K.M. Nyholm, W. Chai, T. Feizi, D. Lingwood, I. Vattulainen, K. Simons, Lateral sorting in model membranes by cholesterol- mediated hydrophobic matching, PNAS, 108 (2011) 16628–16633.
[58] K. Mitra, I. Ubarretxena-Belandia, T. Taguchi, G. Warren, D.M. Engelman, Modulation of the bilayer thickness of exocytic pathway membranes by membrane proteins rather than cholesterol, Proc. Natl. Acad. Sci. U. S. A., 101 (2004) 4083–8.
[59] R. Šachl, I. Boldyrev, L.B. a Johansson, Localisation of BODIPY-labelled phosphatidylcholines in lipid bilayers, Phys. Chem. Chem. Phys., 12 (2010) 6027–6034.
[60] M. Cebecauer, R. Šachl, Lipophilic Fluorescent Probes: Guides to the Complexity of Lipid Membranes, in: M. Wilhelmsson, Y. Tor (Eds.), Fluoresc. Analog. Biomol. Build. Blocks Des. Appl., John Wiley & Sons, Inc., 2016: pp. 367–392.
[61] A.P. Demchenko, Y. Mély, G. Duportail, A.S. Klymchenko, Monitoring biophysical properties of lipid membranes by environment-sensitive fluorescent probes, Biophys. J., 96 (2009) 3461–3470.
[62] J. Sýkora, P. Kapusta, V. Fidler, M. Hof, On what time scale does solvent relaxation in phospholipid bilayers happen?, Langmuir, 18 (2002) 571–574.
[63] A.L. Obaid, L.M. Loew, J.P. Wuskell, B.M. Salzberg, Novel naphthylstyryl-pyridinium potentiometric dyes offer advantages for neural network analysis, J. Neurosci. Methods, 134 (2004) 179–190.
[64] M.K. Kuimova, G. Yahioglu, J. a Levitt, K. Suhling, Molecular rotor measures viscosity of live cells via fluorescence lifetime imaging, J. Am. Chem. Soc., 130 (2008) 6672–3.
[65] R. Sjöback, J. Nygren, M. Kubista, Absorption and fluorescent properties of fluorescein, Spectrochim. Acta Part A, 51 (1995) 7–21.
[66] J.R. Lakowicz, Principles of Fluorescence Spectroscopy, Third, Springer, 2006.
[67] M. Wahl, Time-correlated single photon counting, Tech. Note PicoQuant, (2014) 1–14.
[68] M.A. Digman, V.R. Caiolfa, M. Zamai, E. Gratton, The Phasor Approach to Fluorescence Lifetime Imaging Analysis, Biophys. J., 94 (2008) L14-16.
[69] J. Ries, P. Schwille, New concepts for fluorescence correlation spectroscopy on membranes, Phys. Chem. Chem. Phys., 10 (2008) 3487–3497.
[70] D. Magde, E. Elson, W.W. Webb, Thermodynamic fluctuations in a reacting system: Measurement by fluorescence correlation spectroscopy, Phys. Rev. Lett., 29 (1972) 705–708.
[71] N.L. Thompson, Fluorescence Correlation Spectroscopy, in: J.R. Lakowicz (Ed.), Top. Fluoresc. Spectrosc. Vol. 1 Tech., Plenum Press, New York, NY, 1991: pp. 337–378.
[72] J. Ries, T. Weldemann, P. Schwille, Fluorescence Correlation Spectroscopy, in: Compr. Biophys., 2012: pp. 210–245.
[73] M. Štefl, A. Kułakowska, M. Hof, Simultaneous characterization of lateral lipid and prothrombin diffusion coefficients by z-scan fluorescence correlation spectroscopy, Biophys. J., 97 (2009) L01-3.
[74] J. Enderlein, I. Gregor, D. Patra, J. Fitter, Art and artefacts of fluorescence correlation spectroscopy, Curr. Pharm. Biotechnol., 5 (2004) 155–61.
[75] A. Benda, M. Benes, V. Marecek, A. Lhotsky, W.T. Hermens, M. Hof, How To Determine Diffusion Coefficients in Planar Phospholipid Systems by Confocal Fluorescence Correlation Spectroscopy, Langmuir, 19 (2003) 4120–4126.
[76] M. Böhmer, M. Wahl, H.-J. Rahn, R. Erdmann, J. Enderlein, Time-resolved fluorescence correlation spectroscopy, Chem. Phys. Lett., 353 (2002) 439–445.
[77] A. Benda, V. Fagul'ová, A. Deyneka, J. Enderlein, M. Hof, Fluorescence lifetime correlation spectroscopy combined with lifetime tuning: new perspectives in supported phospholipid bilayer

research, Langmuir, 22 (2006) 9580–5.
[78] P. Schwille, E. Haustein, Fluorescence Correlation Spectroscopy: An Introduction to its Concepts and Applications, 2001.
[79] R. Peters, R.J. Cherry, Lateral and rotational diffusion of bacteriorhodopsin in lipid bilayers: experimental test of the Saffman-Delbrück equations, Proc. Natl. Acad. Sci. U. S. A., 79 (1982) 4317–4321.
[80] R. Peters, A. Brünger, K. Schulten, Continuous fluorescence microphotolysis: A sensitive method for study of diffusion processes in single cells, Proc. Natl. Acad. Sci. U. S. A., 78 (1981) 962–966.
[81] R. Macháň, Y.H. Foo, T. Wohland, On the Equivalence of FCS and FRAP: Simultaneous Lipid Membrane Measurements, Biophys. J., 111 (2016) 152–161.
[82] M. Amaro, R. Šachl, P. Jurkiewicz, A. Coutinho, M. Prieto, M. Hof, Time-Resolved Fluorescence in Lipid Bilayers : Selected Applications and Advantages over Steady State, Biophys. J., 107 (2014) 2751–2760.
[83] M.L. Horng, A. Gardecki, A. Papazyan, M. Maroncelli, Subpicosecond Measurements of Polar Solvation Dynamics: Coumarin 153 Revisited, J Phys Chem, 99 (1995) 17311–17337.
[84] B. Valeur, Molecular Fluorescence: Principles and Applications, Wiley-VCH Verlag GmbH, 2001.
[85] T. Parasassi, G. De Stasio, A. D'Ubaldo, E. Gratton, Phase fluctuation in phospholipid membranes revealed by Laurdan fluorescence, Biophys. J., 57 (1990) 1179–86.
[86] F. Jähnig, Structural order of lipids and proteins in membranes: evaluation of fluorescence anisotropy data, Proc. Natl. Acad. Sci. U. S. A., 76 (1979) 6361–6365.
[87] K. Kinosita, A. Ikegami, S. Kawato, On the wobbling-in-cone analysis of fluorescence anisotropy decay, Biophys. J., 37 (1982) 461–464.
[88] D.W. Piston, G.-J. Kremers, Fluorescent protein FRET: the good, the bad and the ugly, Trends Biochem. Sci., 32 (2007) 407–414.
[89] W.L.C. Vaz, F. Goodsaid-Zalduondo, K. Jacobson, Lateral diffusion of lipids and proteins in bilayer membranes, FEBS Lett., 174 (1984) 199–207.
[90] P.F. Almeida, W.L.C. Vaz, T.E. Thompson, Lateral diffusion in the liquid phases of dimyristoylphosphatidylcholine/cholesterol lipid bilayers: a free volume analysis, Biochemistry, 31 (1992) 6739–6747.
[91] R. Macháň, M. Hof, Lipid diffusion in planar membranes investigated by fluorescence correlation spectroscopy, Biochim. Biophys. Acta, 1798 (2010) 1377–91.
[92] G. Saffman, M. Delbrück, Brownian motion in biological membranes, Proc. Natl. Acad. Sci. U. S. A., 72 (1975) 3111–3113.
[93] S. Ramadurai, A. Holt, V. Krasnikov, G. van den Bogaart, J.A. Killian, B. Poolman, Lateral diffusion of membrane proteins, J. Am. Chem. Soc., 131 (2009) 12650–6.
[94] K. Weiß, A. Neef, Q. Van, S. Kramer, I. Gregor, J. Enderlein, Quantifying the diffusion of membrane proteins and peptides in black lipid membranes with 2-focus fluorescence correlation spectroscopy, Biophys. J., 105 (2013) 455–62.
[95] T. Förster, G. Hoffmann, Die Viskositatsabhängigkeit der Fluoreszenzquantenausbeuten einiger Farbstoffsysteme [Effect of viscosity on the fluorescence quantum yield of some dye systems], Z Phys Chem, (1971) 63–76.
[96] B.D. Allen, A.C. Benniston, A. Harriman, S.A. Rostron, C. Yu, The photophysical properties of a julolidene-based molecular rotor, Phys. Chem. Chem. Phys., 7 (2005) 3035.
[97] J. Sýkora, K. Kaiser, I. Gregor, W. Bönigk, G. Schmalzing, J. Enderlein, Exploring fluorescence antibunching in solution to determine the stoichiometry of molecular complexes, Anal. Chem., 79 (2007) 4040–9.
[98] M. Moertelmaier, M. Brameshuber, M. Linimeier, G.J. Schütz, H. Stockinger, Thinning out clusters while conserving stoichiometry of labeling, Appl. Phys. Lett., 87 (2005) 1–3.
[99] J. Baumann, M.D. Fayer, Excitation transfer in disordered two-dimensional and anisotropic three-dimensional systems: Effects of spatial geometry on time-resolved observables, J. Chem. Phys., 85 (1986) 4087.
[100] M. Stöckl, J. Nikolaus, A. Herrmann, Visualization of Lipid Domain-Specific Protein Sorting in Giant Unilamellar Vesicles, in: V. Weissig (Ed.), Liposomes Methods Protoc. Vol. 2 Biol. Membr. Model., Humana Press, Totowa, NJ, 2010: pp. 115–126.
[101] M.A. Haidekker, T. Ling, M. Anglo, H.Y. Stevens, J.A. Frangos, E.A. Theodorakis, New fluorescent probes for the measurement of cell membrane viscosity, Chem. Biol., 8 (2001) 123–131.
[102] M.A. Haidekker, E.A. Theodorakis, Environment-sensitive behavior of fluorescent molecular rotors, J. Biol. Eng., 4 (2010) 11.
[103] M.K. Kuimova, Mapping viscosity in cells using molecular rotors, Phys. Chem. Chem. Phys., 14

(2012) 12671–86.
[104] R.O. Loutfy, Fluorescence probes for polymer free-volume, Pure Appl. Chem., 58 (1986) 1239–1248.
[105] Y. Wu, M. Štefl, A. Olzyńska, M. Hof, G. Yahioglu, P. Yip, D.R. Casey, O. Ces, J. Humpolíčková, M.K. Kuimova, Molecular rheometry: direct determination of viscosity in Lo and Ld lipid phases via fluorescence lifetime imaging, Phys. Chem. Chem. Phys., 15 (2013) 14986–93.
[106] J.A. Levitt, P.H. Chung, M.K. Kuimova, G. Yahioglu, Y. Wang, J. Qu, K. Suhling, Fluorescence anisotropy of molecular rotors, ChemPhysChem, 12 (2011) 662–672.
[107] I. López-Duarte, T.T. Vu, M.A. Izquierdo, J.A. Bull, M.K. Kuimova, A molecular rotor for measuring viscosity in plasma membranes of live cells, Chem. Commun. (Camb)., 50 (2014) 5282–4.
[108] M.R. Dent, I. López-Duarte, C.J. Dickson, N.D. Geoghegan, J.M. Cooper, I.R. Gould, R. Krams, J.A. Bull, N.J. Brooks, M.K. Kuimova, Imaging phase separation in model lipid membranes through the use of BODIPY based molecular rotors, Phys. Chem. Chem. Phys., 17 (2015) 18393–18402.
[109] H.M. Kim, H.-J. Choo, S.-Y. Jung, Y.-G. Ko, W.-H. Park, S.-J. Jeon, C.H. Kim, T. Joo, B.R. Cho, A Two-Photon Fluorescent Probe for Lipid Raft Imaging: C-Laurdan, ChemBioChem, 8 (2007) 553–559.
[110] N. Bag, X.W. Ng, J. Sankaran, T. Wohland, Spatiotemporal mapping of diffusion dynamics and organization in plasma membranes, Methods Appl. Fluoresc., 4 (2016) 34003.
[111] S. Veatch, P. Cicuta, P. Sengupta, A. Honerkamp-Smith, D. Holowka, B. Baird, Critical fluctuations in plasma membrane vesicles, ACS Chem. Biol., 3 (2008) 287–293.
[112] A.R. Honerkamp-Smith, S.L. Veatch, S.L. Keller, An introduction to critical points for biophysicists; observations of compositional heterogeneity in lipid membranes, Biochim. Biophys. Acta - Biomembr., 1788 (2009) 53–63.
[113] F.A. Heberle, J. Wu, S.L. Goh, R.S. Petruzielo, G.W. Feigenson, Comparison of three ternary lipid bilayer mixtures: FRET and ESR reveal nanodomains, Biophys. J., 99 (2010) 3309–3318.
[114] R. Šachl, J. Bergstrand, J. Widengren, M. Hof, Fluorescence correlation spectroscopy diffusion laws in the presence of moving nanodomains, J. Phys. D. Appl. Phys., 49 (2016) 114002.
[115] R. Šachl, J. Humpolíčková, M. Štefl, L.B. Johansson, M. Hof, Limitations of electronic energy transfer in the determination of lipid nanodomain sizes, Biophys. J., 101 (2011) 60–62.
[116] C. Dietrich, Z.N. Volovyk, M. Levi, N.L. Thompson, K. Jacobson, Partitioning of Thy-1, GM1, and cross-linked phospholipid analogs into lipid rafts reconstituted in supported model membrane monolayers, Proc. Natl. Acad. Sci. U. S. A., 98 (2001) 10642–10647.
[117] A.T. Hammond, F. a Heberle, T. Baumgart, D. Holowka, B. Baird, G.W. Feigenson, Crosslinking a lipid raft component triggers liquid ordered-liquid disordered phase separation in model plasma membranes, Proc. Natl. Acad. Sci. U. S. A., 102 (2005) 6320–5.
[118] A.K. Smith, J.H. Freed, The Determination of Tie-Line Fields for Coexisting Lipid Phases: an ESR Study, J Phys Chem B, 113 (2010) 3957–3971.
[119] M. Amaro, R. Šachl, G. Aydogan, I.I. Mikhalyov, R. Vácha, M. Hof, GM1 Ganglioside Inhibits beta-Amyloid Oligomerization Induced by Sphingomyelin, Angew. Chemie - Int. Ed., 55 (2016) 9411–9415.
[120] D.H. de Jong, C.A. Lopez, S.J. Marrink, Molecular view on protein sorting into liquid- ordered membrane domains mediated by gangliosides and lipid anchors, Faraday Discuss., 161 (2012) 1–19.
[121] I. Levental, D. Lingwood, M. Grzybek, Ü. Coskun, K. Simons, Palmitoylation regulates raft affinity for the majority of integral raft proteins, PNAS, 107 (2010) 22050–22054.
[122] L. V Schäfer, D.H. de Jong, A. Holt, A.J. Rzepiela, A.H. de Vries, B. Poolman, J.A. Killian, S.J. Marrink, Lipid packing drives the segregation of transmembrane helices into disordered lipid domains in model membranes, Proc. Natl. Acad. Sci. U. S. A., 108 (2011) 1343–8.
[123] M.E. Fastenberg, H. Shogomori, X. Xu, D. a Brown, E. London, Exclusion of a transmembrane-type peptide from ordered-lipid domains (rafts) detected by fluorescence quenching: extension of quenching analysis to account for the effects of domain size and domain boundaries, Biochemistry, 42 (2003) 12376–90.
[124] J. Domanski, S.J. Marrink, L. V Schäfer, Transmembrane helices can induce domain formation in crowded model membranes, Biochim. Biophys. Acta, 1818 (2011) 984–94.
[125] B. Bechinger, M. Zasloff, S.J. Opella, Structure and orientation of the antibiotic peptide magainin in membranes by solid-state nuclear magnetic resonance spectroscopy, Protein Sci., 2 (1993) 2077–84.
[126] J.C. Huschilt, B.M. Millman, J.H. Davis, Orientation of α-helical peptides in a lipid bilayer,

Biochim. Biophys. Acta - Biomembr., 979 (1989) 139–141.
[127] S.J. Ludtke, K. He, Y. Wu, H.W. Huang, Cooperative membrane insertion of magainin correlated with its cytolytic activity, Biochim. Biophys. Acta - Biomembr., 1190 (1994) 181–184.
[128] B. Bechinger, J.M. Ruysschaert, E. Goormaghtigh, Membrane helix orientation from linear dichroism of infrared attenuated total reflection spectra, Biophys. J., 76 (1999) 552–63.
[129] P. V Nazarov, R.B.M. Koehorst, W.L. Vos, V. V Apanasovich, M.A. Hemminga, FRET study of membrane proteins: determination of the tilt and orientation of the N-terminal domain of M13 major coat protein, Biophys. J., 92 (2007) 1296–1305.
[130] J. Ren, S. Lew, J. Wang, E. London, Control of the transmembrane orientation and interhelical interactions within membranes by hydrophobic helix length, Biochemistry, 38 (1999) 5905–12.
[131] P. Jurkiewicz, L. Cwiklik, P. Jungwirth, M. Hof, Lipid hydration and mobility: an interplay between fluorescence solvent relaxation experiments and molecular dynamics simulations, Biochimie, 94 (2012) 26–32.
[132] B. Bechinger, Towards membrane protein design: pH-sensitive topology of histidine-containing polypeptides, J. Mol. Biol., 263 (1996) 768–775.
[133] J. Sýkora, V. Mudogo, R. Hutterer, M. Nepras, J. Vaněrka, P. Kapusta, V. Fidler, M. Hof, ABA-C15: A new dye for probing solvent relaxation in phospholipid bilayers, Langmuir, 18 (2002) 9276–9282.
[134] P. Jurkiewicz, L. Cwiklik, A. Vojtíšková, P. Jungwirth, M. Hof, Structure, dynamics, and hydration of POPC/POPS bilayers suspended in NaCl, KCl, and CsCl solutions, Biochim. Biophys. Acta - Biomembr., 1818 (2012) 609–616.
[135] L. Beranová, J. Humpolíčková, J. Sýkora, A. Benda, L. Cwiklik, P. Jurkiewicz, G. Gröbner, M. Hof, Effect of heavy water on phospholipid membranes: experimental confirmation of molecular dynamics simulations, Phys. Chem. Chem. Phys., 14 (2012) 14516–22.
[136] S.A. Sanchez, M.A. Tricerri, E. Gratton, Laurdan generalized polarization fluctuations measures membrane packing micro-heterogeneity in vivo, Proc. Natl. Acad. Sci. U. S. A., 109 (2012) 7314–9.
[137] A.D. Dupuy, D.M. Engelman, Protein area occupancy at the center of the red blood cell membrane, Proc. Natl. Acad. Sci. U. S. A., 105 (2008) 2848–52.
[138] D. Marsh, Protein modulation of lipids, and vice-versa, in membranes, Biochim. Biophys. Acta - Biomembr., 1778 (2008) 1545–1575.
[139] P.C. Jost, O.H. Griffith, R. a Capaldi, G. Vanderkooi, Evidence for boundary lipid in membranes, Proc. Natl. Acad. Sci. U. S. A., 70 (1973) 480–484.
[140] M.R.R. De Planque, D. V Greathouse, R.E. Koeppe, H. Schäfer, D. Marsh, J.A. Killian, Influence of lipid/peptide hydrophobic mismatch on the thickness of diacylphosphatidylcholine bilayers A 2H NMR and ESR study using designed transmembrane α-helical peptides and gramicidin A, Biochemistry, 37 (1998) 9333–9345.
[141] M.R.R. de Planque, E. Goormaghtigh, D. V Greathouse, R.E. Koeppe, J. a Kruijtzer, R.M. Liskamp, B. de Kruijff, J.A. Killian, Sensitivity of single membrane-spanning alpha-helical peptides to hydrophobic mismatch with a lipid bilayer: effects on backbone structure, orientation, and extent of membrane incorporation, Biochemistry, 40 (2001) 5000–10.
[142] A. Holt, J.A. Killian, Orientation and dynamics of transmembrane peptides: the power of simple models, Eur. Biophys. J., 39 (2010) 609–21.
[143] E. Sparr, W.L. Ash, P. V Nazarov, D.T.S. Rijkers, M. a Hemminga, D.P. Tieleman, J.A. Killian, Self-association of transmembrane alpha-helices in model membranes: importance of helix orientation and role of hydrophobic mismatch, J. Biol. Chem., 280 (2005) 39324–31.
[144] S. Mall, R. Broadbridge, R.P. Sharma, J.M. East, A.G. Lee, Self-Association of Model Transmembrane alpha - Helices Is Modulated by Lipid Structure, Biochemistry, 40 (2001) 12379–12386.
[145] P.C.A. Van Der Wel, T. Pott, S. Morein, D. V. Greathouse, R.E. Koeppe, J.A. Killian, Tryptophan-anchored transmembrane peptides promote formation of nonlamellar phases in phosphatidylethanolamine model membranes in a mismatch- dependent manner, Biochemistry, 39 (2000) 3124–3133.
[146] M.J. Saxton, Two-dimensional continuum percolation threshold for diffusing particles of nonzero radius, Biophys. J., 99 (2010) 1490–1499.
[147] K. Weiß, J. Enderlein, Lipid diffusion within black lipid membranes measured with dual-focus fluorescence correlation spectroscopy, ChemPhysChem, 13 (2012) 990–1000.
[148] D. Kozma, I. Simon, G.E. Tusnády, PDBTM: Protein Data Bank of transmembrane proteins after 8 years, Nucleic Acids Res., 41 (2013) D524-9.
[149] R.K. Hite, Z. Li, T. Walz, Principles of membrane protein interactions with annular lipids deduced

from aquaporin-0 2D crystals, EMBO J., 29 (2010) 1652–1658.
[150] M. Frick, K. Schmidt, B.J. Nichols, Modulation of lateral diffusion in the plasma membrane by protein density, Curr. Biol., 17 (2007) 462–7.
[151] P.S. Niemelä, M.S. Miettinen, L. Monticelli, H. Hammaren, P. Bjelkmar, T. Murtola, E. Lindahl, I. Vattulainen, Membrane proteins diffuse as dynamic complexes with lipids, J. Am. Chem. Soc., 132 (2010) 7574–5.
[152] T. Róg, M. Pasenkiewicz-Gierula, I. Vattulainen, M. Karttunen, Ordering effects of cholesterol and its analogues, Biochim. Biophys. Acta, 1788 (2009) 97–121.
[153] T. Róg, K. Murzyn, M. Karttunen, M. Pasenkiewicz-Gierula, Nonpolar interactions between transmembrane helical EGF peptide and phosphatidylcholines, sphingomyelins and cholesterol Molecular dynamics simulation studies, J. Pept. Sci., 14 (2008) 374–382.
[154] M.C. Pitman, A. Grossfield, F. Suits, S.E. Feller, Role of Cholesterol and Polyunsaturated Chains in Lipid − Protein Interactions : Molecular Dynamics Simulation of Rhodopsin in a Realistic Membrane Environment Role of Cholesterol and Polyunsaturated Chains in Lipid-Protein Interactions : Molecular Dynami, Biochim. Biophys. Acta, (2005) 4576–4577.
[155] J.H. Nyström, M. Lönnfors, T.K.M. Nyholm, Transmembrane peptides influence the affinity of sterols for phospholipid bilayers, Biophys. J., 99 (2010) 526–33.
[156] S.R. Shaikh, M. Edidin, Polyunsaturated fatty acids, membrane organization, T cells, and antigen presentation, Am. J. Clin. Nutr., 84 (2006) 1277–1289.
[157] S.E. Feller, K. Gawrisch, A.D. MacKerell, Polyunsaturated Fatty Acids in Lipid Bilayers: Intrinsic and Environmental Contributions to Their Unique Physical Properties, J. Am. Chem. Soc., 124 (2002) 318–326.
[158] M.A. Haidekker, T.P. Brady, D. Lichlyter, E.A. Theodorakis, A Ratiometric Fluorescent Viscosity Sensor, JACS, 128 (2006) 398–399.

9 List of abbreviations

16-Doxyl	1-palmitoyl-2-stearoyl-(16-doxyl)-sn-glycero-3-phosphocholine
Arachidonic acid	Eicosa-5Z,8Z,11Z,14Z-tetraenoic acid
biotinyl Cap PE	1,2-dipalmitoyl-sn-glycero-3-phosphoethanolamine-N-(cap biotinyl)
BODIPY	Boron-dipyrromethene based probe
BSA	Bovine serum albumin
C_2-LW21	Dimeric LW21
Chol	Cholesterol
CTxB	β-subunit of cholera toxin protein complex
DiD	1,1'-Dioctadecyl-3,3,3',3'-Tetramethylindodicarbocyanine Perchlorate
DMPC	1,2-dimyristoyl-sn-glycero-3-phosphocholine
DOPC	1,2-dioleoyl-sn-glycero-3-phosphocholine
DOPG	1,2-dioleoyl-sn-glycero-3-phosphoglycerol
DPH	1,6-diphenyl-1,3,5-hexatriene
DPPC	1,2-dipalmitoyl-sn-glycero-3-phosphocholine
F(C)CS	Fluorescence (cross-)correlation spectroscopy
FLIM	Fluorescence lifetime imaging microscopy
FRAP	Fluorescence recovery after photobleaching
FRET	Förster resonance energy transfer
GFP	Green fluorescent protein
GM1	Monosialotetrahexosylganglioside lipid
GP	Generalized polarization
GPMVs	Giant plasma membrane vesicles
GUV	Giant unilamellar vesicles
HEPES	4-(2-Hydroxyethyl)piperazine-1-ethanesulfonic acid
HPLC	High-performance liquid chromatography
iFCS	Imaging fluorescence correlation spectroscopy
IRF	Instrument response function
Laurdan	6-lauroyl-2-dimethylaminonaphthalene
LAH_4	Model antimicrobial peptide used in the thesis

LAT	Transmembrane peptide used in thesis derived from TMD of Linker for Activation of T cells protein
Ld	Liquid disordered phase
Lo	Liquid ordered phase
LUV	Large unilamellar vesicles
LW21	Model transmembrane peptide used in thesis
MLV	Multilamellar vesicles
NA	Numerical aperture
NADH	Nicotinamide adenine dinucleotide
NMR	Nuclear magnetic resonance
PA	Phosphatidic acid
PC	Phosphatidylcholine
PE	Phosphatidylethanolamine
POPC	1-palmitoyl-2-oleoyl-sn-glycero-3-phosphocholine
PI	Phosphatidylinositol
PMS	Plasma membrane spheres
PS	Phosphatidylserine
PUFA	Polyunsaturated fatty acids
SD model	Saffman-Delbrück hydrodynamic model
SM	Palmitoyl sphingomyelin
So	Solid/gel lipid phase
SP	Structure parameter
Sph	Sphingomyelin
SUV	Small unilamellar vesicles
TCSPC	Time correlated single photon counting
TDFS	Time dependent fluorescent shift
TFE	2,2,2-trifluoroethanol
TICT	Twisted intramolecular charge transfer state
Tm	Phase transition temperature
TMD	Transmembrane domain
TOCCSL	Thinning Out Clusters while Conserving the Stoichiometry of Labeling
TRES	Time resolved emission spectra
UV	Ultraviolet light

10 Appendices

List of attached publications and contribution of Mgr. Marie Olšinová (the author) to the publications presented in the submitted thesis:

Paper I

Di- and Tri-Oxalkyl Derivatives of a Boron Dipyrromethene (BODIPY) Rotor Dye in Lipid Bilayers

Olšinová, Marie, Piotr Jurkiewicz, Michal Pozník, Radek Šachl, Tereza Prausová, Martin Hof, Václav Kozmík, Filip Teplý, Jiří Svoboda, and Marek Cebecauer

2014 *Physical Chemistry Chemical Physics* 16: 10688-97

The author prepared samples in the form of MLVs and GUVs and performed FLIM and anisotropy measurements, FLIM-FRET experiments and quenching experiments with doxyl quenchers. She analyzed data from FLIM measurements and was involved in the analysis of anisotropy, FLIM-FRET and quenching data. The author participated in discussion about results and all experimental procedures.

Supplementary information containing Matlab code for anisotropy analysis is not attached due to its extensivness. It can be downloaded at http://www.rsc.org/suppdata/cp/c4/c4cp00888j/c4cp00888j2.pdf

Paper II

Dynamics and Size of Cross-Linking-Induced Lipid Nanodomains in Model Membranes

Štefl, Martin, Radek Šachl, Jana Humpolíčková, Marek Cebecauer, Radek Macháň, **Marie Kolářová**, Lennart B-Å Johansson, and Martin Hof

2012 *Biophysical Journal* 102: 2104–13

The author was involved in GUVs preparation by gentle hydration method, measurement of cross-linker and lipid dynamics by z-scan FCS, detection of nanodomains by FLIM-FRET measurements, analysis of FCS data, FLIM-FRET data by phasor plot analysis and diffusion law analysis and in discussion of results.

Paper III

Peripheral and Integral Membrane Binding of Peptides Characterized by Time-Dependent Fluorescence Shifts: Focus on the Antimicrobial Peptide LAH_4

Macháň, Radek, Piotr Jurkiewicz, Agnieszka Olzyńska, **Marie Olšinová**, Marek Cebecauer, Arnaud Marquette, Burkhard Bechinger, and Martin Hof

2014 *Langmuir* 30: 6171–79

The author prepared samples for TDFS measurements of Laurdan in lipid membranes in

the presence or absence of transmembrane peptides LW21 and LAT and measured the samples by TDFS method. The author was involved in data analysis and discussions about the results and project.

Paper IV

Roughness of a Transmembrane Peptide Reduces Lipid Membrane Dynamics

Olšinová, Marie, Piotr Jurkiewicz, Jan Sýkora, Ján Sabó, Martin Hof, Lukasz Cwiklik, and Marek Cebecauer

2016 *BioRxiv*: 1–14 (DOI: 10.1101/093377)

The author prepared model lipid membranes for the fluorescence measurements, performed the fluorescence measurements (FCS, TDFS, homo-FRET, peptide incorporation) and analyzed diffusion data and peptide incorporation data. She was involved in TDFS and homo-FRET analysis. The author participated in discussions about the results, experimental procedures and project in general.